UNIVERSITY OF SOUTHAMPTON

FACULTY OF PHYSICAL SCIENCES AND ENGINEERING

ELECTRONICS AND COMPUTER SCIENCE

Counter-flow Dialysis for Microvolume Desalting

by

Prameen Chacko Kalikavunkal

Thesis for the degree of Doctor of Philosophy

August 2015

Supervisors: Dr. Maurits de Planque

Prof. Hywel Morgan

ABSTRACT

Some analytical techniques are not compatible with physiological salt concentrations. An array of desalting approaches exists, but the conventional implementation requires large sample volumes, which is not compatible with fingerprick blood samples for molecular diagnostics. With dialysis being identified as the most suitable method for on-chip microvolume desalting, the aim of this work was to develop a microvolume dialyser that can desalt biological samples to any required salt concentration. Phase-separation ultrafiltration membranes were first characterised to determine their porosity, an important parameter for the dialysis efficiency. Desalting of a microchamber-confined sample over these membranes was then systematically investigated, first by static dialysis against a bulk water phase and next in a dialyser where also the water phase was enclosed in a laser micromachined chamber, with periodic water refreshment. Although the water content of the channel was approximately 400-fold smaller than the initial bulk water volume, similar salt removal rates could be achieved with high refreshment rates. A dialyser that enables a continuous flow of the sample and of the water phase in opposite directions was then constructed. It was established that by selecting the appropriate combination of flow rates the extent of desalting can be exactly controlled. This extensive experimental data set was in good agreement with predictions from mass transfer theory, which also indicated that a further increase in dialysis performance would require a different membrane structure. The developed counter-flow microvolume dialyser could be operated for a prolonged period of time, also for samples with a high protein content and also for blood serum. Finally, protein samples were dialysed under different sample and water flow conditions and the effect of a range of residual salt concentrations on the quality of mass spectrometer analysis was explored.

Contents

DECLARATION OF AUTHORSHIP

I, Prameen Chacko Kalikavunkal declare that this thesis and the work presented in it are my own and has been generated by me as the result of my own original research.

Counter Flow Dialysis for Microvolume Desalting

I confirm that:

1. This work was done wholly or mainly while in candidature for a research degree at this University;
2. Where any part of this thesis has previously been submitted for a degree or any other qualification at this University or any other institution, this has been clearly stated;
3. Where I have consulted the published work of others, this is always clearly attributed;
4. Where I have quoted from the work of others, the source is always given. With the exception of such quotations, this thesis is entirely my own work;
5. I have acknowledged all main sources of help;
6. Where the thesis is based on work done by myself jointly with others, I have made clear exactly what was done by others and what I have contributed myself;
7. None of this work has been published before submission.

Signed:.....

Date:.....

ACKNOWLEDGEMENT

Thanks God, the almighty, merciful and the passionate, for being so kind, blessing and forgiving.

First and foremost, I would like to express my sincere and deep appreciation to my supervisor Dr. Maurits de Planque for his encouragement, invaluable support, guidance and friendship throughout this work. I am honoured to have the opportunity to work under his supervision. There are no words enough to thanks him. Another person I want to thank is Prof. Hywel Morgan who was also a part of my supervisory team. His assistance and valuable time in critical stages of this project has substantially benefitted this project and is greatly appreciated.

My sincere thanks to Mr. Anton Page of the Biomedical Imaging Unit for his help with imaging membranes, and Mr. Neville Wright for his help with mass spectrometry. A big thanks to my friends Sumit, Hang, Hend, Mark, Chunxiao Hu, Gayan, Andy Farida, Roy, Toda for their help whenever I needed and being so supportive and encouraging. Special word of thanks to Dr. Marie, Dr. Martin and Dr. Gareth, who were kind enough to lend me help and support during my PhD in the lab. . I would also like to express gratitude towards other members in Bio-ECS group and clean room technical team for lending a helpful hand in general.

Finally, I would like to thank my parents and my sister Priya for their endless support and encouragement, to cheer me up when I am down.

List of abbreviations and symbols

SEC	Size Exclusion Chromatography
MWCO	Molecular weight cut-off
µL, mL	microlitre, millilitre
SiNW	Silicon nanowire
MTC	Mass transfer coefficient
k	Mass transfer coefficient (moles/s)
Sh	Sherwood number
MT	Mass transfer (moles/s)
Re	Reynolds number
Qs	Sample flow rate
Qw	Water flow rate
D_c	Diffusion coefficient of electrolyte ion in water at 25^{o}C, 1.29x10^{-9}m^{2}/s
km	Membrane mass transfer coefficient (m/s)
ks	Mass transfer coefficient in the sample channel
kw	Mass transfer coefficient in the water channel
C_{sin}	Sample input concentration (moles/litre)
C_{sout}	Sample output concentration (moles/litre)
C_{win}	Water input concentration (moles/litre)
C_{wout}	Water output concentration (moles/litre)
Da, kDa	Dalton, kilo Dalton
S	Conductance (Siemens)
mS/cm, µS/cm	Conductivity

UF	Ultrafiltration
RO	Reverse Osmosis
nm	nanometre
ε	membrane porosity
τ	membrane tortuosity
t	membrane thickness (micrometre)
A	Ampere
MS	Mass Spectrometry
Wc	Width of the channel (m)
Hc	Height of the channel (m)
Lc	Length of the channel (m)

Chapter 1: Introduction

1.1 Background and motivation

Detection and quantification of molecular biomarkers, biomolecules that are associated with a specific disease or even a specific stage of a disease, promises significant advantages for medical diagnostics, especially for complex diseases such as cancer. However, the concentration of these biomarkers in, for example, blood plasma can be very low and their detection is complicated by the high abundancy of many plasma proteins (1-3). A further limitation is the emerging preference, particularly in the context of point of care applications, for small sample volumes such as a blood droplet obtained by fingerprick and simple and robust one-step assays. Two techniques that are of interest in this context are mass spectrometry and nanoscale field effect transistor technology such as silicon nanowire (SiNW) biosensors. The latter technology, which is still in an early phase of development, promises high sensitivity and label-free real-time detection but a physiological salt concentration is an obstacle due to Debye screening (4), whereas in the case of mass spectrometry, salt ions interfere with the mass spectrum analysis through the formation of salt adduct species that broaden all signals (5). Salt concentrations in the sample for good detection scheme would depend on the individual methods used. For eg., SiNW favours low salt concentration (~1mM) whereas mass spectrometry requires <15mM for good detection. It is thus necessary to desalt the sample of interest prior to mass spectrometry or SiNW measurements, but conventional desalting approaches require large sample volumes, at least several millilitres, and are hence not suitable for small-volume samples.

1.2 Aims and scope of work

This project aimed to develop a device for the rapid one-step desalting of microvolume protein samples. Requirements are that the sample should not be diluted and that all of the sample can be recovered from the device. The desalting strategy was based on a conventional well-established desalting method and is in this sense a miniaturisation engineering project. However, the device should also be capable to reduce the salt concentration of a sample to a specific value, i.e. the desalting should be tuneable. This requires incorporation of a sensor to measure the salt concentration. The performance of such a tuneable microvolume desalting device should be systematically evaluated and optimised for a range of samples of increasing complexity, from simple salt solutions to high-concentration protein solutions and an actual biomedical sample. The desalting characteristics should also be underpinned by a theoretical model so that limiting factors can be identified. The construction of all parts of the device will

follow a rapid prototyping approach to facilitate rapid design iterations and to concentrate on achieving proof of concept. The focus will therefore be on system integration rather than on the development of any specialized individual device component. Finally, microlitre samples that have been desalted to various specific salt concentrations with the use of the developed device should be measured with a salt-sensitive analytical technique that is relevant for protein biomarker detection, e.g. mass spectrometry.

1.3 Concept of dialysis

Dialysis was selected as the salt separation mechanism. It is a classic laboratory technique used for a wide variety of applications, including desalting, buffer exchange, removal of labelling reagents, drug binding studies, cell growth and feeding, virus purification and blood treatment. Dialysis involves the separation of particles in a liquid on the basis of differences in their ability to pass through a porous membrane, with transport across the membrane being driven by a concentration gradient. The separation capability of dialysis is determined by the pore size-range of the membrane, which for biomolecular separation processes is often quantified as an empirical molecular weight cut-off (MWCO) value.

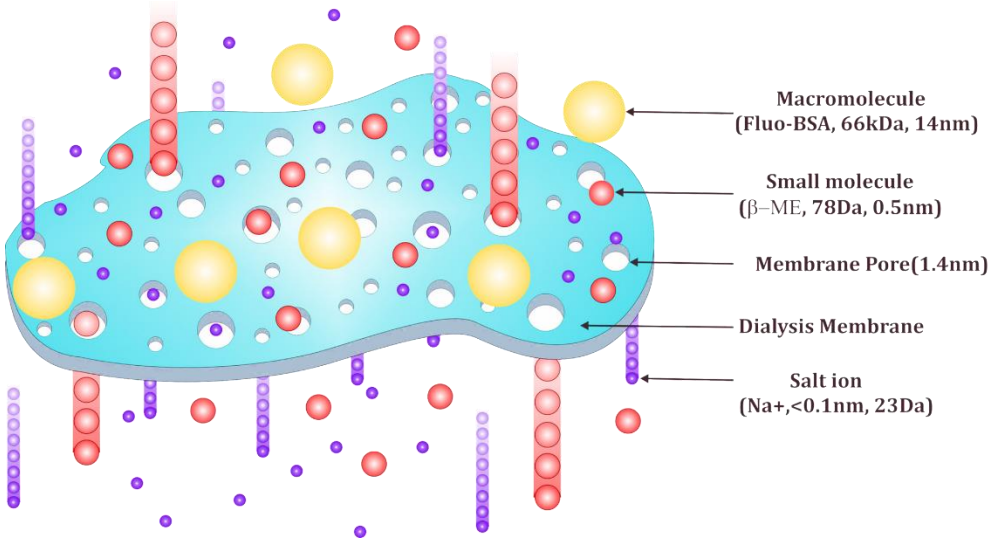

Figure 1.1: : In dialysis, small molecules diffuse over a porous membrane if their concentration in the dialysate phase (below the membrane in the diagram) is lower. Molecules larger than the membrane pore size are retained in the retentate phase (above the membrane in the diagram).

Conventional dialysis applications involve large sample volumes, from tens of millilitres to litres. However, microvolume dialysis has also been explored in recent years for a variety of applications (6-10), including desalting (11). In all these applications of microfluidic dialysis the crucial parameter is the selection of the appropriate membrane, which should sustain a high permeate flux (12).

1.4 Summary of main achievements

A compact platform capable of tuneable microvolume dialysis was developed using an economical and simple method, laser micromachining of acrylic, to integrate millifluidic channels with an ultrafiltration membrane and customized benchtop conductivity meters. Established devices for dialysis fails to offer microvolume dialysis, while at the same time offer no control over desalting efficiencies. This research has overcame such problems which forms the novelty of the work. The performance of this counter-flow dialyser, capable of 99.88% salt removal, was systematically characterized for a wide range of flow conditions. The experimental data were found to be in good agreement with the theoretical performance as predicted by mass transfer theory and identified the membrane itself as the limiting device component. Furthermore, microvolume counter-flow dialysis was performed with solutions with a high, plasma-like, protein content as well as with plasma itself, and the desalting performance was characterized for a range of dialyser operation conditions. Continuous dialysis for 16 hours was demonstrated and desalting down to 1mM salt was achieved. For SiNW and mass spectrometry analysis, salt concentration of approximately 1mM is favourable since it would overcome Debye screening in SiNW and formation of salt adducts in the latter. The salt concentration range that is compatible with mass spectrometry was addressed in preliminary experiments.

1.5 Structure of thesis

The work involves designing a microvolume desalting device and analysis of its desalting efficiency using theoretical equations. Hence the literature review has been divided into two distinct chapters. Chapter 2 reports the working and the advantages and disadvantages of using untreated samples in analytical instruments in the context of desalting requirements. Conventional methods of desalting, along with any on-chip desalting devices or applications, are reviewed. The principles behind each of the methods are explained and their advantages and disadvantages are discussed, concluding with a summary of the optimal choice of desalting strategies with reference to existing on-chip applications. Chapter 3 focuses on dialysis, addressing flow conditions in a microchannel and its influence on diffusion, possible method of analysing the results of desalting, their efficiency and calculation of mass transfer rate of a dialyser. Chapter 4 then describes the construction of different device configurations for desalting the sample and investigating its performance. The fabrication of the dialysis platform using laser micromachining and a simple method to quantify the desalting efficiency are outlined. Configurations to test the dialysis and diffusion, as well as different configurations to obtain good desalting using the membranes are discussed. Chapter 5 concerns the membranes used for dialysis, explaining the different fabrication methods and different structures.

Electron microscopy imaging of commercially obtained membranes is presented and experiments to determine approximate porosity values for the membranes by electrical and diffusional methods are described. Chapter 6 deals with the systematic evaluation of the desalting performance of the various dialysers and reports the optimal flow conditions, combined with a theoretical analysis based on mass transfer theory and an overview of possible limiting factors. Chapter 7 forms the last experimental chapter, with an emphasis on desalting of samples with a high protein content and of blood serum, also addressing continuous device operation for a prolonged period of time and presenting mass spectra of protein mixtures that have been desalted to various specific salt concentrations. Finally Chapter 8 concludes this thesis with a recapitulation of the key findings and recommendations for future work.

Chapter 2: Conventional desalting approaches

This Chapter introduces the concept of molecular diagnostics and biomarker analysis of blood samples. The working principle of mass spectrometry and silicon nanowire (SiNW) biosensors are explained. It also highlights the importance of how the presence of salt in the sample affects the mass spectra analysis and importance of Debye Length which determines the sensitivity limits of the nanoscale field effect transistors. Common strategies to desalt biomolecular samples of millilitre volume are highlighted, with reference to microliter volume (on-chip) adaptations where these have been implemented. Desalting methods such as size exclusion chromatography (SEC), ultrafiltration, reverse osmosis and electrodialysis are outlined first. The traditional method of blood purification by haemodialysis and the principles involved in dialysis as well as the necessary conditions to achieve good dialysis efficiency are subsequently explained. The two most commonly employed microvolume dialysis strategies, using a hollow fibre membrane and using a planar membrane sandwiched between two channels, are then discussed. This chapter ends with a brief summary of previous work about on-chip microvolume dialysis for desalting and other applications.

2.1 Molecular diagnostics

Blood circulates throughout every part of the body, and has a high degree of intimacy with the body. Therefore, it possesses information concerning the overall pathophysiology of a patient. For instance, alterations in protein abundance can serve as an indicator to pathological abnormalities: diseases, toxic effects of clinical treatments and so forth. Blood plasma is a straw-coloured, clear liquid making up 55% of the total volume of blood of which 90% is water. It also consists of salt like sodium, potassium, calcium, magnesium, chloride, and bicarbonate etc. These salts function in many important body processes. Apart from the salt, the plasma does have a sea of biomarkers which could be a useful diagnostic tool. Few of the key biomarkers useful in medical diagnostics such as human growth hormone, prostate specific antigen are available in low concentrations (10pM) and diluting such samples are not favourable. Detecting such low concentration of biomarkers in the samples are simple and straight forward using SiNW or mass spectrometry provided the samples are not diluted further. Current diagnostic tools employ or look for employing undiluted plasma. Mass spectrometry (MS) is an established method for proteomics, including blood serum proteomics (13, 14) while nanoscale field effect transistors are a novel technology that is under development for biomarker detection (15, 16).

2.1.1 Mass spectrometry

Mass spectrometry (MS) is an analytical tool used for measuring the molecular mass of a sample. This technique is useful in identifying the compounds based on the atomic sample composition of the molecules and their charge state. MS does not require the prior knowledge of the sample composition and hence offers blind analysis of unknown sample. Atoms can be deflected by magnetic fields, provided the atoms are first turned into an ion. The sequence for analysis using MS begins with ionisation. Inside the ionization source, the molecules are ionized because they are easier to manipulate than neutral molecules. The small sample is ionized into cations by knocking one or more electrons. The positive ions are obtained even in the case of argon or chlorine which normally do not form positive ion. These ions are then accelerated so that all the ions have the same kinetic energy.

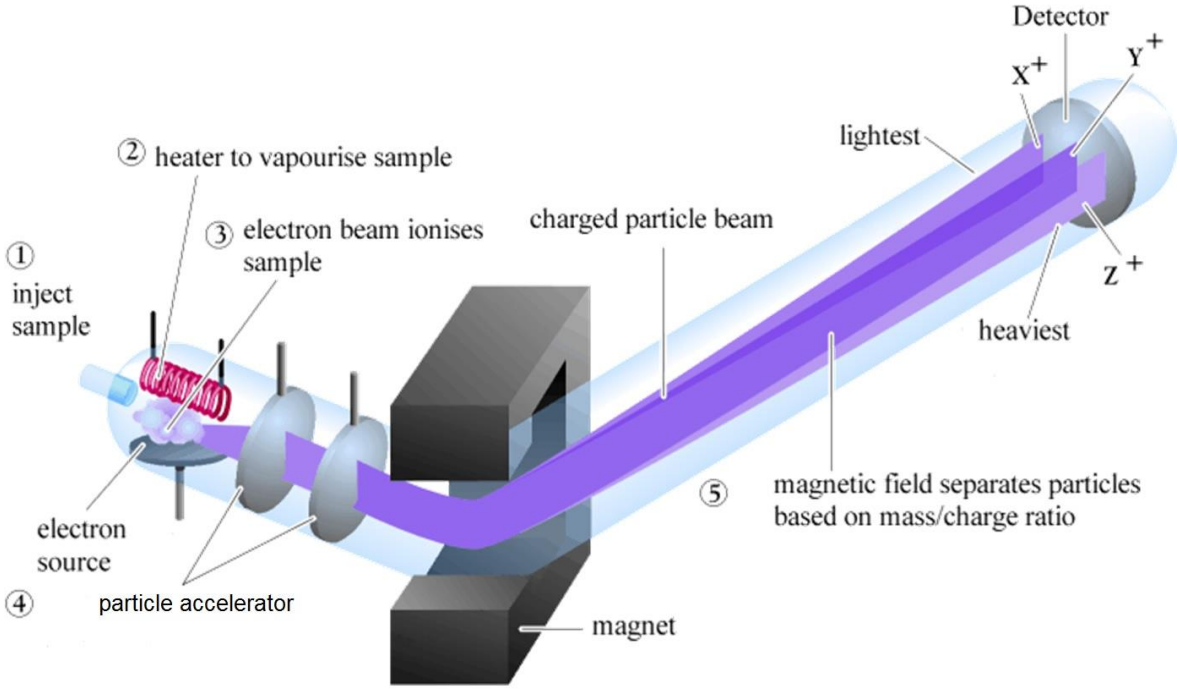

Figure 2.1: Working principle of a mass spectrometer (17)

The ions are extracted to a mass analyser of the MS where they are separated according to their mass (m) -to-charge (z) ratios (m/z). The ions are deflected by a magnetic field according to their masses- the lighter the ions are, the more they are deflected. The deflection also depends on the number of electrons knocked out to form the positive ions- the more the ion is charged, the more it gets deflected. The readout from the detector is then sent to a data system where the signal intensity at each m/z value, corresponding to the relative abundance of each species, is stored along with their relative abundance in the format of a mass spectrum (Figure 2.2). The setup- the analyser, detector, and the ionisation source are maintained under high vacuum to allow the ions to travel from one end of the instrument to the other without any hindrance

from air molecules. The sample under test can be directly inserted into the ionisation source or has to undergo chromatography en-route to the ionization source. Electrospray ionisation is the most common ionisation technique and is well suited for analysis of polar molecules ranging from 100Da-1,000,000Da. The mass spectrum for acetone can be seen from the Figure 2.2. The relative abundance of each ion are detected, and the most abundant ion, called the base peak, is set to 100%. All the other peaks are recorded relative to the base peak. For acetone, the base peak is at m/z = 43. The molecular weight of acetone is 58, so it is possible to identify the peak at m/z = 58 corresponding to the molecular ion peak**,** or parent peak**.**

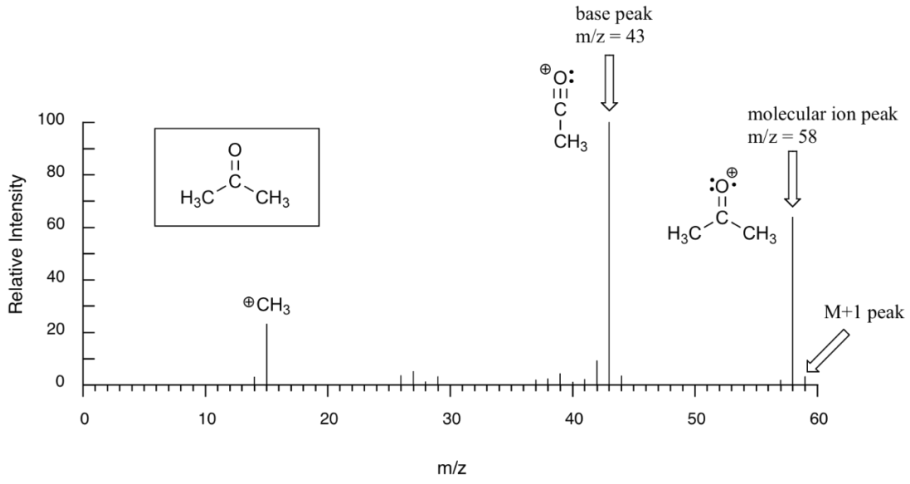

Figure 2.2: A typical output of an electron-ionization MS experiment of acetone sample (18)

Sample preparation prior to Electrospray Ionisation (ESI) is an important determinant of the quality of the resulting mass spectrum. Normally protein samples are dissolved in 90% formic acid and then desalted. Salts and other compounds of fixed charge often dominate the ESI spectrum when present in the sample (19). Salts are problematic in mass spectrometers because MS identify the mass of a charged ion of an analyte molecule. Excess salt can interfere with the performance of the mass spectrometer by overloading the system with charged salt ions. These salt ions can also assist in ionization and generate multiple salt adducts of the analyte. Metal salts such as those of sodium and potassium are usually more problematic than ammonium salts. For matrix assisted laser desorption/ionization (MALDI) type MS, metal salt concentrations of 100mM are usually tolerated whereas in Liquid Chromatography (LC)/MS, salts should be washed through the HPLC column prior to initiating a gradient for elution of the analyte molecules and starting mass spectral analysis. This being said, there are cases where MS requires high concentration of essential salts for a noncovalent protein complex as reported by Sterling et al (20).

Prior to loading the samples into the mass spectrometer, reverse phase desalting columns or high-performance liquid chromatography (HPLC) are commonly used to desalt the samples.

Although these devices provide good desalting as shown in Figure 2.3, they fail to offer any control over desalting efficiency. Pierce C18 Tips were used to desalt the sample. Mass spectrum obtained for the samples prior to desalting fails to show any peaks of interest due to the presence of high salt concentration, whereas the spectrum after desalting clearly showed multiple peaks.

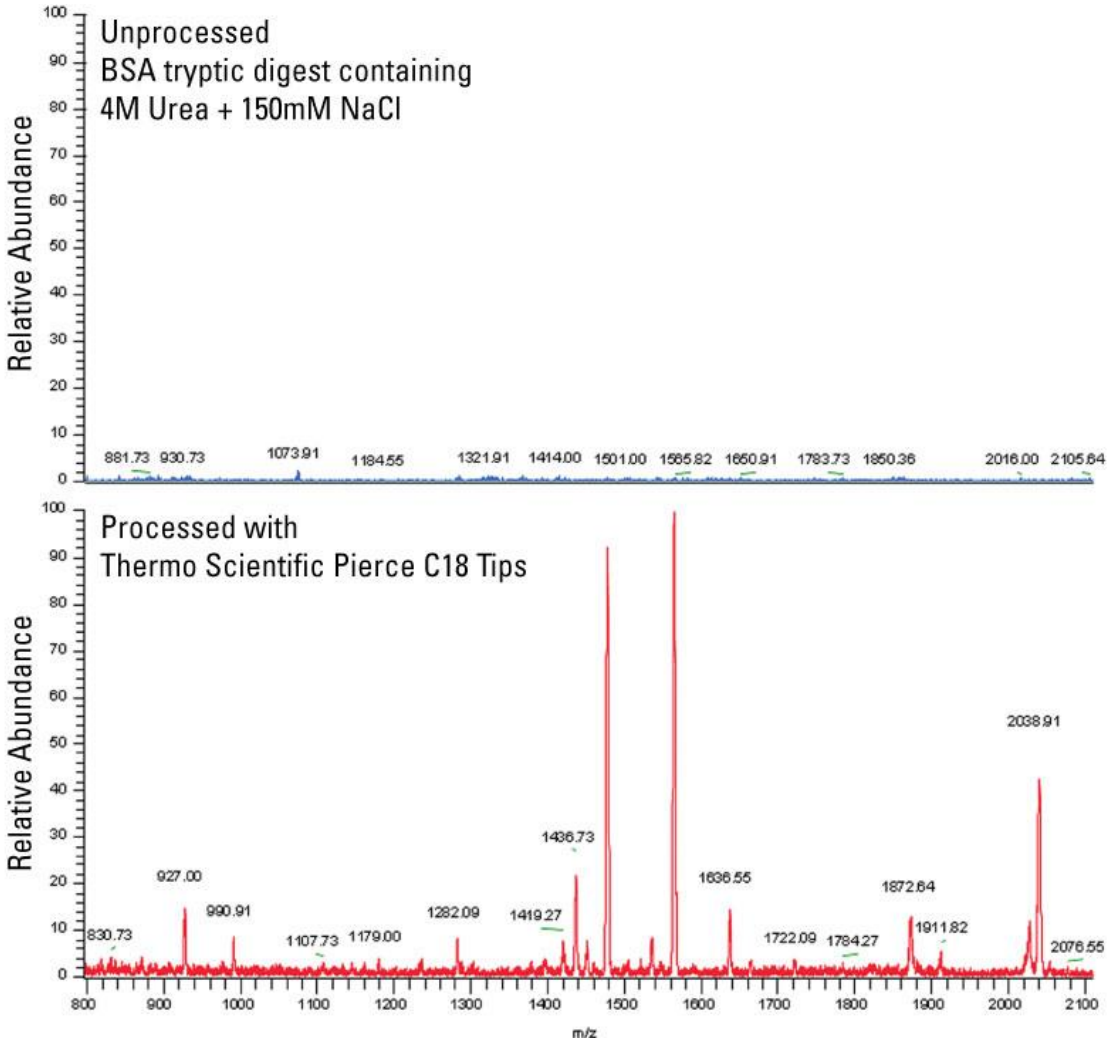

Figure 2.3: The spectrum of the sample before and after removal of salt by desalting using Pierce C18 Tips. Desalting of the sample prior to analysing showed clear peaks (21).

MS has been employed in industry and academia for both routine and research purposes. The most common application of MS can be seen for the analysis of proteins, peptides, oligonucleotide, drug discovery, combinatorial chemistry, pharmacokinetics, drug metabolism, neonatal screening, haemoglobin analysis, drug testing. One of the common interference in analysis of sample using MS is the presence of salt in the sample which mask or interfere with proper spectrum analysis (5; 22).

2.1.2 NanoFET biosensors

An emerging nanotechnology application in the form of electronics for biological application is the use of nano-FET (nanoscale-Field Effect Transistors) biosensors. The sensor utilizes a quasi-1D semiconducting nanostructure. The nanowires form the active sensing element to detect the presence of local electric field produced by charged biological molecules (analyte). Use of nanowires for biosensor recognises label free detection, higher surface to volume ratio coupled with higher sensitivity. The electronic detection rather than having the chemical detection for the analyte is an added advantage. The sensor is also compatible with CMOS with the possibility of on-chip integration, circuitry and microfluidic systems, direct electrical readout. With the conventional methods being limited to labelled proteins (time consuming) with optical detection techniques, using nanowire biosensor is advantageous.

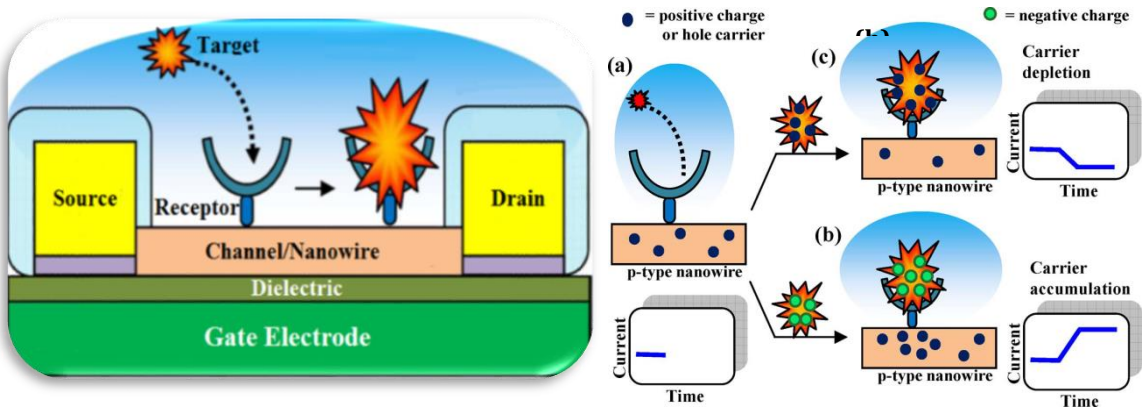

Figure 2.4: Silicon nanowire biosensor configuration and working principle (3)

The bridging nanowire between the source and drain of the transistor has its surface functionalized with a layer of specific receptors. These provide specificity to the sensor element for detection. The functionalisation of the nanowires was achieved through chemical bonding using bi-functional linker molecules, absorption, Van der Waals forces or weak electrostatic forces. The nanowire FET biosensor detects the presence of charged molecules in the immediate vicinity around the nanowire. With an electric potential applied externally between the source and the drain of the nanoFET, it is capable to modulate the number of free charge carriers within the semi-conductive material, this leading to a measurable change in electrical conductance. Sensitivity is measured in terms of change in conductance before and after binding of biomolecules to the receptor probes. Detection in the case of nanowire sensors are due to field effect and not by the change in capacitance as in the case of carbon nanotubes (CNT) (2-4).

Target analyte has to be closer to the sensor surface in order to effectively realize the conductance change. This is due to the electrostatic screening by the mobile charges (ions in the solution) in the vicinity of the analyte molecule. The fluid surrounding the NW sensor can significantly affect the sensor system (1). NanoFET sensors are label free since they recognize the change of electric field induced by biomolecules binding. However this is not feasible in physiological conditions due to screening. In this regard, the Debye length becomes important. The Debye length (λ_D) is the distance over which a charge *z* is shielded by the ions in a solution. Hence on decreasing the ion concentration in the solution the Debye length increases as shown in Figure 2.5.

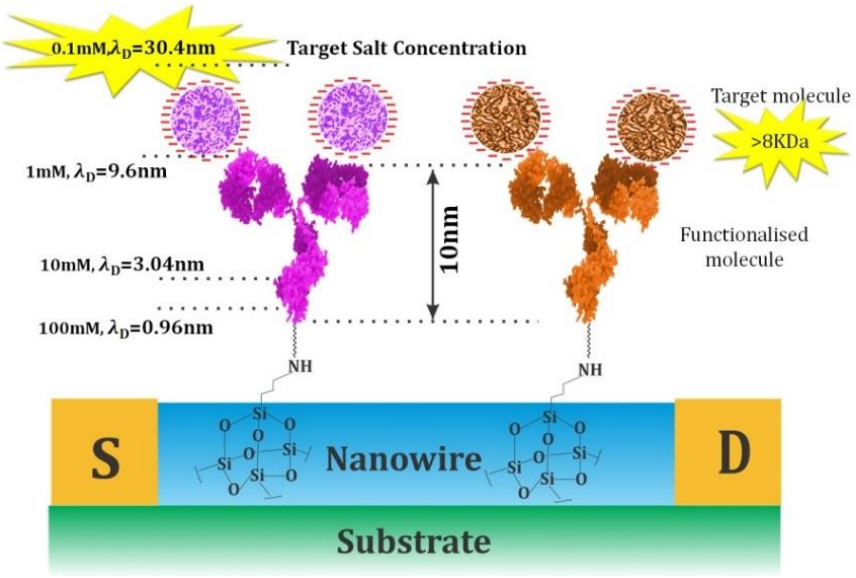

Figure 2.5: Importance of salt concentration and Debye length for the nanowire biosensor.

2.2 Conventional desalting strategy

Desalting of sample has been carried out for long by filtration and other techniques. However, these methods have some common problems. The volume of the sample and the buffer volume used in case of removing salt from the sample in any of the conventional method are quite large. Samples volume ranging from 200µL to 2mL are generally required and at the same time buffer volumes range between 100mL and 2000mL. Long-time duration such 24-48hrs are required to desalt a sample efficiently.

2.2.1 Size exclusion chromatography (SEC)

The size difference between the proteins and the low molecular solute such as salts makes it possible to select a gel filtration that will exclude the protein from the porous network while allowing full permeation of salts through them. Molecular separation occurs in the SEC column based on the stationary phase which consists of an inert gel of porous beads and a mobile phase which is the eluent of the liquid (sample) running through the column. The gel particles contain

pores of definite size with tunnels through which the molecules are separated depending on the size. The larger molecules bigger than the pores in the beads pass around the beads eluting first from the column. Followed by this, the medium sized molecules may find some pores in which they enter and spend some time and eluate second while the smaller-sized molecules have more pores that are accessible to them and therefore spend more time inside the pores eluting last.

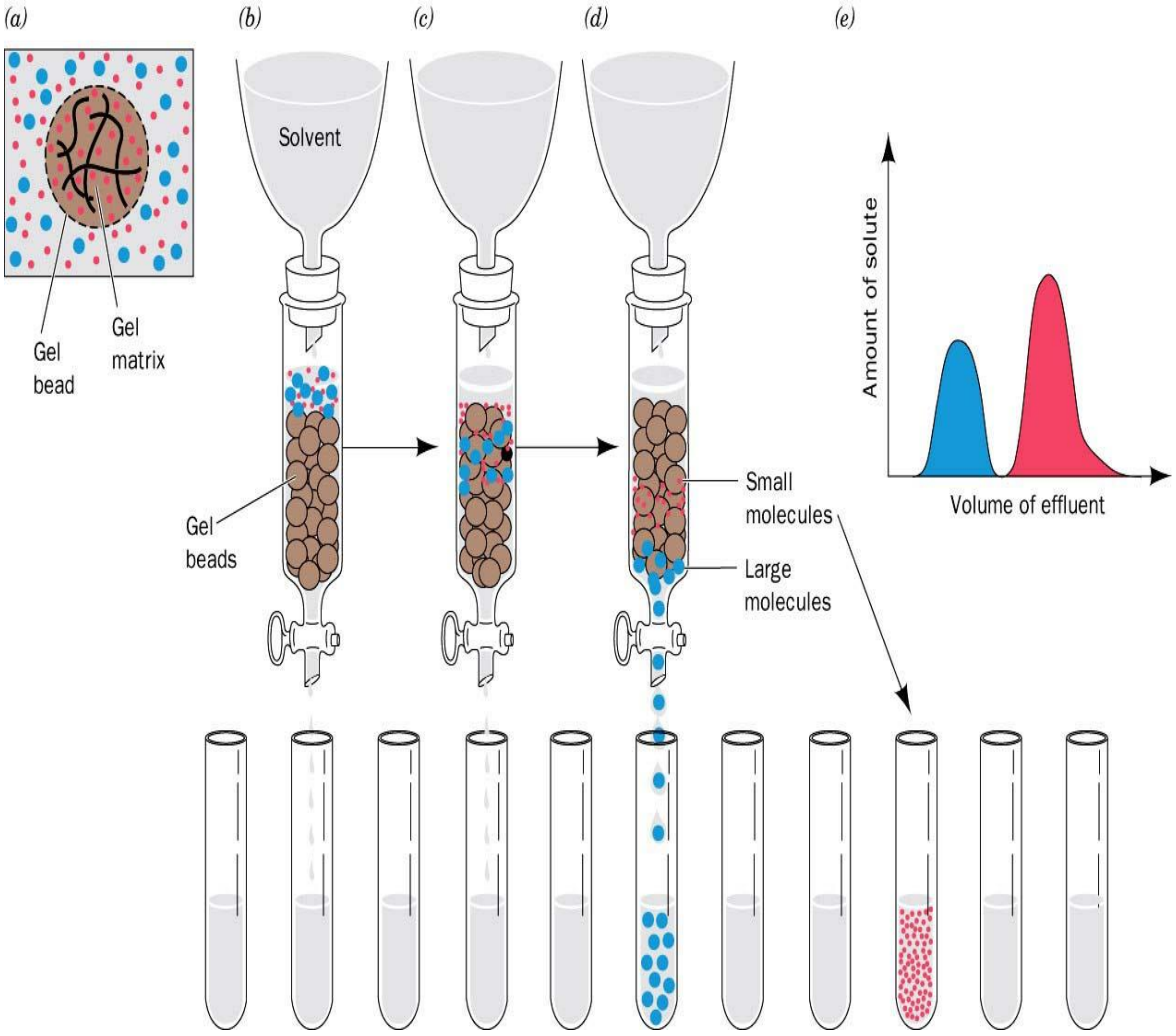

Figure 2.6: Mechanism of Size exclusion chromatography. (a) Shows the gel beads. Each beads has pores and a matrix within them through which smaller particles enter and elute slowly compared to the larger particles. (b) Applying the sample to the gel column containing a mixture of small and large molecules. (c & d) Larger molecules fails to enter the pores of the beads and elute first while the smaller particles enter and elute slowly. (e)Graph showing the detection of two different peaks corresponding to the eluted larger molecule eluted first and the smaller molecule that eluted later (23).

Size is a difficult parameter to accurately measure for a molecule as in the case of proteins due to their 3-D structure. Hence molecular weight is used to define the size of the proteins and the beads are classified based on the molecular weight cut-off (MWCO). Microns are a measure of a 2-dimensional distance and Daltons (Da) are a measure of 3-dimensional size based on atomic weight units, there is no direct conversion from one to the other. However the conversion chart shown in Figure 2.7 could be used to determine an approximate range. SEC is not a high resolution technique and requires high quality pumps for controlling flow rates. The

separation efficiency comes only from the stationary phase, hence for better separation an increased number of passes through the column or using long columns is necessary (24).

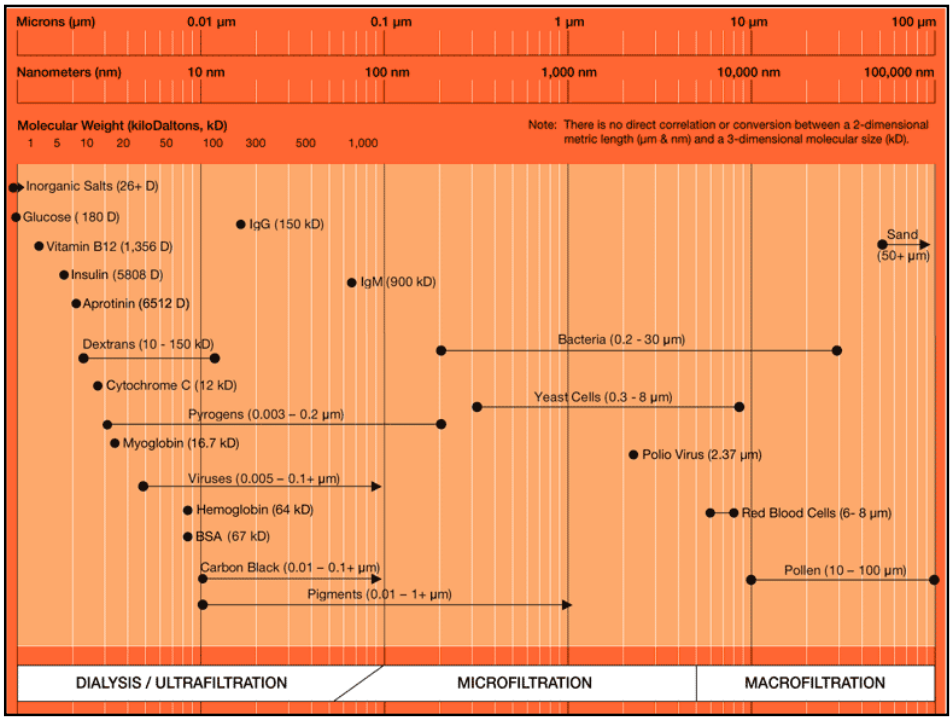

Figure 2.7: Conversion chart between MWCO & particle size (25)

The typical chromatographic beads used in most of the desalting can be seen in the Table 2.1.

Table 2.1: List of typical chromatographic beads available for desalting.

Material	Exclusion Limit	Particle size
Sephadex G-10	700Da	55-165µm
Sephadex G-15	1500Da	60-180µm
Sephadex G-25 Superfine	1000-5000Da	>20µm
Sephadex G-25 Fine	1000-5000Da	>20µm
Sephadex G-25 Medium	1000-5000Da	85-260µm
Sephadex G-25 Coarse	1000-5000Da	>100µm
Bio-Gel P-6DG polyacrylamide gel	6000Da	90-180µm
TSKgel BioAssist DS polyacrylamide gel	6000Da	15µm

Different desalting columns are commercially available. HiTrap desalting columns makes use of 5mL sample using a syringe or pipette is available from Agilent. Similarly GE Healthcare Life Science has marketed Disposable PD-10 Desalting columns (2.5ml) and also PD MidiTrap G-25 (0.5-1mL) both making use of Sephadex beads. Thermo Fisher Scientific provides Zeba Desalting Columns. Gravity based desalting columns as well as centrifugal based desalting columns are commercially available. In the case of the gravity column larger volume of the sample (2.5-4mL) is required and the desalting process is slower than the latter which uses sample of lower volumes (<1.75mL).

2.2.2 On-chip desalting using Size Exclusion Chromatography

Desalting of sample by SEC is generally carried out using beads packed in a column on microfluidic devices. Off-chip desalting has been reported widely. Recently Millet et al (26), show cased how SEC was employed for various applications. Cell lysate was purified using affinity chromatography, ion exchange chromatography and size exclusion chromatography for concentrating, desalting or separate molecules in the samples. Sephadex G-10 (27) and Sephadex G-25 (28) are the most commonly employed beads for desalting columns. Although the columns are capable of desalting microlitre volume of samples, it is important to note that for all application of protein purification, desalting has been carried out off-chip.

Figure 2.8 Commonly used Zeba desalting spin columns for desalting microlitre volume samples for mass spectrometry (29).

Desalting on chip is made possible by making use of surface-tethered octadecyl carbon chains (C18) by reversed phase chromatography (RPC). RPC uses a hydrophobic stationary phase for separation. In RPC, any inert non-polar substance capable of achieving a compact packing can be employed with octadecyl carbon chain (C18) bonded silica being the most popular column (30-32).

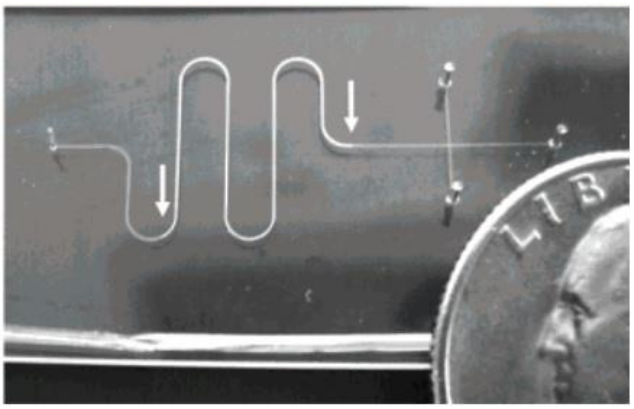

Figure 2.9: Reversed phase chromatography beads (C18) packed in microfluidic channel made of PDMS chip (30).

The same beads (~3-5µm) are available in C18 desalting tip which would bind peptides while allowing the salts to be washed off. Agilent macroporous reversed-phase C18 column (mRP-

C18) having unique silica-based C18 column packing. They have been shown to provide an optimized desalting of the human serum and concentrating it after the depletion of the high-abundance proteins using the Agilent Multiple affinity removal system. They are capable of reproducing the desalting efficiency at the same time recovering 99% of the protein in the sample. The mRP-C18 was used in most of the cases to desalt the sample. Columns with a flow of about 0.75mL/min, and a pressure limit of 250bar and a time frame of 13minutes was required for desalting/concentrating the sample (33). Although this being said, the desalting efficiency in most of the case of testing is not discuss as the prime importance is given to protein recovery.

SEC offers good desalting but at the same time offers few problems. Samples are diluted since they are collected as eluates from the column and not as a whole sample. Hence for detection of analyte of very low concentration in sample would be difficult. Another problem is that incorporating the principle of SEC onto a microfluidic chip. Most of the beads employed are polymer beads which swell in water. So having the beads in the microchannel and maintain its integrity would be difficult.

2.3 Filtration

Desalting of sample by filtration is another conventional technique for removing or purifying the sample and has been employed in various fields for a long time. Generally filtration is membrane separation process, allowing molecules to be retained or removed from the fluid depending on the separation mechanism. The membrane separation processes can be carried out either by using a pressure difference, electric field or by concentration difference.

2.3.1 Ultrafiltration, reverse osmosis

Reverse Osmosis and ultrafiltration are pressure driven separation mechanism suitable for aqueous low molecular mass solutions, macromolecular solutions, emulsions etc. Both the processes are capable of extracting the solvent from the solution to high efficiency. This being said, it is important to note that, the pressure required to drive this separation process varies between 10-100bar. In principle, reverse osmosis, is a membrane process with a high transmembrane pressure difference, in which a semipermeable membrane is suspended and a solution which is to be purified is on top of the membrane (Figure 2.10). Pressure is applied on the feed side of the membrane and molecules smaller than the pores in the membrane, the solvent generally water pass through, while the solute- the salts (ions), particles, colloids, organics, bacteria are held back on the membrane. During this process of solvent removal, the retained solutes collects on the feed side of the membrane forming a cake layer and its thickness increases with time while reducing the permeate flux. Cross flow filtration where an

incoming feed stream passes across the surface of a crossflow membranes is generally applied to overcome such cake formation (34; 35).

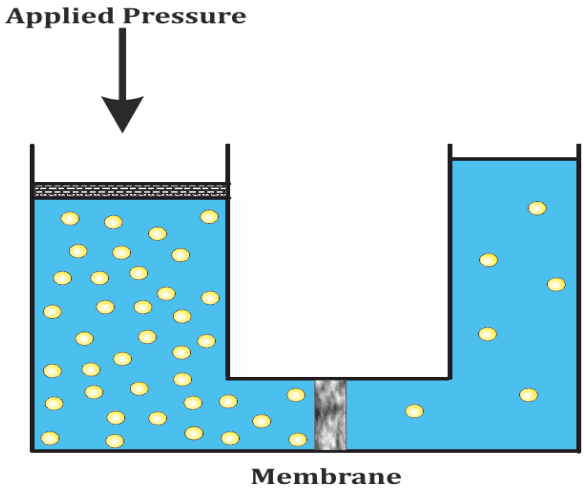

Figure 2.10: Principle of Reverse osmosis. Pressure is applied on one side of the sample to force the fluid through the membrane while restricting most of the macromolecules from passing through.

Reverse osmosis is applicable for purifying the water. Applying this method for purification of physiological sample would help in concentrating the target molecules on one side depending on the pores sizes of the membrane. But the complexity of having a high pressure to filter or concentrate the sample has made it difficult for RO to be employed in lab-on-chip application and hence difficult to realise it for microvolume RO.

2.3.2 Electrodialysis

Electric field is used as a driving force for separation in Electrodialysis compared to a pressure driven separation as in the case of RO or ultrafiltration. Electrodialysis is characterised by the use of ion-selective membranes and electric field applied orthogonal to the membranes. This separation method makes use of two membranes as opposed to one used in the previous method. The membranes used in this method of separation are ion selective as in anion- and cation-selective membranes placed alternatively between the anode and cathode as shown in the Figure 2.11. This is a single electrodialysis cell (34; 36). The ion-selective membranes are essentially sheets of ion-exchange resins and contain other polymers to improve mechanical strength and flexibility. Cation-exchange membrane would have a resin consisting of negatively charged groups (e.g., $-SO_3^-$) chemically attached to the polymer chains (e.g., styrene/divinylbenzene copolymers). Ions with a charge opposite to the fixed charge (counter ions) are freely exchanged at these sites (37).

Dialysis procedure is accelerated with an electric field. This method has the solution flowing between the two ion-selective semipermeable membranes. On applying an electric field, positive ions will travel towards the cathode and the negative ions towards the anode. This

leads to dilution or removal of ions in between the membranes while ions get concentrated next to the membrane. Multiple electrodialysis cells like the one shown in the Figure2.11 are used to form electrodialysis stack providing high purification of water.

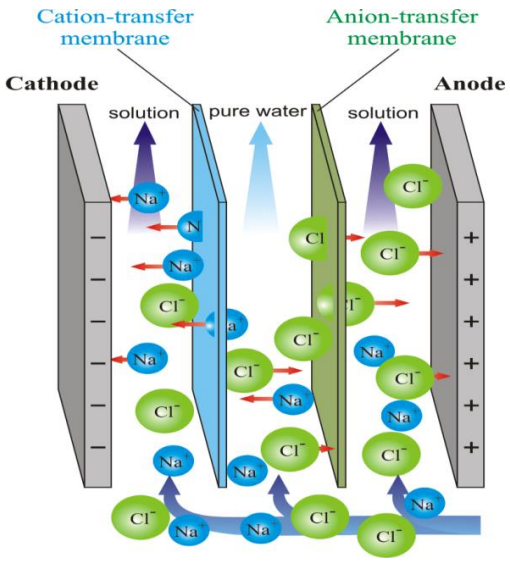

Figure 2.11: Working principle of Electrodialysis. Three compartment device with two ion selective membranes to remove the ions (38).

When extremely low salt concentrations are required, this method becomes less economical. Large membrane areas are an additional requirement to satisfy capacity requirements for low concentration feed solutions. Pre-treatment of the feed sample is another necessity in electrodialysis to remove species that coat or precipitate or foul the surface of the ion-exchange membranes. Fouling of the membranes reduces the efficiency of the separation process (35; 36; 39; 40). These membrane separation processes are commonly used for desalination of sea water or brackish water and commonly employed for macrovolume of feed solution or water. Scaling down these methods to suit microvolume membrane separation is also difficult using the above mentioned method. Employing two different membranes on-chip for microscale separation is also difficult. More importantly, when the feed is a physiological sample such as blood, it becomes increasingly difficult to separate or purify the sample using the methods mentioned above.

2.3.3 Dialysis

Dialysis is the movement of molecules by diffusion from high concentration to low concentration through a semi-permeable membrane. Molecules that are smaller than the pores present in the membrane are capable of diffusing through the membrane. Molecules larger than the pores present in the membrane will not diffuse through. The diffusion of the molecule will continue until equilibrium is attained between two concentrations on both sides of the membrane. Equilibrium condition is the point at which concentration of solutes on either side

of the membrane is equal. On attaining equilibrium in the system (in the entire volume), there is no further movement of the molecules across the membrane because molecules will be moving through the pores into and out of the dialysis unit at the same rate. Large molecules present on the side of the membrane during the start of the dialysis will remain on the same side as when the dialysis was initiated. In order to remove the small molecules furthermore, it would be necessary to replace the dialysis buffer so that a new concentration gradient can be established. However with the change in the buffer, movement of particles from high concentration to low concentration will again resume until equilibrium is once again reached. With each change of dialysis buffer, substances inside the membrane are further purified by a factor equal to the volume difference of the two compartments. By replacing the buffer just as the rate of diffusion slows down and the solutions are approaching equilibrium, the rate of dialysis can be improved or maintained. There are a number of factors that affect the completeness of dialysis includes *dialysis buffer volume*- large volume of the buffer facilitates increased diffusion of molecules across the membrane because of the higher concentration gradient; *buffer composition*- having a pure buffer containing no small molecules that would interfere with the removal of similarly sized particles (e.g. DI water for removal of salts) ; *the number of buffer changes*- this is also another important factor since it allows more volume of the buffer to come in contact the sample to be purified; *time*-the longer the time allowed for the buffer to be in contact sample to be purified, more molecules diffuse across the membrane; *temperature* – increase in the temperature will increase the kinetic energy enabling faster diffusion of molecules across the membrane and *particle size vs. pore size*- the size of the molecule to be removed from the sample should be comparable to the size of the pores present in the semi-permeable membrane. Substances that are very much smaller than the pore size will reach equilibrium faster than substances that are only slightly smaller than the pores. Convoluted pores allow small molecules to pass through the twists and turns of the pores with greater ease than do larger molecules. The greater the difference in molecular weight of the molecule to be removed vs. the molecular weight cut-off (MWCO) of the pore size, the greater the rate of dialysis since it is easy for the molecule to pass through.

The rate of dialysis is also directly proportional to the surface area of the membrane and inversely proportional to the thickness of the membrane. Though the liberty of changing the membrane thickness is limited, it is possible to improve dialysis by changing the surface area of the membrane. If the volume of sample can be spread over a membrane, increased rate of dialysis would be seen. This is because all the molecules in the sample are closer to the membrane and can diffuse easily. The thickness of the membrane also has a key influence on the rate of diffusion of molecules across the membrane. A thin membrane would mean the samples are very much closer to dialysis buffer and molecules can be removed faster.

2.3.4 Haemodialysis

One membrane separation process which has been successful in filtering complex samples such as blood is dialysis. Haemodialysis has proved to be an exceptional method to remove waste products from blood. Most of the common haemodialysis setup employs a hollow fibre membrane or a collection of hollow fibre membrane which is enclosed in cylindrical tube. The blood flows inside the membrane while the dialysate flows around them facilitating removal of waste products such as urea, creatinine, potassium etc. from blood. Typically the flow rates are quite high in these devices and at the same time uses large volume of blood and dialysate (41; 42).

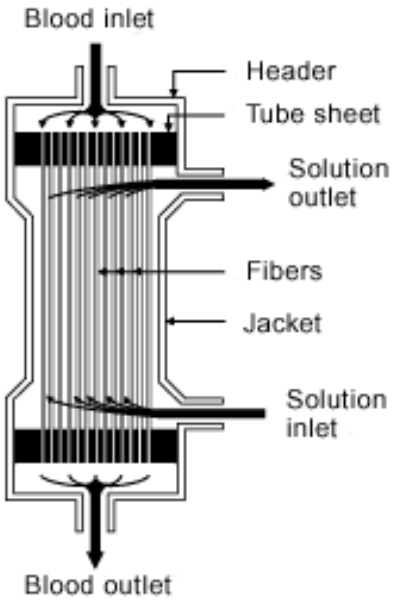

Figure 2.12: Haemodialysis. Commercially available blood purification system (43).

2.3.4.1 Dialysis tubing

Dialysis can be performed based on the conditions of the sample and buffer that are present. The traditional practice of performing dialysis is based on using a semipermeable membrane bag or tube which contains the sample that is to be dialysed. This is then suspended in a large tub or beaker containing buffer/water (~600-1800mL). The setup is then left for a long period of time (24-48hrs) during which the particles of interest are either removed from the bag or retained with in it. In this traditional practice, the key point to note is that the entire set up is in static mode. This would mean that the process of molecules being removed from the sample is purely based on diffusion and so is the movement of the removed particle within the water. This is a type of *no-flow device.* In this method, the dialysis slows down gradually over the course of time. When the low molecular weight solutes diffuses into the buffer, they form a microenvironment termed as Nernst diffusion layer near the surface of the membrane. This region is about 200-300 molecules thick and the small molecules are at a higher

concentration in relation to the rest of the dialysate. This would effectively slow the rate of dialysis because now molecules can re-enter the dialysis membrane pores and return to the sample.

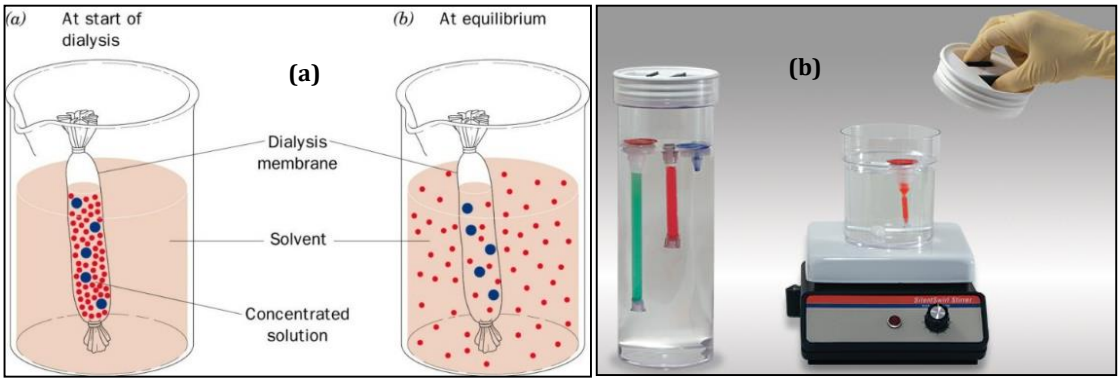

Figure 2.13: Conventional dialysis. (a) Mechanism of dialysis. (b) Spectro/Por dialysis kit with static set up and Spectro/Por dialysis kit with buffer stirred (44).

In order to overcome this problem of thin Nernst diffusion layer, introducing a flow or stirring would improve the dialysis mechanism (45). Commercial suppliers provide a number of dialysis tubings of various MWCO depending on the requirements. The typical lengths of the dialysis tubings are about 1m with a flat diameter 6-20mm which might be cut to required size for different applications (46). Some suppliers, including Spectrum labs, also offer equipment for dynamic dialysis.

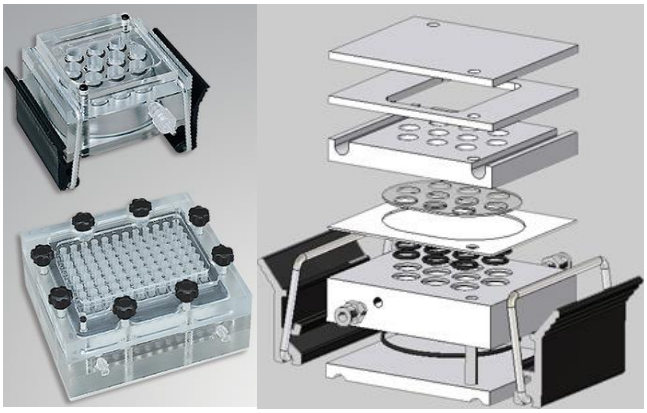

Figure 2.14: Commercially available rapid dialysis of micro-volume samples from Spectra/Por MicroDialyzers. Capable of simultaneous dialysis of multiple micro-volume samples. The dialysate chamber is capable of accommodating magnetic stir for agitation in static mode or using a luer fitting for a circulation of a larger buffer volume to maintain a more effective concentration gradient in dynamic dialysis. Typical sample volumes ≥100µL (47).

The one-flow design makes use of either having the sample in flow or the buffer in motion. But in most cases buffer in motion is commonly used. This would enable the sample to be more in contact with the buffer and carry away molecules that has diffused into the buffer. Using a cross-flow design would further improve the dialysis, since both the sample and the buffer are in motion.

2.3.4.2 On-chip dialysis

The increasing demand for the capability to handle small sample volume with high throughput and less time has directed research into miniaturisation of analytical instrumentation. On-chip dialysis offers numerous advantages compared to the traditional dialysis techniques. They offer much reduced sample volume consumption (~5-100 μL), less buffer volume consumption (>50mL). Another important factor that is greatly advantageous is the time required for the process which is very short compared to the former method and the size of the device required for carrying out the operation.

With diagnostic devices and other biomedical applications requiring small volumes and faster testing time, numerous method of desalting the sample by on-chip microdialysis has been carried out. Most of the work reported so far, was intended on the removal of the salt interfering with mass spectrometry analysis. The on-chip microdialysis device is composed of either having a planar membrane sandwiched between two microchannels or having a hollow fibre membrane enclosed in a tube.

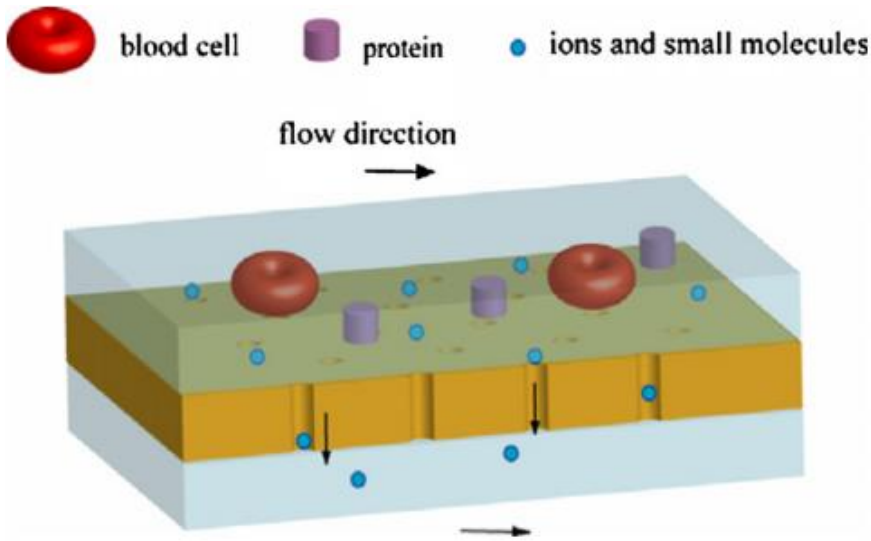

Figure 2.15: Microdialysis across a membrane. Pores present in the membrane allow ion molecules to pass through while blocking the passage of larger molecules like blood cells and proteins (48).

2.3.4.3 Hollow fibre membrane dialysis

The first hollow fibre for dialysis was clinically used in artificial kidney in the 1960s and consisted of a 1.0m^2 unmodified cellulosic membranes. Most of the hollow fibres have an inner diameter 180-220μm and length 20-24cm. A relatively small hollow fibre with smaller inner diameter is desirable because it provides a short diffusive distance for the solute mass transfer (49). Hollow fibre module of dialyser typically takes its principle from the commercially available blood purification system which has numerous dialysis fibres densely packed in them for high throughput. Researchers have taken individual fibres of smaller sizes in order to carry out microvolume purifications of the sample.

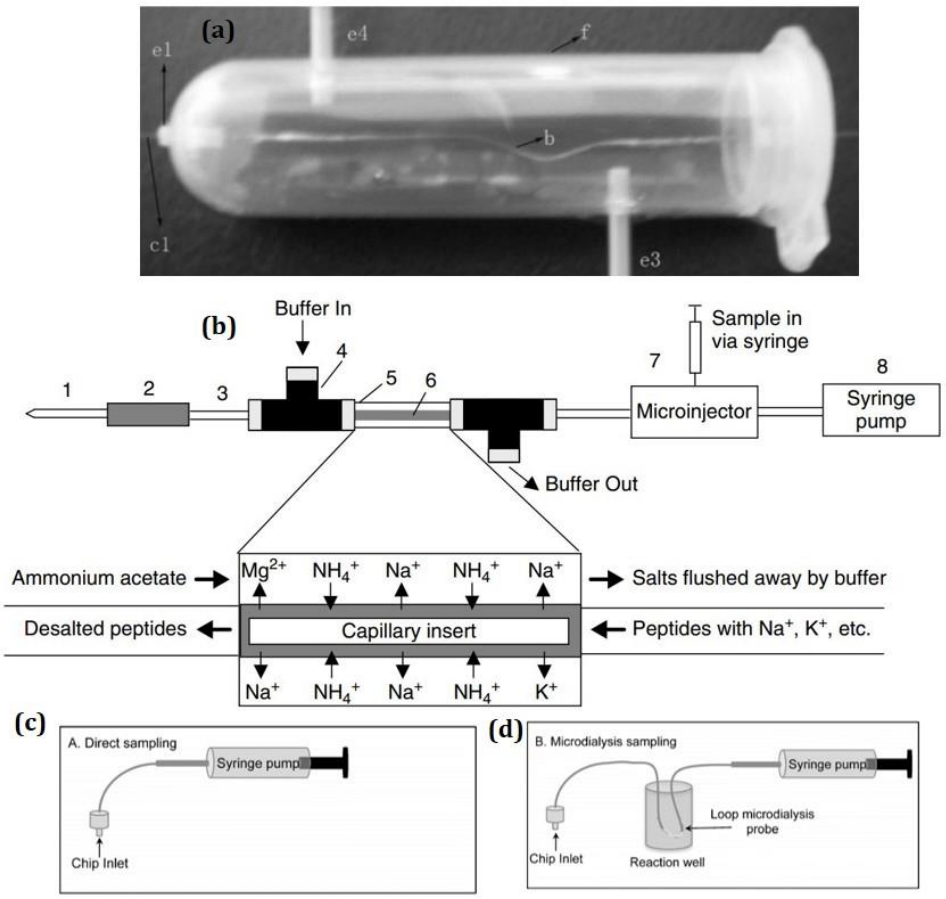

Figure 2.16: Schematic of the microdialysis using hollow fibre membrane. (a)Sun et al., b-hollow fibre membrane of MWCO-3kDa, c: capillary; d: epoxy glue; e: Teflon tube; f: centrifugal tube (2mL) (50). (b) Jakubowski et al., (1) Taper Tip, (2) grounded metal union, (3) fused-silica capillary, (4) Tee connecting buffer inlet, (5) Teflon tubing, (6) hollow fibre membrane with MWCO-13kDa inside Teflon tubing, (7) microinjector used to inject 1- µl samples, and (8) syringe pump with flowing solvent. The inset illustrates the exchange of cations occurring across the dialysis membrane (51). (c & d) Off chip dialysis with a membrane having a MWCO-30kDa was used in microdialysis of sample in the works of Scott et al (52).

Sun et al., has made use of a hollow fibre membrane of cellulose acetate (MWCO 3000 Da) to perform microdialysis (50). Microdialysis of small volume of less than 1µL is made possible using hollow fibre membranes. In the set up reported by Sun et al., the fibre was enclosed in an eppendorf, which had a counter flow arrangement accelerating the dialysis. Dialysis of the sample was done within 1min and the device maximum desalting. Salt concentration of 100mM and 1M having a flow rate of 1µL/min with a buffer flow rate of 1.3mL/min and 3.9mL/min yielded a desalted sample of about 1.3mM and 2.7mM. Another result that is of considerable importance is the effect of buffer flow rate which can be understood from the report. Desalted samples had low salt concentration in the cases where the buffer flow rate was high and the amount of salt removed from the sample increases with the increase in the flow rate of the buffer. Earlier to this work, Jakibowski et al. also showed microdialysis but made use of a membrane of much higher molecular weight cut-off 13kDa. The set up can been in Figure 2.16 (51). Liu et al, also showed a similar method of dialysis for mass spectrometry with a 13kDa membrane made of regenerated cellulose (20cm x 216µm o.d. x 200µm i.d.) from Spectrum Labs (53). With counter current flow to be set up, flow rates

of 2-5μL/min for the sample and 300μL/min for the dialysis buffer was chosen. Further, the work also reports that with higher flow rate (10μL/min) of the sample desalting was incomplete and significant sodium peaks were seen in the mass spectrum. Canarelli et al., also made use of one such membrane to carry out the dialysis (54).

2.3.4.4 Sandwiched membrane dialysis

The sandwiched membrane device forms one of the basic method of realising on-chip dialysis. The device consists of a semipermeable membrane sandwiched between a sample channel and a buffer channel (55). Dual microdialysis with two dialysis membrane of different MWCO (100kDa & 50kDa) sandwiched between three polymer layers micromachined with serpentine flow channels was reported by Xiang et al as shown in Figure 2.17d. The serpentine channels were fabricated on 30x30x6mm chip using laser. Poly carbonate track etch membrane of 100nm pore size was reported to be used in glucose dialysis (56; 57; 58). Polyethersulfone (PES) is another type of membrane that is commonly employed. PES membrane has been sandwiched between PDMS using clamps with two channels and depending on the pore size of the membrane, it is possible to remove various particles (59; 60). An artificial kidney microchip using PES membrane on PDMS was designed by Ould-Dris et al. (61) They have shown the separation of molecules of different weights (40k-500kDa) with concurrent flow where the sample and the buffer flow in the same direction.

Xu et al. designed a sandwiched device for microdialysis for mass spectrometry. This was achieved by making use of a Spectra/Por Biotech 1.1 dialysis membrane with a molecular weight cut-off (MWCO) of 8000Da sandwiched between two micromachined serpentine channels. One of the channels is bigger (500μm) containing the buffer at a flow rate of 100μL/min while the other is smaller (200μm) for the sample with a slower flow rate of 0.5μL/min with counter flow arrangement. The channels where micromachined on polymide sheets rather than being made from PDMS. The results from the mass spectrometry analysis in Xu et al, as shown in the Figure 2.17e&f showed more than 20-fold increase in S/N (62). A hydrophobic poly (vinylidene difluoride) membrane was used by Lion et al., for on-chip proteins sample desalting for mass spectrometry (63). Lion et al constructed a device as shown in Figure 2.17c in which the salt solution was pumped through the membrane at 0.2μL/min to 5μL/min. When the desired volume of the sample was pumped through the membrane, salts are washed out by pumping DI water with the same flow rate as before. The reported work was intended for sample clean-up for the application in electrospray ionisation mass spectrometry and hence no clear value on the desalting efficiency was mentioned. The effect of varying the sample flow rate was briefly reported by George et al (64).

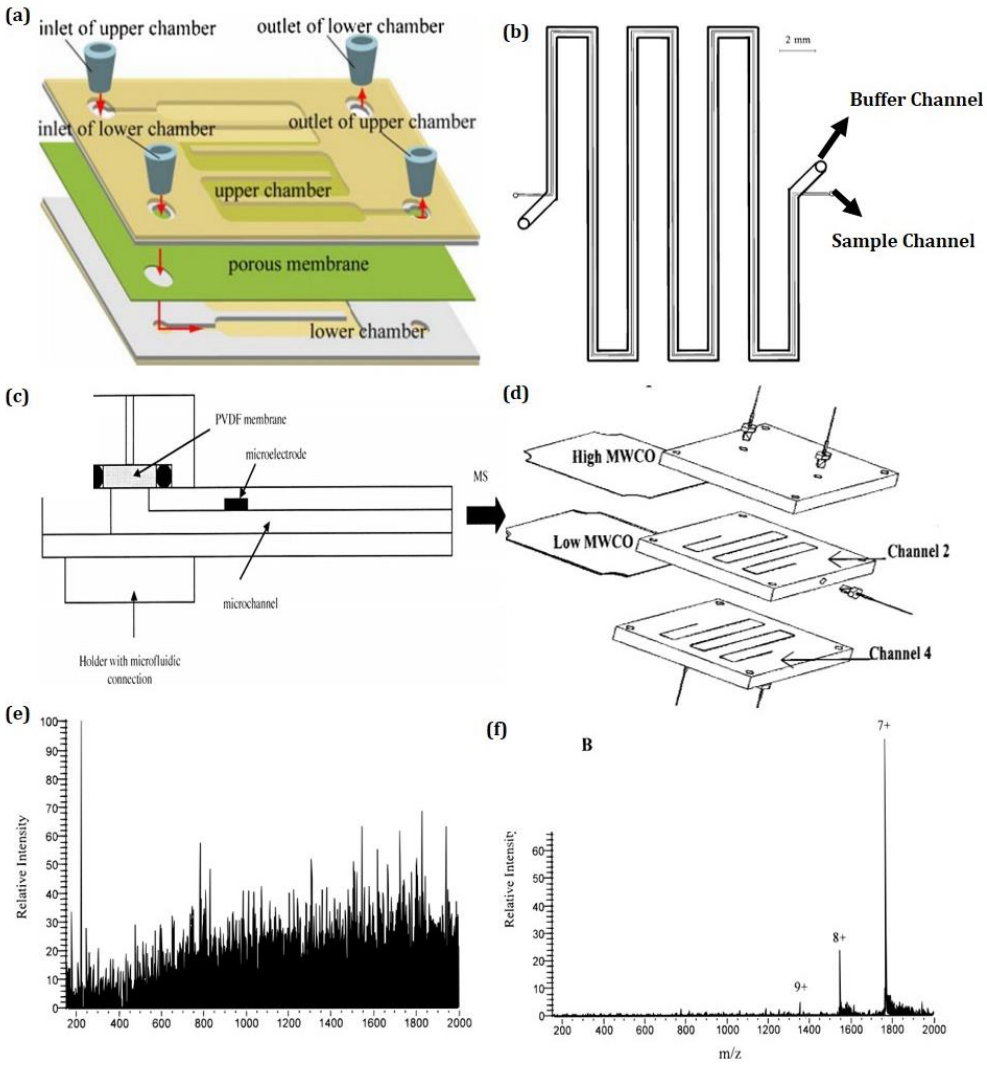

Figure 2.17: Schematic of the sandwiched membrane based dialysis. (a) Ye Gu et al, bonded two pieces of fluidic chips fabricated using PDMS with layers designed on it to the PES membrane (MWCO-4800Da) using PDMS glue. Sample flowed in the upper chamber while the pure water flowed in the lower chamber (59), (b) Xu et al., had a microdialysis membrane (MWCO-8KDa) sandwiched between two chips having a micromachined serpentine channels with a cross flow arrangement (62) (c) Lion et al. made use of a PVDF membrane sandwiched between a microchannel reservoir and a fluidic connection to carry out the dialysis (63)and (d) Xiang et al showed dual microdialysis setup comprising of two membrane of different MWCO sandwiched between three polymer layers micromachined with serpentine flow channels (55) (e &f): ESI-mass spectrum before and after dialysis using Xu et al's arrangement. 20 fold S/N improvement is seen (62).

Most of the work reported so far on chip-based dialysis, have been used for removing the salt that would interfere with the mass spectrometry analysis. Most of the research work on desalting for MS applications do not quantify the desalting performance, but it is known from the MS literature that a salt concentration of 10mM or lower should be obtained for proper analysis. This being said, it is also clear from the information provided here that, it is easy to construct a sandwiched dialysis device which would form the first base for experimentation later on.

Similar principle can be employed in different application than just desalting by varying the type of membrane employed. The effect of varying the sample flow rate was briefly reported by George et al (64). A microdialysis chip in which cellulose acetate film was created using the

phase separation process and suspended over silicon microchannels fabricated with the cleanroom microfabrication equipment. The feed side (sample) of the membrane had fluorescein (MW-332Da) while the other side had buffered saline perfusate creating a concentration gradient. The concentration gradient drove the fluorescein molecule across the membrane. By varying the flow rate and fluid volume, the concentration of the collected dialysate was varied as in Figure 2.18. It can be noticed that with increase in the flow rate, fluorescein concentration decreases.

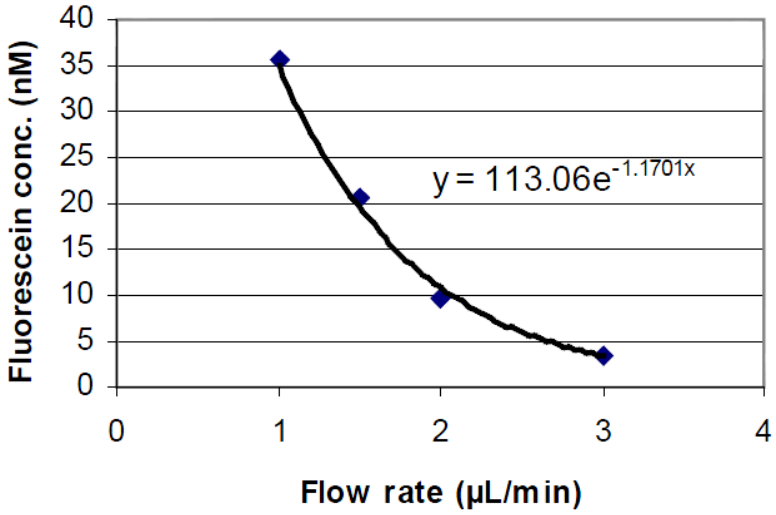

Figure 2.18: Plot showing the permeability of cellulose acetate membrane to 62nm Fluorescein solution for various flow rates [55]

Hsieh and Zahn reported an On-chip microdialysis intended for glucose sensing using a PDMS sample channel and a SU-8 perfusion flow channel sandwiching a polycarbonate track-etch membrane as the microdialysis membrane (57). The importance of the flow rate in case of the perfusion channel or the buffer channel was clearly noted as in Figure 2.19.

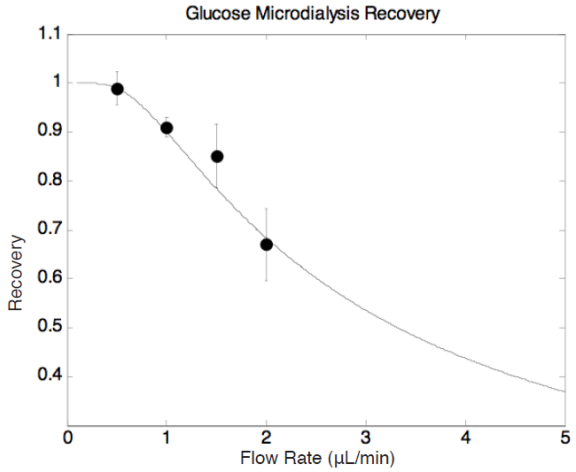

Figure 2.19: Glucose microdialysis recovery as a function of perfusion flow rate (57).

From the two works mentioned, one important conclusion can be deduced. Recovery of target solute is high at slow flow rate of the sample containing the solute and increasing sample flow rate, the recovery decreases.

Song et al (65) designed a low MWCO and a high MWCO microdialysis system by using a novel method for in situ photo-patterning of porous polymer. A counter flow microdialysis system with MWCO- 5700Da was fabricated in a 5-mm long microchannel by patterning membranes in the middle of the microchannel to separate the sample (top) and perfusion (bottom) flows. The result of using a counter flow dialysis configuration can be seen from the Rhodamine 560 concentration in the sample channel decreases along the flow.

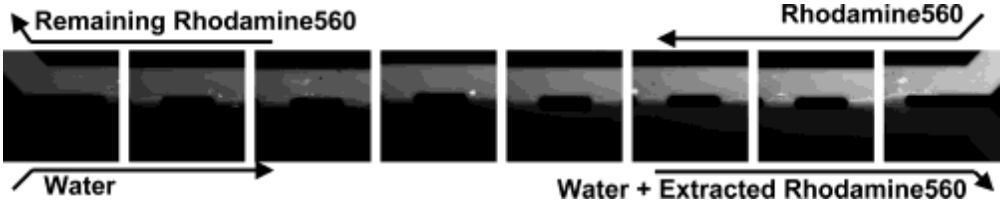

Figure 2.20: Rhodamine 560 extraction in a counter-flow dialysis configuration with the low MWCO membrane (65).

Figure 2.20 shows that Rhodamine560 is removed considerably at the water inlet. At the water inlet, the concentration gradient between the sample containing Rhodamine and water without it is high.

Kurita et al (66) showed how a thin dialysis membrane with double flow channels was used for measuring blood samples. Clearance or removal of solutes of different molecular weights were investigated by Eloot et al. using a combined dialyzer flow configurations (67). Sheng et al. (68) showed how using a nanoporous membrane in a PDMS microfluidic device was helpful in selecting the size of DNA using a counter-flow arrangement.

2.4 Summary

Biomarkers detection using advanced diagnostic tools such as mass spectrometry and nanowire field effect transistors requires samples to be desalted prior to testing. Physiological concentrations of salt ions result in the formation of a large number of different salt adduct protein segments in mass spectrometry and, for nanoscale field effect transistors, in a Debye length that is too short for the nanowire surface to experience a change in charge density upon biomarker binding. A number of conventional macroscale desalting strategies have been highlighted in this chapter. Size exclusion chromatography is an easy method of desalting by selecting gel/resin of appropriate MWCO to sort the target from the sample mixture. Filtration schemes using membranes with different driving forces – pressure driven, electric field, concentration gradient are also possible. However, employing these methods on-chip for

microvolume desalting is complicated. Dialysis is the easiest method that has already been employed on microscale (on-chip). Dialysis using a semipermeable membrane is either designed by suspending the membrane in a tube or sandwiching it between plates containing microchannels to make up a dialyser. Some examples of microvolume desalting using dialysis have been given, with an emphasis on the influence of flow rate on dialysis performance. In the next Chapter, the theory about mass transfer by dialysis over a semi-permeable membrane will be addressed.

Chapter 3: Dialysis theory

This Chapter focuses on analysing the performance of a dialysis device. The first section discusses diffusion, the key principle of dialysis. The basic formula underlying diffusion, – Fick's Law, is explained with a reference to the importance of the concentration gradient which is the driving force in the case of dialysis. With the basic idea of the dialysis device introduced in the previous chapter, the project look to investigate the theoretical performance for a device based on several assumptions. The concept of the Reynolds number and its influence on the flow conditions of the fluid in the microchannel is also highlighted. Prediction of dialysis/desalting efficiency is not straightforward and requires consideration of the mass transfer coefficient and the mass transfer rate over a semi-permeable membrane. The discussion on the performance parameters of the device will be based on the principles of a parallel plate dialyzer.

3.1 Fick's laws of diffusion

The principle force behind dialysis is diffusion of molecules across a semi-permeable membrane form a region of high concentration to a region of low concentration. A number of works on quantifying the efficiency of dialysis has been reported. The key principle and factors involved in dialysis are explained below.

Molecules are constantly in a random motion due to collision with the other molecules. Mass transfer is a physical process, which involves the transport of molecules within a system. The driving force behind this transfer is a difference in the concentration of a given molecule between two regions. Diffusion is the process that allows ions or molecules to move from a region of high concentration to a region of low concentrations. In biological cells, this process accounts for the transport of many different molecules across a cell membrane for metabolism or signalling (69). The movement of molecules i.e., diffusion continues until the molecules are equally distributed and the concentration of the molecules becomes the same throughout the area that contains them. Molecules of different sizes can be separated by diffusion by making use of a semi permeable membrane with an appropriate pore size. A solution (retentate or sample phase) containing different sized molecules of higher concentration on one side of the membrane and the other side with significantly lower concentration of these molecules or no molecules at all (dialysate or water/buffer phase) would facilitate the diffusion of molecules smaller than the membrane pores (70).

Diffusion can be expressed mathematically using Fick's law as

$$J = -D\frac{dc}{dx} \qquad \textit{Equation 3.1}$$

J is the diffusion flux (mol/m²s) or rate of mass diffusion, D is the diffusion coefficient (m²/s), $\frac{dc}{dx}$ is the change in concentration across the distance.

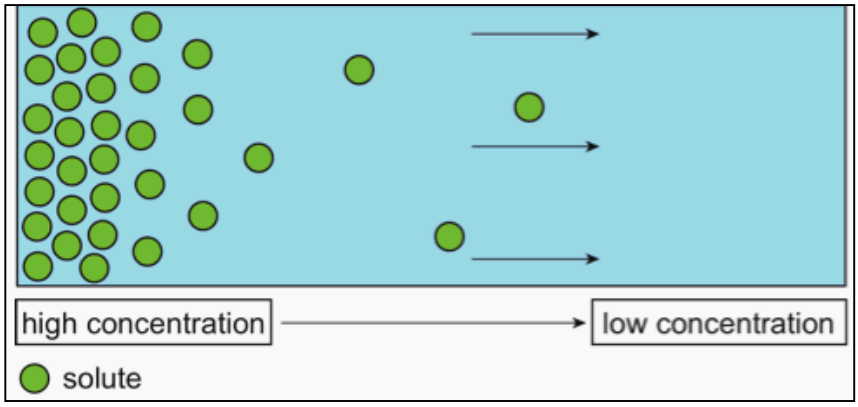

Figure 3.1: Definition of Fick's Law. Solute moves from a region of high concentration to low concentration.

Diffusion coefficient 'D' is a proportionality constant between the molar flux due to molecular diffusion and the gradient in the concentration of the species and is given by

$$D = D_o e^{-\left(\frac{E_A}{kT}\right)}$$

Where D is the diffusion coefficient (m² / s), D_0 is the maximum diffusion coefficient (at infinite temperature; m² / s), E_A is the activation energy for diffusion in dimensions of (J atom^{-1}), T is the absolute temperature (K), k is the Boltzmann constant.

The rate of diffusion may be affected by the steepness of the concentration gradient. The higher the concentration gradient between two region, faster the diffusion of molecules from high to low region. At the same time, the diffusion is also limited by the neighbouring particles which might block the pores in the semi-permeable membrane across which the diffusion occurs. The permeability of the membrane to the diffusing substance is also an important parameter that affects the rate of diffusion. Apart from the permeability of the membrane, the surface area of the membrane is also directly proportional to the rate of diffusion. Diffusion is also dependent on the thickness of the membrane. Diffusion across a thick membrane will be rather slow than across a thin membrane. This is because of the movement of the particles through a large area within the membrane. Temperature also plays an important role in the rate of diffusion due to the kinetic energy. Increase in temperature would increase the diffusion. The rate of diffusion is directly proportional to the concentration of the molecule while inversely proportional to its molecular weight (71).

Fick's first law gives the relation between flux of the material across a given plane which is proportional to the concentration gradient across the plane. Fick's second law also consider

the fact that the gradient and local concentration of the impurities in a material decreases with an increase in time. Fick's second law is represented by the following equation

$$\frac{dc}{dt} = D\frac{d^2c}{dx^2} \qquad \textit{Equation 3.2}$$

Where c is the concentration in (mole/m^3), t is time(s), D is the diffusion coefficient (m^2/s), x is the position (m).

3.2 Peclet Number

Peclet number (Pe) is a dimensionless number which defines the ratio of the rate of advection of a physical quantity by the flow to the rate of diffusion of the same quantity. In context of mass transfer Peclet number is given as a product of Reynolds number (Re) and Schmidt number (Sc).

$$Pe = \frac{Advective\ transport\ rate}{Diffusive\ transport\ rate} = \frac{Lu}{D} = Re_L Sc \qquad \textit{Equation 3.3}$$

Where L is the characteristic length, u is the local flow velocity and D is the mass diffusion coefficient.

3.3 Reynold's number (Re)

Diffusion of solutes in a channel can be dependent on the flow conditions in a channel. The flow regime of a fluid in a microfluidic channel can be defined and characterised by Reynolds number (Re). The number is a ratio between inertial forces to the viscous force and is capable to classify the fluid flow into laminar flow or turbulent flow (Figure 3.2).

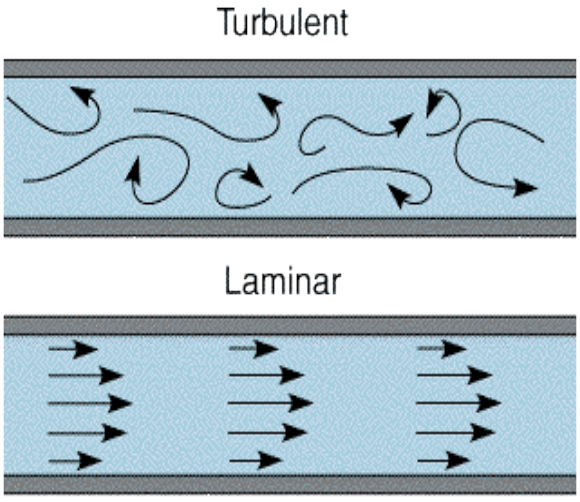

Figure 3.2: Flow regime in microfluidic channel (72)

Reynolds number is defined as

$$Re = \frac{\rho v D_h}{\mu} = \frac{v D_h}{\omega} = \frac{Q D_h}{\omega A} \qquad \textit{Equation 3.4}$$

Where

D_h is the hydraulic diameter of the pipe; its characteristic travelled length, L, (m), Q is the volumetric flow rate (m^3/s), A is the pipe *cross-sectional* area (m^2), υ is the mean velocity of the fluid (SI units: m/s), μ is the dynamic viscosity of the fluid (Pa·s or N·s/m^2 or kg/(m·s)), ω is the kinematic viscosity ((m^2/s), ρ is the density of the fluid (kg/m^3).

The hydraulic diameter of the pipe can be obtained from the following relationship

$$D_{h=}\frac{4\ x\ Area\ of\ the\ channel}{Perimeter} \qquad \textit{Equation 3.5}$$

In case of using a rectangular channel of height '*h*' and width 'ω' the hydraulic diameter is given by

$$D_{h=}\frac{2h\omega}{h+\omega} \qquad \textit{Equation 3.6}$$

At low Reynolds number, the viscous forces are dominant in the microchannel, laminar flow occurs in the channel characterized by smooth constant fluid motion. When the flow is dominated by the inertial forces which are at high Reynolds number, turbulent flow is seen in the channel which produces chaotic eddies, vortices etc. (73; 74).

3.4 Schmidt number

Schmidt number defines the ratio between viscous diffusion rates to the molecular diffusion rate and is given by

$$Sc = \frac{Viscous\ diffusion\ rate}{Molecular\ diffusion\ rate} = \frac{\mu}{\rho D}$$

Where μ is the dynamic viscocity of the fluid (Pa.s or kg/m.s) , ρ is the density of the fluid (kg/m^3) and D is the mass diffusivity or diffusion coefficient (m^2/s).

3.5 Single parallel plate dialyser

Diffusion can be analysed in two ways. The first using the diffusion coefficient from the Fick's law mentioned above and the second by making use of the mass transfer coefficient (MTC). Analysis of dialyzers has been reported in many research papers (42, 61, 75-80). These papers generally use the mass transfer coefficient which is commonly given by the dimensionless

number –Sherwood Number (Sh). Mass transfer rate can then be determined by using the mass transfer coefficient as reported by Yeh et al (81- 89). Mass transfers for dialysis coupled with uniform and non-uniform ultrafiltration fluxes in a cross-flow membrane module had been reported (83). A similar method is used in this thesis, in order to analyse the dialyzer.

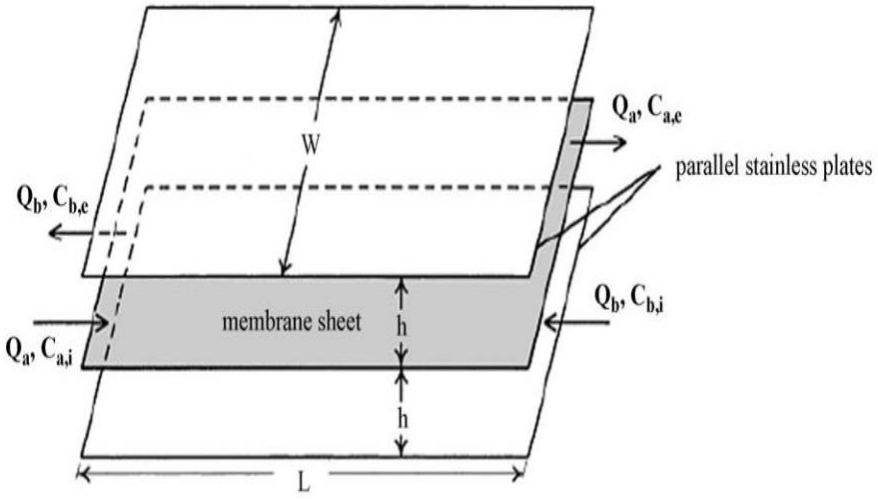

Figure 3.3: Single pass parallel plate dialyzer with counter current flow having the membrane sheet inserted between two parallel plates. (89)

A mass balance for solute over a single-pass mass exchanger (Figure 3.3) operated with flow rates Q_a and Q_b. Q_a and Q_b are the flow rates of sample and water compartment. $C_{a,i}$ and $C_{b,i}$ are the inlet concentration of the sample and the water. $C_{b,i}=0$ since the inlet concentration of the DI water is assumed as zero. $C_{a,e}$ and $C_{b,e}$ are the outlet sample and water concentrations.

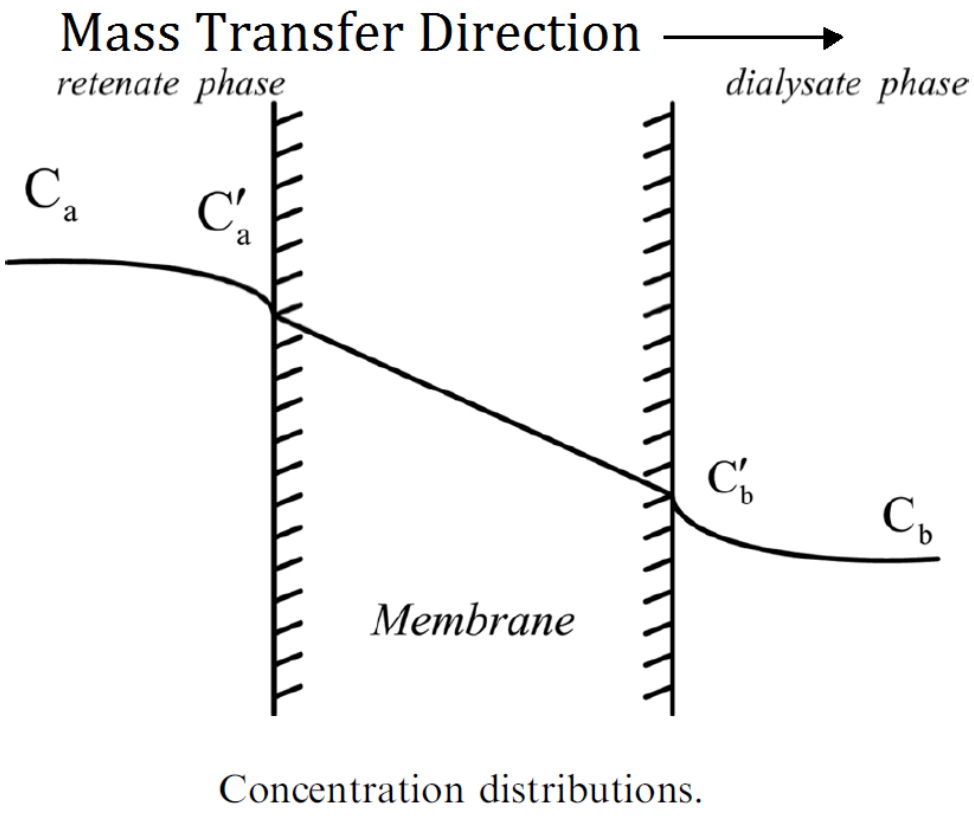

Figure 3.4: Schematic diagram of membrane dialysis different phases in a dialyser for mass transfer analysis (83)

From the schematic of the membrane dialysis (Figure 3.4), three phases can be seen in the in the system. Feed side or the sample side which is phase 1, in the membrane is phase2 and in the water side or the perfusate side is phase 3. The assumptions made in the analysis are as follows: steady state, no chemical reaction, and uniform concentration over the cross section of flow, constant rates of flow, constant distribution coefficient and constant physical properties of the fluid.

3.5.1 Mass transfer co-efficient (MTC)

Analysing diffusion with mass transfer coefficients requires assuming that changes in concentration are limited to a small part of the systems near its boundaries. MTC is commonly used in the study of diffusion when the diffusion occurs across an interface. MTC is used to describe the ratio between the actual mass flux of a species into or out of a flowing fluid and the driving force that causes that flux. In other words, the MTC is a diffusion rate constant that relates the mass transfer rate, mass transfer area and the concentration gradient as driving force. The mass transfer coefficient determines the rate of mass transfer across a medium in response to a concentration gradient. It is an important principle in chemical engineering and fluid dynamics. It depends on the relevant physical properties of the fluid, the geometry used along with relevant dimensions, and the average velocity of the fluid in cases of flow. The mass transfer coefficient can be written as

$$k = \frac{M}{A\Delta C} \qquad \textit{Equation 3.7}$$

where M is the mass transfer rate(mol/s), A is the effective mass transfer area(m^2), ΔC is the concentration gradient (mol/m^3) and k is the mass transfer coefficient (m/s)

Kolev and Linden reported the importance of the term in one of their works. Under steady state conditions the performance of a parallel-plate dialyser is determined mainly by the values of its mass-transfer coefficient (90). The dimensionless version of mass transfer co-efficient is the Sherwood number Sh. For laminar flow in a thin rectangular channel, the “film-theory” mass transfer coefficient (k) may be related to the Sherwood number through the following equation (75).

$$Sh = k\frac{d_h}{D} = 1.62\left(ReSc\frac{d_h}{L}\right)^{\frac{1}{3}} \qquad \textit{Equation 3.8}$$

Where Re is the Reynolds number (dimensionless), Sc is the Schmidt’s number (dimensionless), k is the mass transfer coefficient (m/s), D is the diffusion coefficient (m^2/s), L is the channel length (m), d_h is the channel hydrodynamic diameter (m).

by expanding the individual components and rearranging, the mass transfer coefficient (48) can be given as

$$k = 0.816\left(\frac{6QD^2}{W_c{H_c}^2 L_c}\right)^{\frac{1}{3}} \qquad \textit{Equation 3.9}$$

Where Q is the feed flow rate (m^3/s), D is the diffusion coefficient (m^2/s), W_c is the width of the channel (m), H_c is the channel height (m),L_c is the length of the channel(m)

The above equation is used to obtain the value of mass transfer coefficient in a rectangular channel. In the case of the membrane, the mass transfer coefficient can be obtained from

$$k_m = \frac{D_c \varepsilon}{\tau t} \qquad \textit{Equation 3.10}$$

Where k_m- mass transfer coefficient in the membrane (m/s), τ and ε are the tortuosity and porosity of the membrane, D_c is the diffusivity of the solute in the membrane and 't' is its thickness.

In the case of a counter flow dialysis device, the overall mass transfer coefficient can be obtained from the three phases of the system. From the mass transfer coefficient in the sample channel, water channel and the membrane as we get the overall mass transfer coefficient as (85)

$$\frac{1}{k} = \frac{1}{k_s} + \frac{1}{k_m} + \frac{1}{k_w} \qquad \textit{Equation 3.11}$$

Where k_s- mass transfer coefficient in the sample channel (m/s), k_m- mass transfer coefficient in the membrane(m/s), k_w- Mass transfer coefficient in the water channel (m/s)

The importance of the mass transfer coefficient was shown by Leypoldt et al. (91) in their research. The work showed that, the mass transfer area coefficient for urea and creatinine in case of a haemodialzyer were independent of blood and ultrafiltration flow rate but decreased with decreasing dialysate flow rate.

3.5.2 Overall mass-transfer (M)

Mass transfer is the net movement of mass of substance from one location to another. This forms like one of the important principle in case of dialysis. Mass transport with a phase up to the phase boundary is called mass transfer while when the mass transport occurs over the phase boundary into another phase, it is known as the overall mass transfer

Flow regimes can be either cross-flow, counter-flow or cocurrent flow. Yeh et al (85) has observed that among the three cases, counter-flow or the counter current flow provides better separation efficiency than its counterparts. The total mass-transfer rates for single pass of

counter current flow (M) can be derived analogous to the heat transfer in single-pass heat exchangers (92)as

$$M = kA(\Delta C) \qquad \textit{Equation 3.12}$$

$$(C_{sin} - C_{win}) = M \frac{\left(\left(\frac{1}{Q_s}\right) - \left(\frac{1}{Q_w}\right) e^{-KS\left[\frac{1}{Q_s} - \frac{1}{Q_w}\right]}\right)}{1 - e^{-KS\left[\frac{1}{Q_s} - \frac{1}{Q_w}\right]}} \qquad \textit{Equation 3.13}$$

where M-total mass transfer rate(mol/s),

k-overall mass transfer coefficient (m/s),

A- overall mass transfer area of the membrane sheet(m^2),

ΔC- mean concentration difference between two phases(mol/m^3),

Q_s=Q_a, Q_w=Q_b- volume flow rate in the retentate phase(sample) and dialysate phase (water),

$C_{a,i}$=C_{sin}, $C_{a,e}$=C_{sout}, $C_{b,i}$=C_{win}, $C_{b,e}$=C_{wout}- concentration at the inlet and outlet of the dialyzer.

3.6 Summary

Diffusion, the movement of a substance from a region of higher concentration to region of lower concentration, is the main principle behind dialysis. The diffusion of solute was explained by Fick's law which shows that flux depends on the concentration gradient in the system. Diffusion in a microchannel can be affected by Reynold's number. A high value of the Reynolds number indicate a turbulent flow in the microchannel which is favourable for diffusion while a low value of Reynold's number corresponds to a laminar flow in the microchannel. With a development towards using small sample volumes, for example blood obtained by finger prick for medical diagnostics, those analysis techniques that require sample processing such as desalting would benefit from well-characterized micro-volume dialysis devices. Analysis of the desalting efficiency of a dialyser can be studied and predicted using mass transfer equations, which take into account the mass transfer coefficient in the channels and the membranes. The mass transfer coefficient of the membrane highlights the factors that limit diffusion over the membrane: membrane thickness, membrane porosity and the tortuous nature of the membrane pores. Using the mass transfer coefficient (m/s) and mass transfer (moles/s) over a membrane and knowing the dialysis time (s), it is possible to predict the dialysis and therefore the desalting efficiency of a dialyzer of a specific design.

Chapter 4: Fabrication of microvolume dialysers

In this chapter, the construction of various microvolume (<50μL) dialyzers by rapid prototyping will be discussed. Millimetre scale fluid chambers and channels are defined by laser ablation of the polymer PMMA, with planar ultrafiltration membranes of various pore size as the crucial device component. Track-etch membranes with a wide range of larger pore sizes are employed for reference or control purposes. The dialysis efficiency is quantified by conductance measurements. Initial devices are simple sample chambers covered by a membrane and floating on a bulk water phase, while subsequent designs use a micromachined water chamber. The final device design is a spiralling retentate and dialysis channel separated by a membrane, with syringe pumps that regulate the flow of each phase and in-line conductivity meters for quantification of the post-dialysis salt concentration in each phase.

4.1 Membranes

Ultrafiltration (UF) membranes made of regenerated cellulose (RC) and polyether sulfone (PES) with a molecular weight cut-off (MWCO)-1000, 5000, 10000, 100000, 300000Da were purchased from Sartorius. The datasheet supplied by the manufacturer states that the membranes are 25mm in diameter with a thickness of 180μm. They have a water flux of about 0.08mL/min/cm^3 and give 99% retention of cytochrome c (12.4kDa). Further details on the membrane porosity, pore density, tortuosity were not provided from the supplier and being an UF membranes these data are difficult to obtain which will be discussed in later chapters. Membranes with small MWCO were chosen so as to retain most of the proteins while removing the small molecular weight salts, while membranes with larger pore sizes, with specified pore size and porosity, were used for control experiments as described in subsequent chapters. The membranes were sandwiched between clear cast acrylic which contains the microchannels for both sample and buffer compartments. The acrylic was obtained from RS Components and is about 5mm thick. The acrylic was chosen since it provides an easy means of constructing the device using laser micromachining. Hollow fibre Spectra/Por in-vivo microdialysis membrane (fibre OD: 216μm and fibre ID: 200μm, thickness 16μm) made from regenerated cellulose having a MWCO of 13000Da was purchased from Spectrum Labs. These fibre membranes are about 6 inch long and can be cut into desired pieces.

Polyethylene terephthalate track etch membranes were bought from Avanti for various pore sizes ranging from 50nm-1000nm. The specifications of these membranes can be seen from the following table. With increasing pore size, the porosity increase and pore density decreases to maintain structural stability of the membranes.

Table 4.1: Specification of track-etch membranes.

Pore size (nm)	Pore Radius(m)	Porosity (%)
50	2.50E-08	1.18
100	5.00E-08	4.71
200	10.00E-08	15.70
400	20.00E-08	18.84
1000	50.00E-08	17.27

DI water was Millipore deionized water (18MΩ/cm & 550nS/cm) and was used as a dialysate /water phase in all the dialysis experiments. Prior to using the membranes for making the dialysis device, they were soaked in DI water in a beaker for about a day before use. This is done so as to remove the glycerine coating from them and also to make sure that the membranes are well hydrated before use. When the membranes are needed, they are taken, rinsed with fresh DI water and wiped using a clean laboratory tissue.

4.2 Laser Micromachining

A convenient and cost effective method of fabricating microchannels is by rapid prototyping is laser micromachining. The mechanism of laser ablation involves the removal of the material via vaporisation. A beam of high energy laser increases the internal energy of the substrate, causing the material at the point of incidence to convert into a plasma. The rate of ablation depends on the optical absorptivity of the material, the laser wavelength and pulse length (93). Kawamura et al (94) reported ablating polymethyl methacrylate (PMMA) using a pulsed KrF excimer laser.

4.2.1 CO_2 Laser

The CO_2 laser is a benchtop laser with output wavelengths between 9 and 11μm. To create the microchannels for the on-chip dialysis device, laser micromachining was employed. Epilog Mini 24 laser system was used for high quality engraving on the clear cast acrylic to create the microchannels for the sample and water flow. The laser source is a digitally controlled, air cooled CO_2 laser. The spot size of the laser is 0.003" - 0.005" (0.0762 - 0.127 mm).

Figure 4.1: CO_2 Epilog Laser Mini.

4.2.2 Designing microfluidic channels and printing.

Channels are designed on any graphics editor, and the CorelDRAW® vector graphics editor was used for the present work.

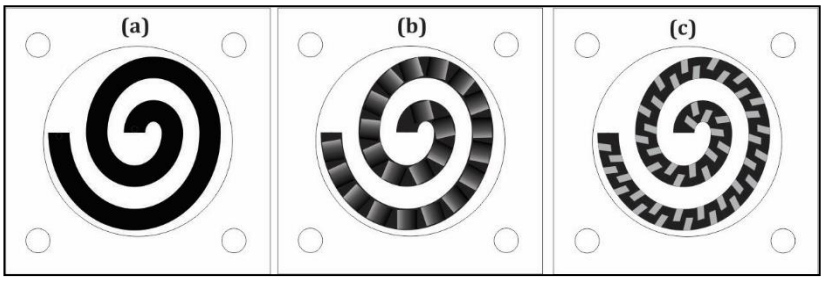

Figure 4.2 Design for laser ablated microchannels. Microchannel with (a) no obstructions in the channel and (b & c) with obstructions.

Channels of different geometry (discussed later in this chapter) can be designed using the application. The Epilog laser is displayed as a printer on the computer and by a simple print option design can be transferred to the machine. The printer dialog box is shown in the Figure 4.3. Using the raster mode it is possible to engrave or ablate layers of PMMA and using vector mode PMMA can be cut according to the design. Using high power and low speed in the settings, large and deep channels can be created since the laser ablates a considerable amount of PMMA.

Deep channels can be obtained by rastering PMMA at slow speed and high power. The Epilog CO_2 laser settings were first optimized to determine the deepest channel that can be rastered in a PMMA at the same time avoiding cracking the channel which was commonly noted when rastering deep channels. Water channels are deep and rastering deep channels makes the surface of the channels rough. Roughness can be reduced by rastering the same channels over again with very high speed. Rastering PMMA at high speed and low power yields a shallow and smooth surface channel.

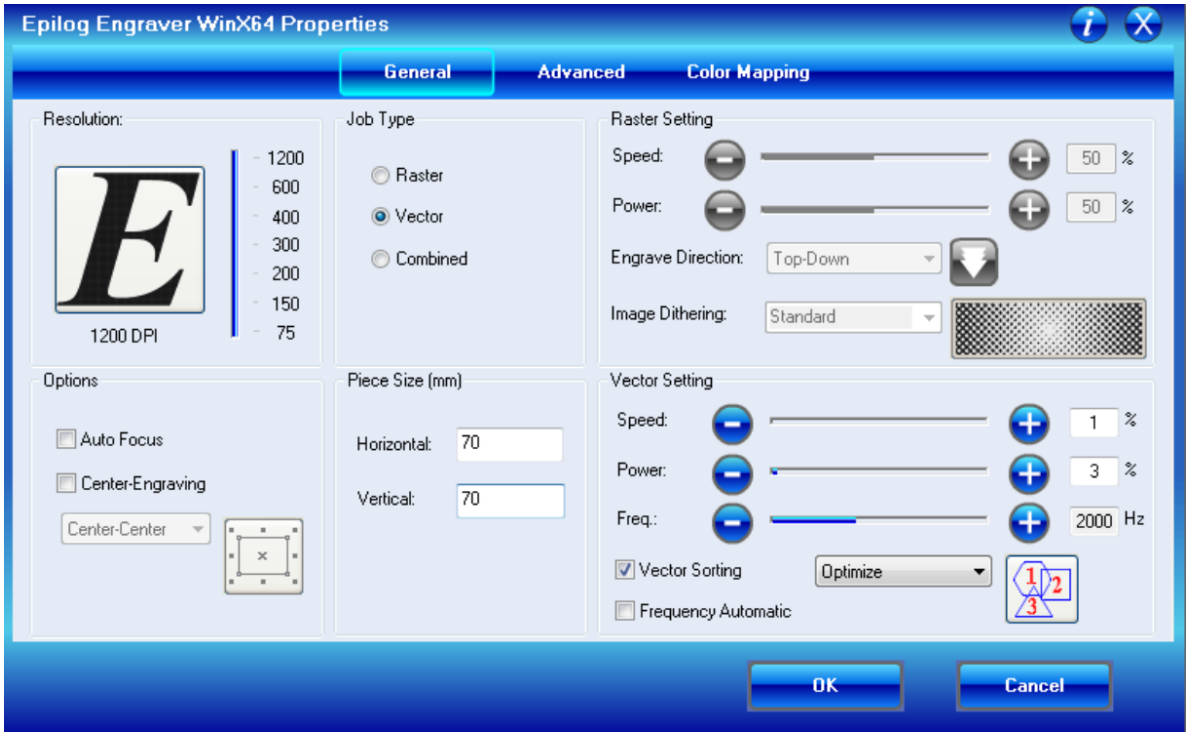

Figure 4.3: Engraver Print Properties control box.

4.2.3 3D mode Engraving

Normal channels are easy to fabricate using the laser cutter. At the same time, it is possible to create channels with chevrons or grooves in them. Turbulent flow or mixing in the channel would be advantageous as discussed in the previous chapter which can be made possible by introducing patterns in the microfluidic channels.

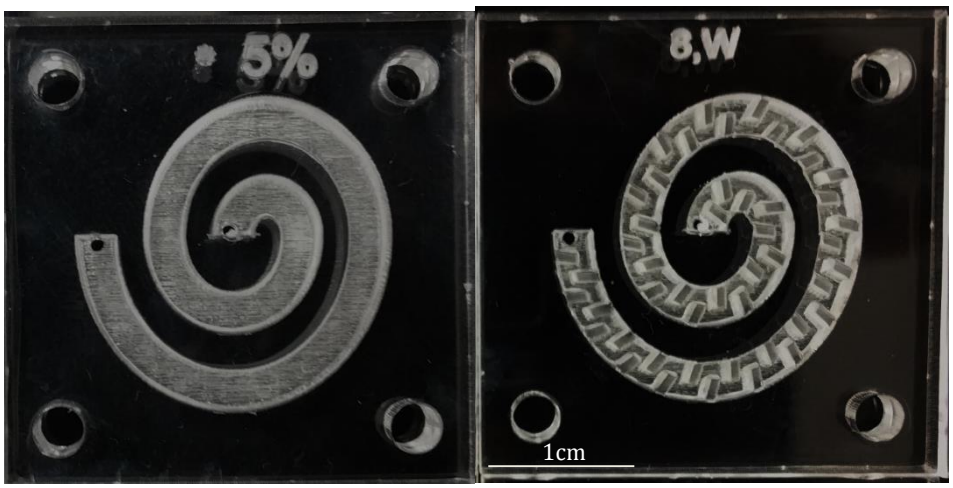

Figure 4.4: Microchannels fabricated using laser micromachining. The devices shown above has a channel without an obstruction (on the left) and with chevrons (on the right). The Devices are 30mm x 30mm and the channels are 4mm deep and 75mm long.

Kwon et al. (95) showed chaotic mixing in microfluidic channel with herring-bone shaped obstacle. Similar designs were made using the laser cutter. In order to achieve this, the necessary condition is to have a CorelDraw design with a greyscale pattern in the design corresponding to the features that are required in the microchannel. Having a greyscale image

makes the laser to raster with each pulse having a different power corresponding to the greyscale value of the design. Unless the 3D mode is selected, the laser would have all the pulse with the same power.

4.3 Conductivity measurements.

Quantifying desalting efficiency of the device is important to understand how it functions under various testing conditions. One of the easiest methods of quantifying, post dialysis, the salt present in the sample or in the water phase after removal is to measure the conductivity of these phases. With a calibration curve of the conductivity of a series of salt solutions of known concentration, this conductivity can be related to the salt concentration. Two different conductivity meters were used in the experiments to measure the salt concentration.

4.3.1 Macrovolume conductivity measurements

YSI 3200 is the conventional bench top conductivity meter used for measuring the conductivity. The meter is capable of measuring conductivity, resistance salinity and temperature. The instrument has a resolution of about .0001µS with a wide range 0-3Seimens and also offers the possibility of data storage and with RS-232 output. The availability of the RS-232 makes it advantageous when recordings with definite time interval are carried out over a period of time. Using software RS-232 Data Logger, it is possible to obtain the read out from the conductivity meter.

Figure 4.5: Bench top conductivity meter YSI 3200.

The meter includes a large conductivity probe/cell and uses resistance ratio measurement technology. The cell uses black platinum electrodes which are stable and linear. The cells can also be replatinized if need be by using the meter with a platinizing solution. The conductivity cell (model 3252/003252) used over here has a cell constant of 1.0/cm and has an overall length of 146mm, 13mm O.D., chamber I.D 10mm and with a depth of 20mm. The cell is also a dip type which requires a minimum of 5mL of sample to measure the conductivity.

4.3.2 Microvolume Conductivity Meter

The pocket sized conductivity meter from Horiba can accurately measure minute samples in its built-in sampling chamber, or measure large samples by sample chamber immersion in the measurement solution. The Horiba B-173 has auto calibration ad features a waterproof flat sensor. The device uses AC bipolar method and has a measurement rage from 1µS/cm to 19.9mS/cm. The measurement modes use sodium chloride salinity conversion which is favourable for our experiment. The readings are displayed over a digital LCD and there is no possibility of recording the measurements like YSI3200. The handheld conductivity meter and the sensor surface can be seen from the Figure 4.6. 100µL of sample is required for measurement. But by modifying the area around the sensor surface, it is possible to reduce the volume required to obtain the conductivity measurement. Sealing the area away from the sensor surface using blu-tag would reduce the sample requirement to 50µL. The sensor is then calibrated using the calibration solution and can be used for further test. Further, by adding an inlet and an outlet port to the device Figure 4.6, it is possible to employ the conductivity meter as a flow cell and record the measurements for a very short period of time (2-5mins).

Figure 4.6: Handheld conductivity meter Horiba B-173. (a) Modified sensor surface of the conductivity meter. Blu-tag was used to cover of the portion of the chamber.

The conductivity meter has two advantages. The meter can be used as a flow cell where an inlet to the sensor surface can be made and have it connected to the outlet of the dialyser for sample measurement and an outlet to remove the sample out by flow after measurement. Another important advantage is that the device is suitable for requires a low sample volumes. This makes it suitable for in-line conductivity measurements as described in the chapter.

4.4 Test Sample

The physiological salt concentration is equivalent to approximately 150mM of a monovalent salt, while of all the salts present in the blood, sodium chloride (NaCl) constitutes about 135-140mM which equates 7.8-8.7g/L. Hence 150mM NaCl it (Fisher Scientific) is used as a test sample in the initial experiments. Human serum albumin constitutes around 86% of the total proteins available in blood hence albumin from bovine serum (97% pure), was purchased from Sigma Aldrich as lyophilized powder. Fluorescein isothiocyanate conjugate bovine albumin and tetramethylrhodamine isothiocyanate bovine (fluo-BSA) were bought from Sigma Aldrich unless otherwise noted, the experiments described in this thesis were carried out with a solution of, 150mM NaCl and 2mg/mL fluo-FBSA. This protein was chosen since it would be easy to detect, by observing a yellow colour in the water phase, if there is any leakage from the sample across the membrane or device. The yellow coloured sample also acts as in indicator to visualise how the sample moves along the sample channel and how it spreads across the membrane.

Table 4.2: Summary of the main requirements for the microvolume dialyzer.

Requirements		Experimental approach
Low sample volume ~50µL	→	Millimetre channel height and width
Removal of salt ions with retention of proteins	→	UF membrane with ~1000Da MWCO pore size
Rapid prototyping of devices	→	Laser ablation micromachining of optically transparent acrylic polymer
Good seal between membrane and dialysate and retentate matrix	→	Use of fluorescent protein to visually ascertain that this is only present in the retentate phase
Do not exceed ~60min dialysis duration	→	1mL/60mL syringe volume for retentate/dialysate phase.
Determine the salt concentration in retentate and dialysate down to ~1 mM	→	Conductivity meters with a dynamic range of 0µS/cm-20mS/cm

4.5 Static Dialyzer

In order to check the performance of the membranes initial experiments were carried out using a static setup, with no flow of either the retentate or the dialysate phase. The sample was static in a chamber rastered on an acrylic. The sample container is shown in the figure below (Figure 4.7). The RC membrane was glued to the acrylic using gel type super glue with care taken so as to not block the region of interest in the membrane, which will be in contact with the sample. When this region is also in contact with the DI water, migration of molecules from the sample

to the water will occurs. Clogging the pores in the active region of the membrane with glue has to be avoided otherwise the active area of the membrane would be underestimated.

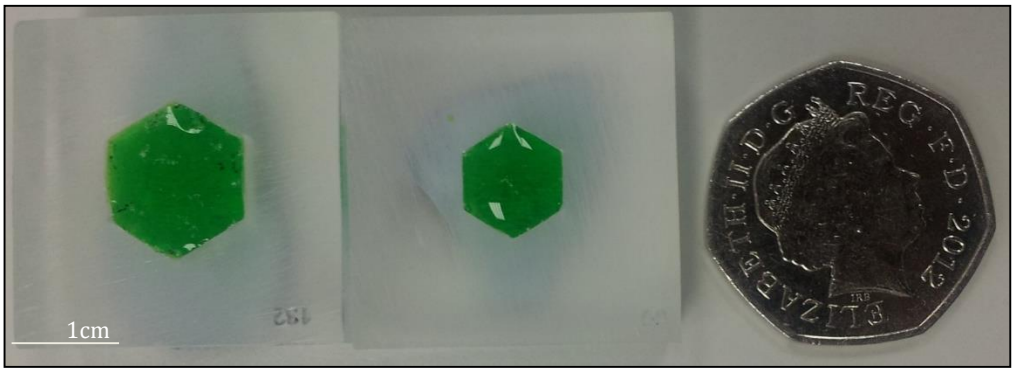

Figure 4.7: Basic dialysis device to check the performance of the membrane. The ultrafiltration membrane is glued to the acrylic. The hexagon has an area of 132mm^2 and 66mm^2.

A hexagonal design was chosen for the sample chamber so as to enable recovery of the sample at the end of the experiment. The influence of the active area of the membrane on the dialysis and the influence of the total volume of the sample in the device can be easily understood from this experiment. Two different hexagonal designs were made using laser micromachining, one having an area of around 132mm^2 while the other was smaller at about 66mm^2. When the ultrafiltration membrane (UF) is glued to the device, the active surface area of the membrane will correspond to the area of the hexagon. In these experiments, the design shown in Figure 4.7 is filled with the sample and allowed to float in a beaker containing about 200mL of DI water. The conductivity cell connected to the YSI 3200 is immersed in the beaker in such a way that, it does not touch the device that is floating at the top of the water. The output port of the YSI 3200 –RS-232 port is then connected to a computer and by using a serial port reader, the conductivity of the DI water is measured and stored every minute.

From the conductivity measurements, it is possible to find the amount of salt removed or left behind as follows.

- Measure the conductivity of the bulk water phase as a function of time; the conductivity increases when NaCl diffuses out of the sample through the membrane.
- Convert the conductivity to a NaCl concentration in the dialysate by using a calibration curve of known NaCl concentrations.
- For each time point, calculate the mass of salt present in the total volume of water dialysate.
- Obtain the amount of salt left in the sample by subtracting the mass of salt present in the water phase from the mass of the salt initially present in the sample.
- Present the dialysis data as a plot of the concentration of salt left in the sample versus time.

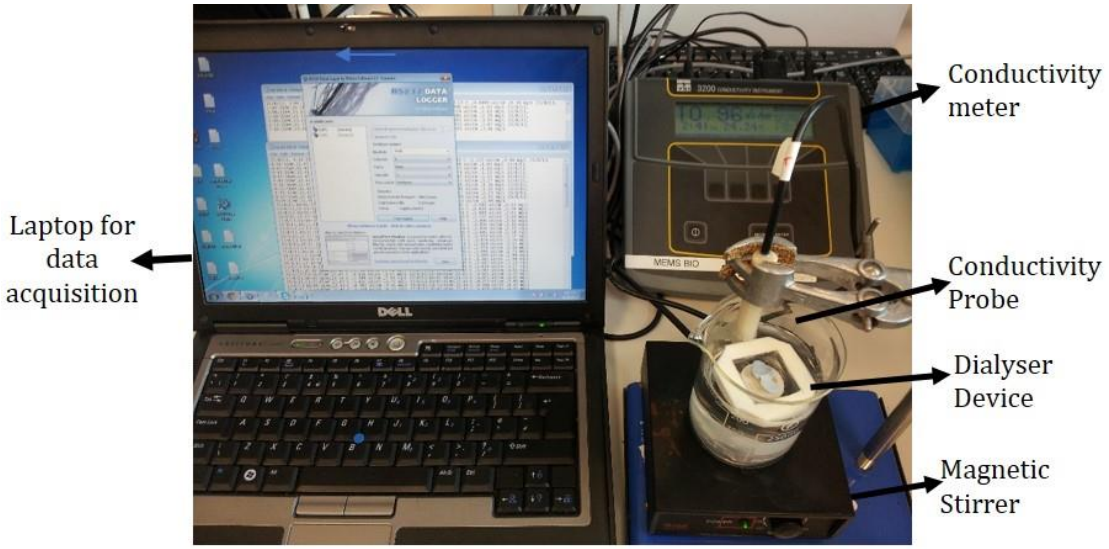

FFigure 4.8: Basic dialysis setup for checking the membrane performance.

In this set of experiments the principle driving force is diffusion because of the concentration gradient between the sample and the water phase across the membrane. Similar set up and experiments were carried out for measuring the porosity of the membranes by diffusion. In this regard, diffusion rate across a membrane of known porosity is measured and compared against the diffusion rate of the membrane of unknown porosity to determine the value. Membranes with 50nm pore size were chosen as a reference membrane of known porosity and compared against all the UF membranes to determine the membrane porosity.

4.6 Stop and flow experiment

A basic system to check the dialysis procedure with microvolume dialysate and retentate volume consists of two rectangular channels. Using CorelDraw, a design was made for the sample and the water channel with the following specifications. In all the designs used for the microvolume dialysis, the diameter of the membrane (25mm) is one the limiting factor in selecting the dimensions of the channel and the other being the volume of the sample used.

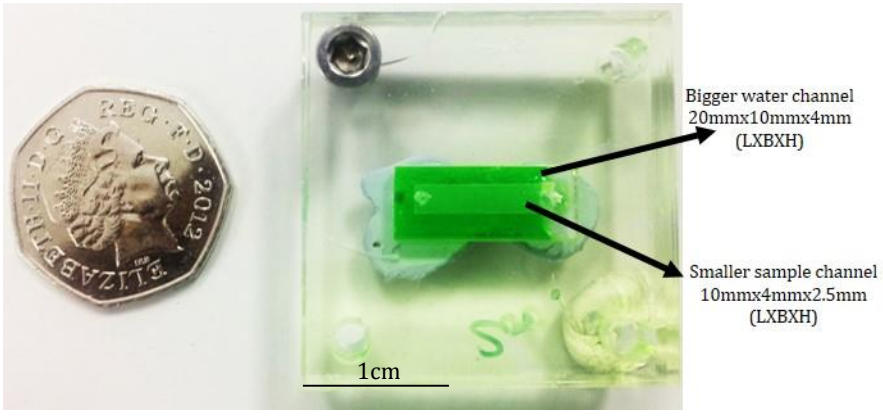

Figure 4.9: A simple dialysis setup containing rectangular sample and water channels for stop and flow experiment

Figure 4.10: Rectangular dialysis setup with 'O' rings to provide tight sealing of the membranes for stop and flow experiment

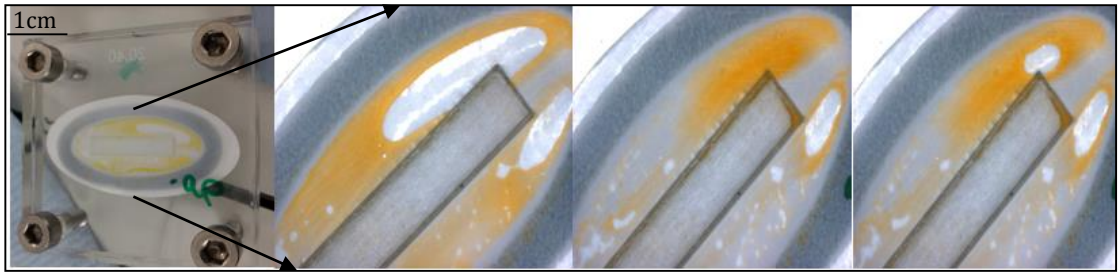

Figure 4.11: Problem with the rectangular dialysis setup for stop and flow experiments. The water channel is too wide with respect to the sample channel, causing the membrane to sag and the sample to flow, over the sagged membrane, out of the sample channel.

The sample channel was made smaller in all aspects length, width and the depth. The sample channel was engraved using the laser with 50% speed and 100% power. The resulting channel gave a depth of about 2.5mm and was able to hold about 100µL of the sample. The water channel was rastered or engraved at 5% Speed and 100% Power to give a depth of about 4mm on an acrylic sheet of 5mm thick. The water channel was about 20mm x 10mm while the sample channel was 10mm x 4mm. The differences in the water and sample channel sizes are advantageous. On aligning the two rastered pieces as shown in the Figure 4.9, it can be noticed that the sample channel fits inside the water channel. In this case, it is possible to have the sample exposed to much large volume of water thereby effectively increasing the diffusion of salts across the membrane.

When the sample was filled into the sample channel using a syringe pump, some problems were observed. First, the sample did not remain within the channel but it spreads over membrane randomly. This would be mean that the active surface area where the sample is present varies from device to device and in each experiment as shown in the Figure 4.11. Secondly, having the design shown above, it was found that the channels are too wide apart leading the membrane to sag in the middle. This leads the sample channel to take in more amount of sample filling the void in the device. In order to overcome this problem and to provide a tight sealing 'O' rings were used. Usage of 'O' rings increased the volume of water and water not being confined to the channel as well (Figure 4.10 & 4.11). This led to re-designing

the device with smaller channel at the same time maintaining the surface area of the membrane.

Smaller serpentine channels were initially engraved using the laser micromachining. Engraving the sample channel in the serpentine design was easy and quick. Unfortunately, this was not the case for the water channel. The serpentine design of the water channel was quite close to each other. Hence when rastering at water channel at high power and low speed the boundary lining the water channel melts away creating no boundary and forms a large chamber instead. This problem was overcome by using a spiral design as shown in Figure4.12.

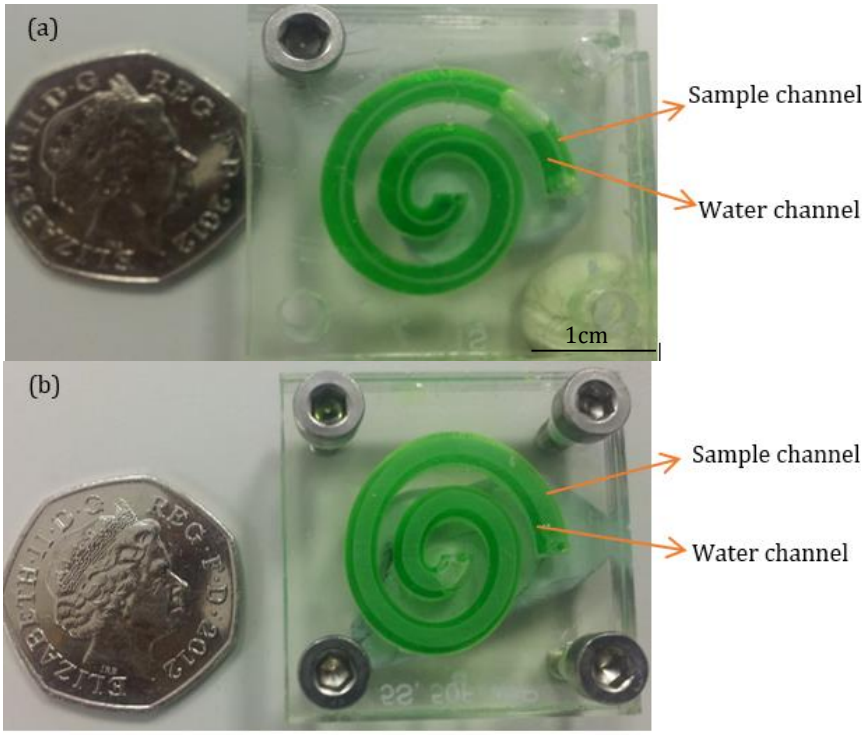

Figure 4.12: Spiral device with water and sample channel. (a)Sample channel width =0.98mm. Water channel width =2.82mm. Width of sample channel <<Width of water channel. Sagging of membrane in the middle of the channel seen. (b) Sample channel width=1.76mm. Water channel width=2.82mm. Sagging of membrane is much reduced

The spiral design of the water and sample channels adhered to the diameter of the membrane. Each of the water and sample channels had a length of about 75mm. The water channel was fixed and maximized to fit inside the membrane diameter and had a width of about 2.82mm or 8pt. To prevent the problem of sagging of membranes at the middle, different dimensions of sample channel was rastered. With respect to the pt scale or points scale, sample channels of 1pt, 2pt, 3pt, 4pt all failed to obtain prevent the membrane from sagging. Sample channel having a width of 5pt= 1.76mm provided the best result from preventing the membrane from sagging. Sample channels of width above 5pt/1.76mm also proved that membrane sagging does not occur when placed in the dialyser. But using wider sample channels would mean more sample is required to flow through the channel. The sample channel was rastered at 50% laser power and 40%speed movement of the laser unit to obtain a channel height of 200µm. The power and the speed of laser rastering were chosen after various trials. Increasing the power

further resulted in an increased channel height while decrease the speed had the same effect. On the other hand, decreasing the power and increasing the speed made the channel shallower making it difficult for the sample to flow in the channel. Hence in all the experiments, the sample channel of width 1.76mm and depth 200μm was used along with a water channel of width 2.82mm and depth 4mm. The total surface area available to the sample is about 132mm^2 which is nearly the same as the test device in Static measurement section. The sample channel was able to hold about 26μL of the sample while the water channel was able to contain about 750μL of DI water.

Experiments were carried out using the Rectangular design with the 'O' rings (Figure 4.10) and last design with a wider sample channel in case of the spiral design (Figure 4.12) in order to calculate the appropriate flow rate of the water that would give the best desalting efficiency. The sample channel and the water channel are aligned with a RC membrane in between them. The acrylics are then squeezed together using M4 screws gently so that the acrylics do not bend due to stress in the middle of the device. For the initial set of experiments, the sample is flown into the sample channel using a syringe pump and then the inlet and outlet port are sealed off using blu-tag. Then DI water is filled in the water channel using a syringe pump and allowed to be in contact with the sample for a stipulated amount of time (1,2,5,10,15,30mins etc) and then flushed out. This water is then collected in an eppendorf and the conductivity of the water is measured and the values are recorded and further processed.

Experiments carried out using the above device were primarily for control experiments such as influence of stirring in dialysis, influence of membranes surface area in desalting, determine flow rate for future experiments and determine membrane parameter such as porosity.

4.7 Counter-flow Measurements

In the last section, experiments with no sample flow were done. In this section, we discuss about experiments involving flow of both the sample and the water across the membrane in their respective channels. From the literature reading and from previous chapter, it is clear that counter current flow is advantageous and results in good desalting/extraction (96). Hence counter current flow of water and sample is set in all the experiments with water flowing in the direction opposite to the flow of the sample.

4.7.1 Micro volume Dialysis with Sandwiched Planar Membrane

The schematic of the counter-flow arrangement can be seen in the Figure 4.13

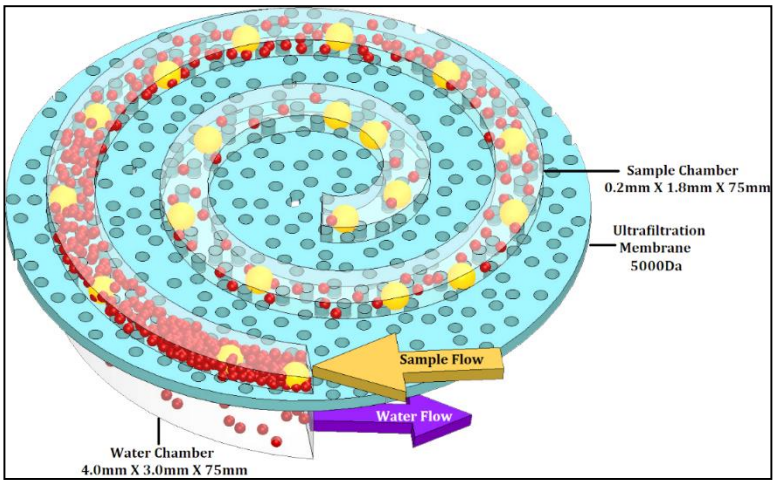

Figure 4.13: Schematic of a counter current flow in a dialyser. An ultrafiltration membrane is sandwiched between two microchannels with water and sample flowing in the opposite direction. Red dots indicates small particles such as salts which can pass through the membrane and yellow dots represents bigger particles such as proteins which doesn't pass through. Small particles are removed across the length of the channel starting from the inlet port.

Figure 4.14: Experimental set up for Counter flow arrangement (1) Water supply from a syringe flow rates 10-750µL/min, (2) Sample supply from a syringe, flow rates 0.5-50µL/min and (3) membrane of MWCO-5000Da used to design sandwiched dialysis device.

The experimental setup shown in Figure 4.14 was used for the counter flow dialyser. The device shown in the Figure 4.12 was used in the experiments with counter flow mechanism. Sample was flown from the inlet port at the centre of the device on the sample side and water was flown in the opposite direction from the inlet port at the outer side of the device as shown. Samples were flown through the device at low speed (0.5-5µL/min) and water was flow at much higher speed (150µL/min). The sample fills in the channel, and passes out from the device, gets collected and the measurement is recorded. On finalising the procedure and the flow rates to obtain the modified conductivity sensor is included at the outlet port. The outlet of the dialysis device is connected to the side of sensor thereby conveying the sample to the sensor surface. Once the small chamber is filled, the measurements are noted and the sample is collected through the outlet port at the top of the sensor surface. With this arrangement, it

was made possible to carry out the in-line conductivity of the sample with various conditions of flow. The flow rates for this set of experiments ranges from Q_s-0.5-50µL/min in case of sample flow while in the case of water flow, the flow rates varied from Q_w-10-750µL/min.

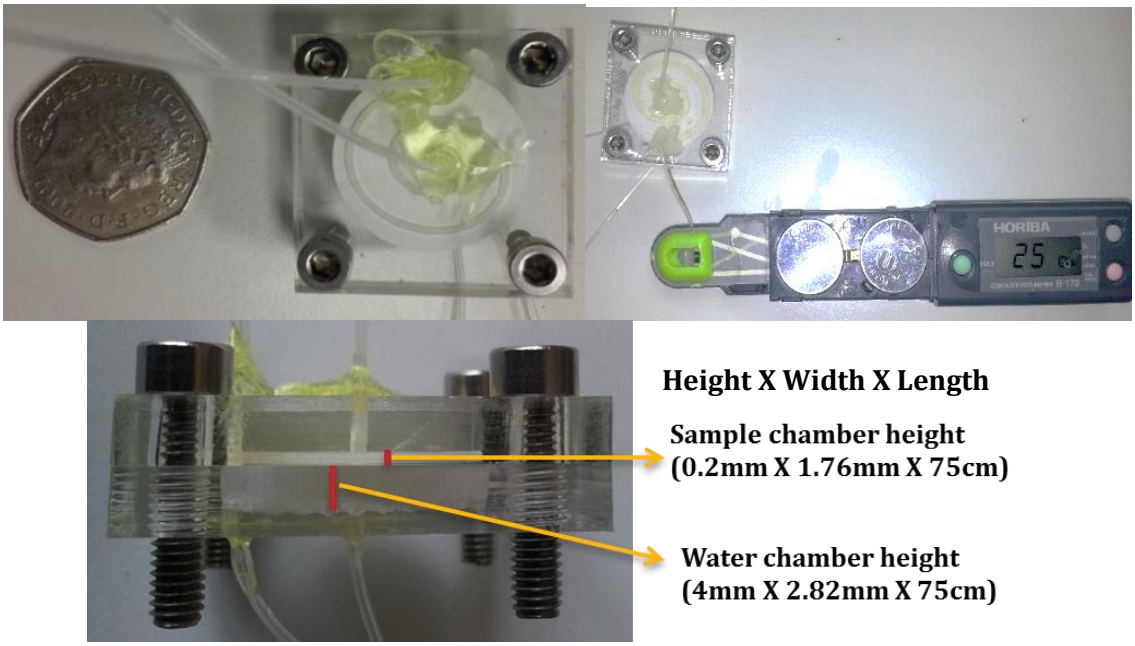

Figure 4.15: (a) Sandwiched membrane dialysis in spiral design using counter flow method. (b) Dialysis device connected to the modified in-line conductivity meter. (c) Side view of the dialyser showing the channel dimensions.

The same set up with camera was used for real-time measurement of the conductivity changes to quantify the desalting efficiency. Two conductivity meters- YSI-3200 bench top conductivity meter along with Horiba's portable meter was used together one for the sample side and the other for the water side to measure the conductivity of individual phases as shown in the figure below.

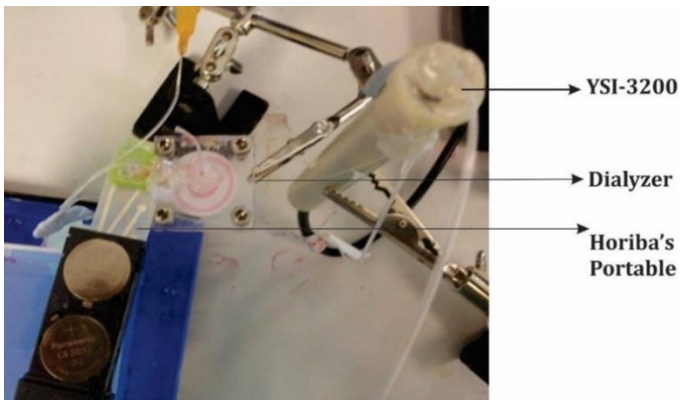

Figure 4.16: Live measurement recording set-up consisting of two conductivity meters attached one on each of the sample and water outlets

4.7.2 Micro volume Dialysis with Enclosed Hollow Fibre Dialysis Membrane

The hollow fibre membrane is about 16µm thick and has an O.D 216µm. In order to connect the dialysis membrane, having an inner diameter of 208µm polythene tubings are used into which the dialysis membrane was inserted and sealed off using an epoxy as shown in the Figure 4.17. This set up primarily selected in order to understand the effect of using a membrane of

different structure for dialysis and the influence of the surface area of the membrane. The sample flows through the membrane while the water flows through an eppendorf. The membrane was first cut into 40mm so as to fit inside an eppendorf. This would give the length of the sample channel to be 40mm. The working volume of the fibre of 150mm length is about 6µL. So for the selected length of the fibre in the eppendorf, the working volume is about 1-1.5µL. The inlet and the outlet for the water flow uses the polythene tube and they are fixed to the eppendorf using epoxy.

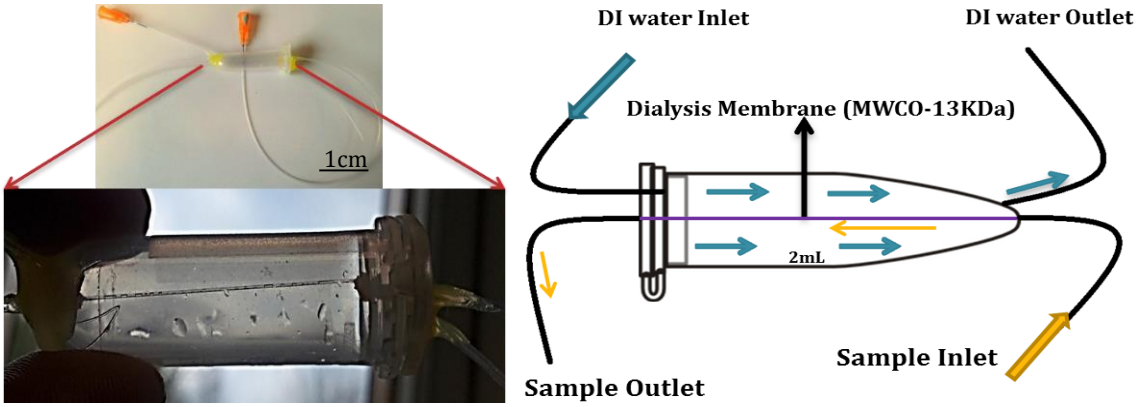

Figure 4.17: Hollow fibre membrane Dialyzer. Dialysis membrane is fixed inside an eppendorf, (b) Schematic of the Counter current flow in the Hollow fibre membrane Dialyzer.

The working of the hollow fibre membrane is first evaluated using a high salt concentration sample 1M with Fluorescent BSA. The counter flow arrangement was set up using the pumps with the initial flow rate of the sample at 1µL/min and water flow rate at 1mL/min. on collecting the initial test results, further experiments were carried out using the sample of 170mM and BSA with different set of flow rates ranging from 0.5-25µL/min in the sample channel while having 250-2000µL/min in case of the water. The in-line conductivity measurements were then used to measure the conductivity of the desalted sample.

4.8 Mass Spectrometry

Mass spectrometry was used to analyse the influence of the presence of salt in the sample at different concentrations. Samples for the mass spectrometry analysis consisted of proteins samples before and after desalting. Protein samples were mixed with an equal volume of $CH_3OH//HCO_2H$ (98:2). Mass spectra were recorded on an LCT™ (Waters,UK) orthogonal acceleration time-of-flight mass spectrometer fitted with a nano-electospray source. Samples (4µL) were loaded into borosilicate capillaries (1.2mm o.d. x 0.69 mm i.d.) (Clark Electromedical Instruments, Reading, UK) that had been drawn to a fine tip using a micro electrode puller (Narishige, Tokyo, Japan) and sputter coated with gold/palladium. Spectra were recorded in the positive ion mode between 500-1750 *m/z* (cytochrome *c*) or 650-1500 *m/z* (myoglobin) using the following instrument settings: capillary 1250-1650V, sample cone

25-31 V, extraction cone 8V, source temperature 80° C. Typically, 50-100 acquisitions were combined and deconvoluted using the maximum entropy algorithm, MaxEnt™ (Micromass, Altrincham, UK) to give relative molecular mass spectra over the range 10000-15000 Da (cytochrome *c*) or 15000-20000 Da (myoglobin) at 1 Da resolution. Spectra were externally calibrated using myoglobin spectra recorded under identical conditions, immediately after each sample. The samples were desalted using the method discussed in section 4.7.2 and handed over to Mr. Neville Wright, Biomolecular Facility, Center for Biological Science, University of Southampton for obtaining the mass spectrum for the samples. Typical samples included 10mg of myoglobin (17kDa) in 1mL of PBS and 10mg of cytochrome c (12.3kDa) in 1mL of PBS. A combination of two proteins cytochrome c and Lysozyme from Chicken egg white (14.3kDa), each of 10mg was taken in 1mL PBS and desalted as before. In order the compare the resolution of the spectrum between the samples before and after desalting, all the samples were desalted at different sample and water flow rates (Q_s=0.5, 5, 10μL/min and Q_w=750μL/min). Blood serum was also used for mass spectrometry analysis after desalting.

4.9 Summary

Ultrafiltration membranes of different molecular weight cut-off were selected for desalting with retention of proteins in the sample, and track-etch membranes with larger pore sizes and known porosity were selected for control experiments. Microvolume dialysis was approached by rapid prototyping of millimeter scale channels fabricated by laser micromachining of the optically transparent acrylic material PMMA. The membranes are bonded to the acrylic matrices with glue to obtain a retentate-membrane-dialysate stack. So that the glue did not block the active membrane area, the relative width of the sample and water channels was optimized to prevent sagging of the membrane into the water channel. The composition of most test samples was chosen to be 140mM NaCl, together with 2mg/mL fluorescent BSA protein to visualise sample flow and to verify that the sample does not leak around the membrane. The conductivity of the post-dialysis sample and/or water phase was measured with customised conductivity meters and the salt concentration can subsequently be determined with reference to a calibration curve. Initial static dialysis experiments involved placing a membrane-covered microvolume on top of a bulk water phase. Devices for dynamic dialysis were designed with straight or spiralling microvolume sample and water channels. These were optimized with respect to channel dimensions and acrylic-to-membrane bonding. The crucial components of these dialyzers are the commercially sourced ultrafiltration and track-etch membranes, which are investigated in the next Chapter.

Chapter 5: Membrane Characterization

The structural characteristics of a separation membrane, which include pore size and porosity, are important parameters for dialysis performance. This chapter highlights the difference between the various membranes employed in this work, which can be distinguished by their fabrication method, which is either phase inversion or track etching. The differences between these techniques are explained and the different membrane materials and especially membrane pore morphologies are highlighted from a literature review perspective. Electron microscopy is then performed to investigate the commercially sourced membranes, and electrical and conductivity measurements are performed to estimate the porosity of the membranes with the smallest pores. The experimentally obtained morphologies and porosities are in agreement with the literature on track etched membranes and on ultrafiltration membranes prepared by phase inversion.

5.1 Introduction

A semi-permeable membrane is an interphase between two adjacent phases acting as a selective barrier. Passive transport of ions or (bio)molecules through membranes can occur as a consequence of a difference in chemical potential across the membrane, e.g. a concentration or pressure gradient, or of an electrical field (97). The barrier structure of membranes can be classified according to their porous character (Table 5.1)

Table 5.1: Classification of membranes and membrane processes for separation via passive transport (98)

Membrane barrier structure	*Transmembrane gradient*		
	Concentration	*Pressure*	*Electrical Field*
Non-porous	*Pervaporation*	*Gas separation*	*Electrodialysis*
		Reverse osmosis	
Microporous pore diameter ≤2nm	*Dialysis*	*Nanofiltration*	
Mesoporous pore diameter 2-50nm	*Dialysis*	*Ultrafiltration*	*Electrodialysis*
Macroporous pore diameter 50-500nm		*Microfiltration*	

Although there are many different commercially available membranes types for separation process, the detailed working principles of membrane separation are not very well understood. One of the reasons for this is that the physical and chemical nature of the applied membranes is intricate, and that the relation between the membrane structure and the actual performance, e.g., the transport efficiency, is complex (99) Membrane should be highly qualities are high selectivity and, highly permeable for the species of interest and also exhibitility, good mechanical stability and chemical resistance (34). In literature, several

parameters for membrane performance are enumerated. Morphology related membrane parameters such as pore size, pore distribution, pore shape and membrane thickness, as well as performance related parameters such as permeability and rejection, are all considered important (99).

Some of the most common membrane process and their basic separation mechanism can be seen in the Table 5.2.

Table 5.2: Membrane separation processes and some of their characteristics (99) and ε- porosity of the membrane.

Membrane Process	Pore Size	Typical Characteristics	Separation Mechanism
Microfiltration	5-0.05μm	ε~10-50%	Size Exclusion
Ultrafiltration	50-2nm	ε~0.1-10%	Size Exclusion
Reverse Osmosis	1-0.1nm		Solution Diffusion
Dialysis	10-0.1nm	ε~50%	Effective Diffusion
Electrodialysis	10-0.1nm		Difference in Charge
Gas Separation	<0.1nm		Solution Diffusion
Prevaporation	<0.1nm		Solution Diffusion

5.2 Molecular weight cut-off vs pore diameter specifications.

In most of the membrane filtration processes, the membranes used are distinguished by their pore size or by their molecular weight cut-off (MWCO), which is defined as the smallest molecular mass (MW) of an approximately globular molecule which is retained at a certain coefficient (the ESMST Standardization Committee suggests 90%) of retention (100). In other words, the term MWCO was developed for certain membranes to define the equivalent spherical size of macromolecules that can be retained by a specific membrane. When comparing MWCO measured with proteins to pore size measured by other techniques in a membrane, it should be noted that proteins differ by 10times in MW may only differ by three times in size in their globular form (97). Most proteins fold into a globular domain and hence they are characterized depending on their molecular weight. A straightforward correlation between nanometre and MWCO is rather difficult and generally the “real” pore sizes are larger than those evaluated from MWCO data (100). There are four different types of separation membrane, which are distinguished by their pore size and/or the molecular weight of the solute they can reject.

1. *Microfiltration (MF)*: The pore size generally spans the 0.1-1μm range, which are measured by porometers. Most of the track etch membranes (section 5.3.1) fall in this category.
2. *Ultrafiltration (UF)*: The pore size generally spans the 0.01-0.1μm range, but pore sizes are often expressed as MWCO values, which range from 1000Da to 300kDa.
3. *Nanofiltration (NF)*: The pore size ranges from 1nm to 10nm and MWCO values may range from 200Da to 1000Da. NF membranes can remove divalent ions with relatively high efficiency, e.g. 70-99%, the efficiency of removing monovalent ions such as Na+, K+, Cl-, etc. is typically lower (30-80%).
4. *Reverse osmosis (RO)*: No pores can be identified by SEM (101).

The basic rejection process for the above mentioned type of membranes can be seen in the Figure 5.1.

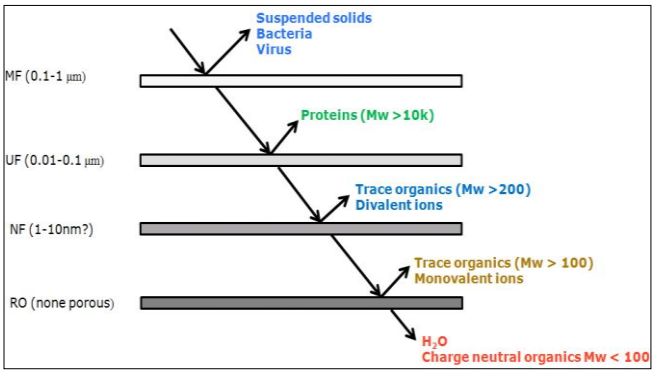

Figure 5.1: The particles rejected by membrane as a function of pore size: An approximate relation (101)

UF membranes are microporous barriers capable to separate the components of mixture on the basis of differences in size and shape. This kind of membranes is very suitable to separate suspended materials, colloidal particles and dissolved solutes with molecular mass at least two orders of magnitude higher than the solvent (usually water). In case of an UF membrane there exists a nominal MWCO in kDa or atomic mass units (amu) such as 1,3,10,100kDa etc. According to the membrane pore size distribution for UF membranes as shown in Figure 5.2, a 1kDa rated UF membrane could have ~20% pore sizes ranging from less than 1kDa (e.g. 0.5kDa) to another 20% of pore larger than 1kDa (e.g. 1.3kDa), with the majority at ~1kDa (100).

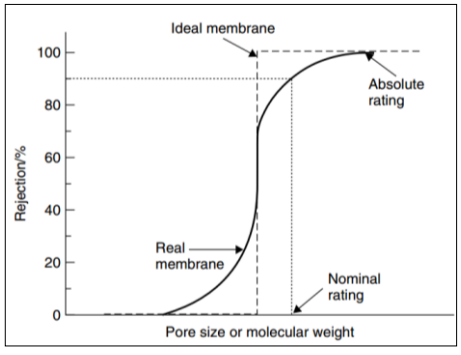

Figure 5.2: Membrane pore size distribution and ratings of ideal and real membranes (100).

This variation in the pore size distribution depends on the membrane fabrication method. Some techniques offers precise control over the pore structure, pore size and pore size distribution while other methods give less control.

5.3 Membrane fabrication technologies.

The functioning of the membrane will depend on its structure as it determines the mechanism of separation. There are two types of structures found in membranes: symmetric or asymmetric. Symmetric membranes mostly have cylindrical pores while the asymmetric membranes are characterized by a non-uniform structure (102). Based on the fabrication method, a membrane can also have different types of pore structure. Figure 5.3 shows a schematic diagram of various pore morphologies commonly observed in separation membranes. There are pores which are cylindrical and run straight through the membrane while other pores are tortuous, consisting of twists and turns, and of irregular diameter.

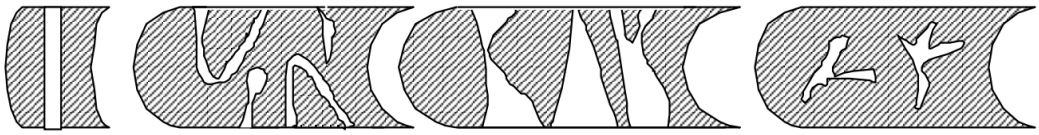

Figure 5.3: Schematic diagram of different pores types in separation membranes (103).

The most commonly used techniques for preparation of polymeric membranes include phase inversion, interfacial polymerisation, stretching, track-etching and electrospinning. Herein we discuss the track etch method and phase inversion method.

5.3.1 Track etch membranes

Track etch membranes are symmetric membranes and offer distinct advantages over conventional membranes such as phase separated membranes (discussed in section 5.3.2) due to their precisely determined structure. Their pore size, shape and density can be varied in a controllable manner so that a membrane with the required transport and retention characteristics can be fabricated.

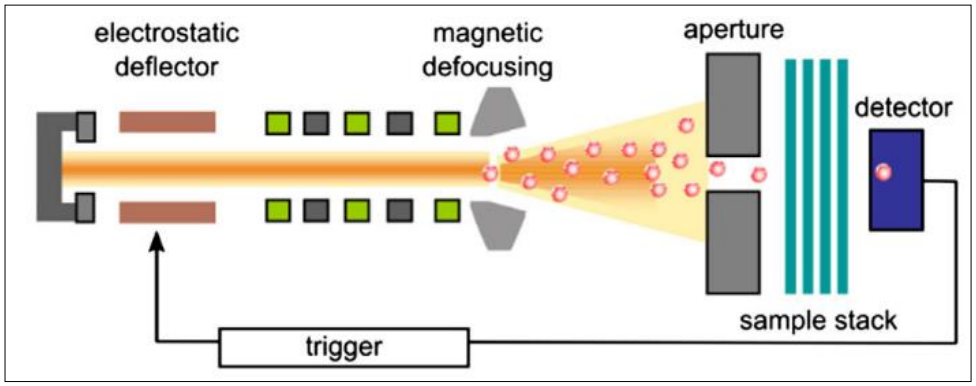

Figure 5.4: Schematic showing single ion-irradiation setup used to fabricate track etched membrane (104; 105)

Track etched membranes consist of a thin polymer foil with channels that run straight from the top surface to the bottom surface. The process of track etch membrane fabrication can be seen in Figure 5.4. A nonporous polymer film is first irradiated with energetic heavy ions leading to the formation of linear tracks across the width of the polymer film. These ion tracks are then chemically etched to transform the latent track into a hollow channel (106). Chemical etching is the pore-size-determining and pore-shape-determining stage of the track etch method (104; 105; 106). The use of accelerated heavy ion beams in combination with beam deflectors makes it possible to vary the angle distribution of pore channels and pore lengths. The pore shape can be made cylindrical or conical, or can have a funnel-like or cigar-like geometry.

Typically for track etch membranes, the film material is polycarbonate (PC), polyethylene terephthalate (PET) or polyimide. The pore size of the track etch membranes can be easily varied from 0.01 to 30μm while pore densities ranging from $1x10^4$ to $6x10^9/cm^2$ can be realized, with a porosity of up to 30%. For a membrane having small pores (e.g. 200nm) the pore density is high (e.g. $5x10^8/cm^2$) while membranes with larger pores (e.g. 10μm diameter) have a low pore density of approximately $1x10^5/cm^2$. This is to maintain the mechanical stability of the membrane (107). Xue et al (108) investigated nanopores which were prepared in thick PET foils. They managed to make a single nanopore membrane of known size by controlling the aperture in the beam path (Fig. 5.4). The foil was first bombarded with a single U-235 particle with energy of 11.4 MeV/u to form a latent ion track. After being irradiated with UV rays for 1 h, the foil was immersed in a 5M NaOH solution at room temperature. Since the etching rate in the ion track region is much faster than that in the bulk material, a cylindrical pore with a radius in the nanometre scale was fabricated in each foil.

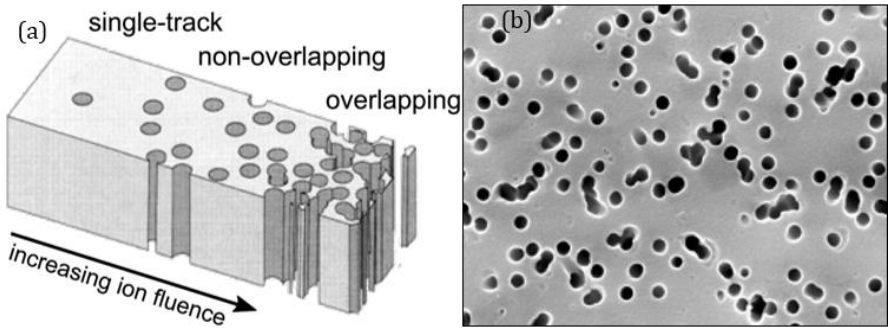

Figure 5.5: (a) Illustration of track etch membrane: single-track channel, multiple non-overlapping channels and multiple over-lapping channels (105) and (b) Top view of a track etch PETE membrane from Sterlitech (109).

The pore size, pore size distribution and pore density of typical track etch membranes are easy to measure with scanning electron microscopy because the pores tend to be >50 nm wide and run straight through the membrane.

5.3.2 Phase inversion membranes.

Ultrafiltration membranes are generally asymmetric or anisotropic membranes produced from a single or multiple polymers. UF polymeric membranes are usually prepared through the so-called phase inversion process starting from a concentrated polymer solution which is first cast on a support material as a thin film and then immersed in a liquid (water) which is miscible with the solvent but leads to precipitation of the polymer. This enables one to manufacture large-area porous membranes in the form of flat sheets, but hollow fibres are also possible. This technique offers the possibility of controlling to some extent the structure and the porosity of the membrane by means of simple variations of the preparative parameters (100). Anisotropic membranes are preferentially used because of their high separation efficiency. The structure of the phase separation membranes are more complex because membranes were obtained from gel (103). This case is observed in all anisotropic membranes. For example, a polyether sulfone (PES) or regenerated cellulose ultrafiltration membrane are asymmetric membranes (110).

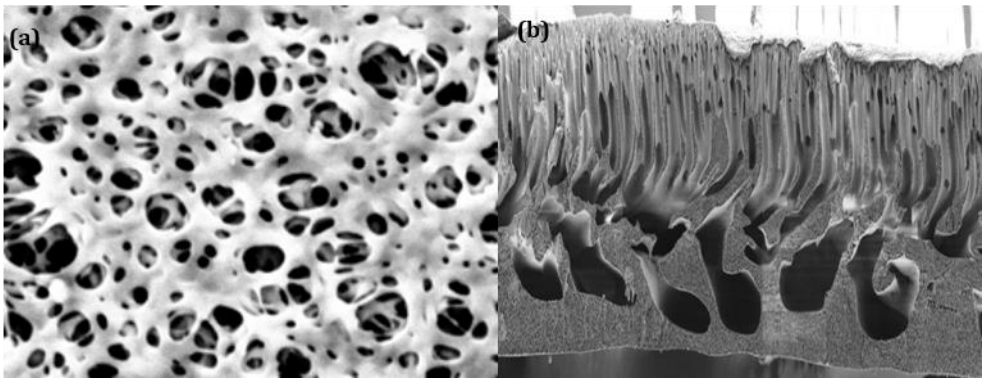

Figure 5.6: (a) Top view of a 30nm PES membrane from Sterlitech Corporation (111) and (b)cross-section of PES membrane. A thin skin layer is present below a thick macroporous support layer (112). Scale for the images are not provided.

Anisotropic membranes prepared by phase inversion consist of a thin skin layer that contains the smallest pores, which determine the separation performance of the membrane (98). Figure 5.6 depicts a top view and a cross-section of such an ultrafiltration membrane. The skin layer is a dense top layer responsible for the separation characteristics of the membrane and for the much higher transmembrane flux compared to the underlying mesh structure (113). The size distribution of the pores present in the skin determines the selectivity of the membrane while the skin thickness co-determines the permeability of the membrane (99; 114). Below the skin layer, there exists a relatively open microporous mesh structure which is basically for support of the membranes. This results in a membrane which has both satisfactory high fluxes and a good mechanical properties. Most of the pores in the asymmetric UF membranes are aligned normal to the membrane surface (115). The skin layer is usually around 100-200nm in thickness (98; 114; 116)

As the skin layer is very thin its porosity or surface porosity is in the order of a few percent (98; 117). The pore size and the surface porosity can be varied in the membrane by varying the concentration of the polymer solutions and solvents. For example, Ghoshb et al. (118), described the preparation of five UF membrane samples using different solvents and additives, including dimethyl formamide (DMF) and N-methyl pyrolidone (NMP). The cross-sectional morphology of a PES ultrafiltration membrane showed tear-shaped elongated macrovoids that extend from the compact skin layer towards the permeate side, as shown in Figure 5.6b. The lower porosity skin layer was found to dominate the transport resistance of the composite membrane (112).

Pore size, pore density and porosity of anisotropic UF membranes can be measured using several methods, including the bubble pressure method, the liquid displacement technique, mercury porosimetry and thermoporometry. The bubble pressure method and mercury porosimetry are based on determining the pressure necessary to blow air through a water-filled or non-wetting liquid such a mercury through a porous membrane. For UF membranes with pores that are small, high pressures (about 1OMPa) are necessary. At these pressures the membrane matrix may deform and the structure may be altered, which could consequently lead to erroneous results. The liquid displacement technique has the disadvantage that polymer membranes may swell or shrink in the alcohol-water system. Thermoporometry is based on the microcalorimetric analysis of solid-liquid transformations in porous materials, but is not suitable for swelling membranes

The thickness of the skin layer is usually determined by scanning electron microscopy (SEM), but the size of the pores in the skin layer is too small to be imaged with SEM. Another complication, from an imaging perspective, is that there is a gradient in the pore size from the top of the skin layer towards the porous sublayer (114).

5.4 Imaging the membranes

The mass transfer theory summarized in Chapter 3 highlights the importance of the thickness and the porosity of the membranes and the tortuosity of the pores for the separation efficiency of the membrane. In this experimental section, electron microscopy was performed to gain insight in the thickness and the pore size of the commercially sourced membranes. The porosity of these membranes was determined experimentally as described in section 5.5.

5.4.1 SEM of membranes.

A scanning electron microscope scans samples with focused beams of electrons. The electrons interact with the atoms in the sample, producing signals which can be detected and contains information about the samples surface topography.

Membranes were first soaked in water and dried properly to remove any water molecules present in the membrane using an oven. Zeiss EVO LS25 with LaB6 thermionic electron gun was used for obtaining the images of the membranes. The membranes were sliced into small pieces to image. It was noticed that, using such membranes failed to provide good results. Hence membranes were coated prior to imaging. The membranes were sputter coated with Gold/palladium to make the surface more conductive. Images produced with a SEM elucidate the structure of particular membranes as well as the thickness of the surface layer of asymmetric membranes. SEM images of the track etch membranes and the UF membranes produced desired results. Membranes having pore sized 1µm, 200µm and 100µm were chosen among the track etch membranes for microscopic images. From the SEM image of 1µm pore sized membrane Figure 5.7, the pore density was found to be around $8x10^6/cm^2$ to $1x10^7/cm^2$. This is approximately similar to the pore density and pore size reported from the specification sheet on the membrane (107). Hence the pore density, pore size are used in future calculations and these values will be discussed later in section5.6. The image also clearly shows the well-structured pores in the membrane surface obtained by track etch process. UF membranes were then scanned to determine the pore size if possible along with its morphology.

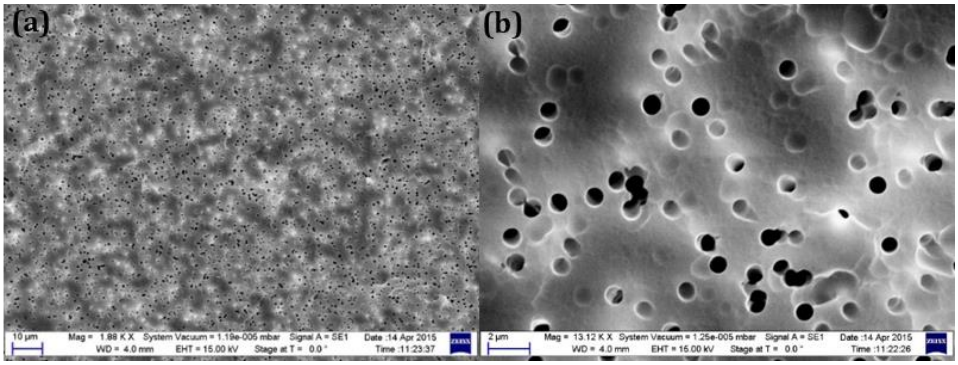

Figure 5.7*:* SEM images of the commercially sourced track etch membranes with a specified pore size of 1µm. Non-overlapping and overlapping pores can be observed. Electron micrograph obtained by Dr. Sumit Kalsi, Nano group, University of Southampton.

Next an ultrafiltration membrane of regenerated cellulose, prepared by phase inversion, were imaged. From Figure 5.8 a & b it can be noted that the membrane is thin and has a fibrous support material underneath it. The fibrous support material has pores of 40-60µm. The membrane without the fibrous support material is very fragile but the fibrous support material can be peeled off to obtain a small bit of the phase inversion polymer membrane itself, and images of this are shown in Figure 5.8 c-f. From the figures, it is obvious that the UF membrane

has a thin skin layer in which the pores are indistinguishable using SEM because the specified MWCO value of 5000Da would equate to a pore size of approximately 1nm, which is close to the resolution limit of SEM. However, the sublayer showed pores of about 100-400nm. But since the skin layer is the part of the membrane that determines the filtration/separation performance, these sub-layer pores do not play a role in the separation efficiency.

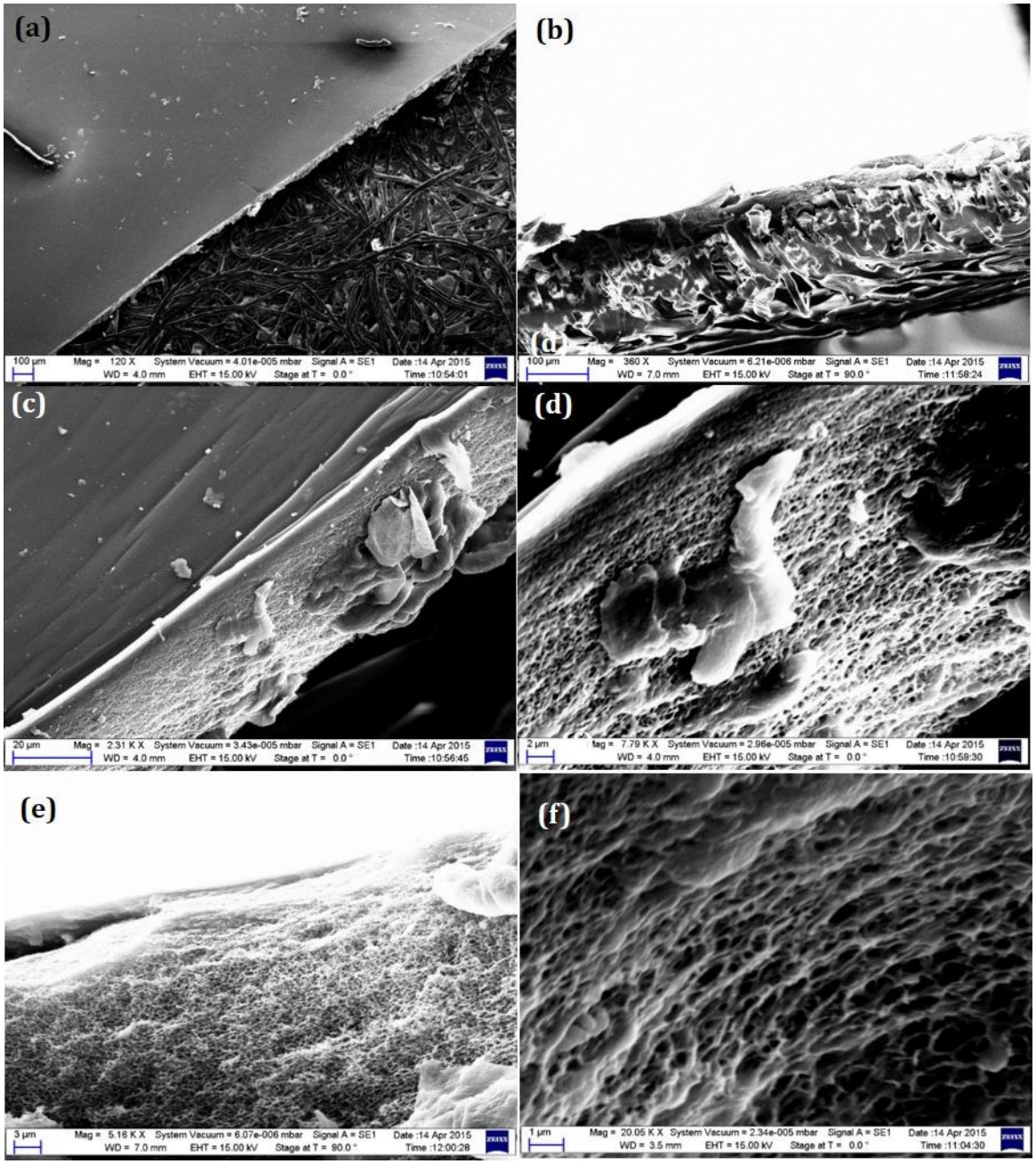

Figure 5.8: SEM images of the Regenerated cellulose UF membrane. (a) Membrane structure with fibrous support material, (b) Side view of the membrane showing the thickness of the support material (~160µm) and the membrane (~20µm), (c) Close up of the membrane which shows no noticeable pore on the surface, (d) zoomed in section of the membrane showing the think skin layer at the top and mesh like bottom sublayer in the membrane and (e) and (f) Mesh like structure of the sublayer in an ultrafiltration membrane. Sublayer exhibits pore of size ~200nm. Electron micrograph obtained by Dr. Sumit Kalsi, Nano Group, University of Southampton.

Determining the pore size of the skin layer of an ultrafiltration membrane prepared by phase inversion is very difficult and has been attempted in only a few studies. A commonly used protein to obtain the MWCO cut-off value of these membranes is cytochrome c, the diameter of

which is approximately 3nm (119). Nripen et al (120), used field emission SEM to visualize the pores in the skin layers of different UF membranes. They estimated the skin layer pore size of 100, 300 and 1000 kDa membranes to be 5, 15 and 30nm, respectively. However, for desalting of (biomedical) protein samples, we are interested in UF membranes with a substantially smaller MWCO, the skin layer pores of which can hence be expected to be smaller than 5nm in diameter.

5.4.2 TEM of membranes.

Transmission electron microscopy (TEM) is an electron microscopic technique in which a beam of electrons is transmitted through an ultra-thin specimen, interacting with the specimen as it passes through. An image is formed from the interaction of the electrons transmitted through the specimen. TEM has resolution up to 0.3-0.5nm and therefore is particularly useful in investigating fine morphology porosity and low thickness of the skin layer. The preparation of cross-sections for the transmission electron microscope (TEM) requires a different and more complicated procedure. a section thin enough (200nm or less) for electrons to penetrate is cut by glass or diamond knife with the aid of an ultramicrotome.

Figure 5.9: Hitachi H7000 TEM in the Biomedical Imaging Unit, University of Southampton.

Figure 5.10: Ultramicrotome used for sectioning the sample

Dr. Anton Page of the Biomedical Imaging Unit, University of Southampton prepared the membranes and carried out the TEM imaging process. The membrane was first placed directly

without any preparation or modification in the TEM and this method failed to obtain any noticeable image of the pores in the membranes. This is because the membranes were of about 120μm in thick. For TEM, the sample needs to be approximately 200nm. In order to cut the sample at a precise size for the TEM, the membranes were first placed in an epoxy resin which was then sectioned using an ultramicrotome. Ultramicrotome is a tool used for cutting materials into very thing sections. From the Figure 5.11, it can be noticed that knife marks from the microtome are present on the membrane. This is one of the main drawbacks of using a TEM especially in case of an UF membrane where the pores are randomly distributed.

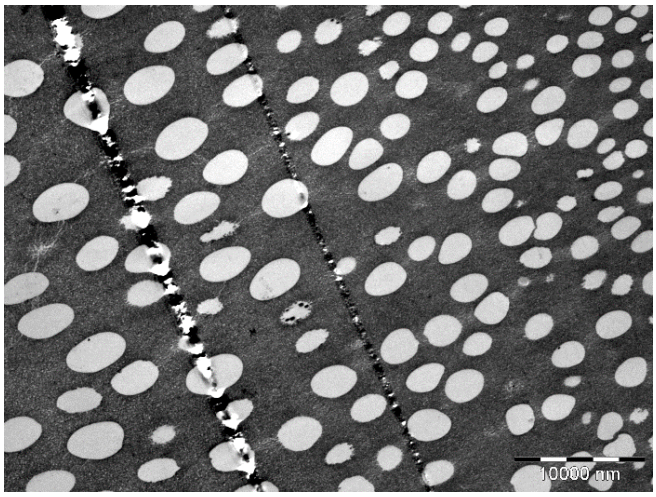

Figure 5.11: TEM of a track etch membrane with a nominal pore size of 400nm. Pores of ~200nm-400nm were observed. The linear features are marks from the ultramicrotome blade. Electron micrograph obtained by Dr. Anton Page, Biomedical Imaging Unit, University of Southampton.

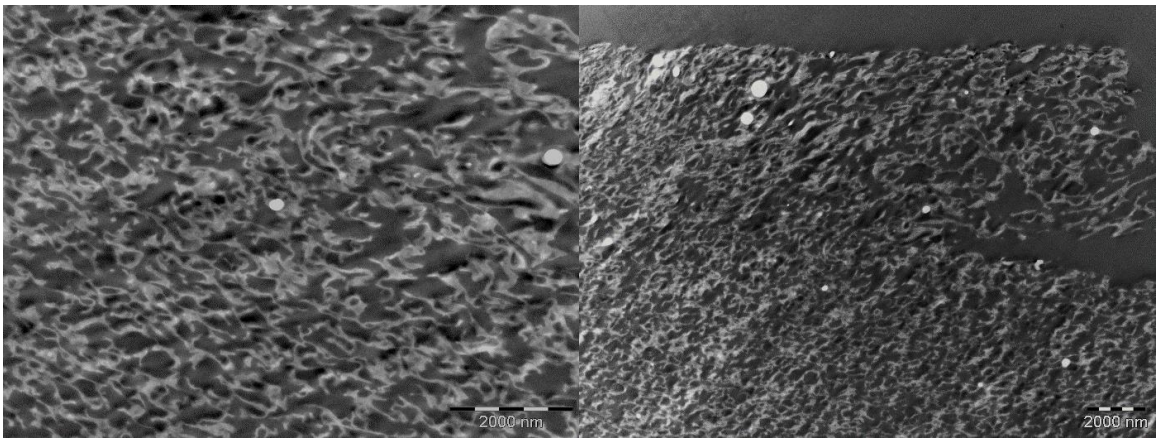

Figure 5.12: TEM images of a regenerated cellulose membrane. Ultramicrotome samples slices of 200nm thickness were imaged. Pores of size ~100nm-200nm are visible, which correspond to membrane sub-layer segments. Electron micrograph obtained by Dr. Anton Page, Biomedical Imaging Unit, University of Southampton.

5.4.3 Problems with electron microscopy

The investigation of the ultrafiltration membranes using electron microscopy is a delicate and difficult task compared to the track etch membranes for a number of reasons. The resolution and depth of field of the microscopy techniques and the structure of the sample itself limit the suitability of SEM and TEM. Preparing the microscopy samples and interpreting and processing the images is time consuming, while sample preparation procedures may also

introduce artefacts, especially with ultramicrotome slicing. A major disadvantage of the UF membrane structure in terms of electron microscopy imaging is that the pores in the skin layer at the surface of the membrane are not always connected to the porous network of the sub-layer mesh structure. Moreover, the resolution of SEM is not sufficient to image the very small skin layer pores (<< 5nm) of the UF membranes with a MWCO suitable for desalting protein samples, while cutting exactly this skin layer out of an UF membrane as a TEM cross-section is a difficulty in itself (99; 100)

5.5 Calculating the porosity of the membranes.

Porosity is defined as the fraction of void space (pore) volume with respect to the total volume of a membrane. It is an important parameter that influences the performance of membrane separation. The mass transfer coefficient of a membrane given by Equation 3.9 in the previous chapter highlights this; the mass transfer coefficient is directly proportional to the porosity.

Observations made by Ravish et al (121), also showed that porosity is the important factor. Electrical conduction across track-etch membranes with different pore size and pore density having same porosity showed nearly identical results. Typical values of porosity ranges from 0-1. For e.g., for a track etch membrane with a pore size 50nm (pore radius r_p=25nm) and Pore density $6x10^8/cm^2$, would have a porosity of 1.18%. Some of the other common track etch membranes with specifications are mentioned below.

Table 5.3: Nominal properties of track etch membranes. Pore size and pore density are provided by the supplier and porosity was calculated (107)

Pore radius (r_p) nm	**Pore Density (pores/cm^2)**	**Porosity (%)**
25	$6x10^8$	1.18
50	$6x10^8$	4.71
100	$5x10^8$	15.7
200	$1.5x10^8$	18.84
500	$2.2x10^7$	17.27

Table 5.3 illustrates that the porosity of track etch membranes decreases with decreasing pore size while the pore density increases. However, for UF membranes it is difficult to obtain these values. UF membranes of different MWCO (1kDa, 5kDa, 10kDa, 100kDa & 300kDa) were chosen. Cuperus et al. (99) stated that UF membranes would have a pore diameter range from 50nm down to 2nm while the porosity ranges from 0.1-10%. Similar observations on pore size were made by Nirpen et al. who estimated that PES membranes of 100kDa, 300kDa and 1000kDa have a pore size of 5, 15 and 30nm, respectively (120). In this section, two methods for obtaining an approximate porosity value for the UF membranes that have been used for the

microvolume dialyzer are discussed. These methods require a reference membrane with known porosity, for which the 50nm track etch membrane was chosen.

5.5.1 Theory of the electrical measurement of porosity

The electrical porosity of the membrane was estimated with a conductometric method as reported by Kumar et al. (122; 123) and Ravish et al (121). They sandwiched a track etch membrane between two chambers filled with an electrolyte solution to study the transport of this electrolyte through the membrane pores. The electrical conduction of electrolyte thorough the cylindrical pores of a track etch membrane follows Ohm's law. The resistance offered by the pores filled with the electrolyte to transport the electrolyte ions is determined by V-I measurements. According to Ohm's law:

$$V = IZ \qquad \textit{Equation 5.1}$$

Where V- Voltage applied (Volts)

I-Current measured (Ampere)

Z-Impedance (ohm)

For DC measurements Z is replaced by R_t- resistance (ohm) and assuming resistance offered is high compared to the capacitance from the membrane.

$$R_t = \frac{V}{I} \qquad \textit{Equation 5.2}$$

The membrane pores can be represented in a circuit diagram as shown in Figure 5.13

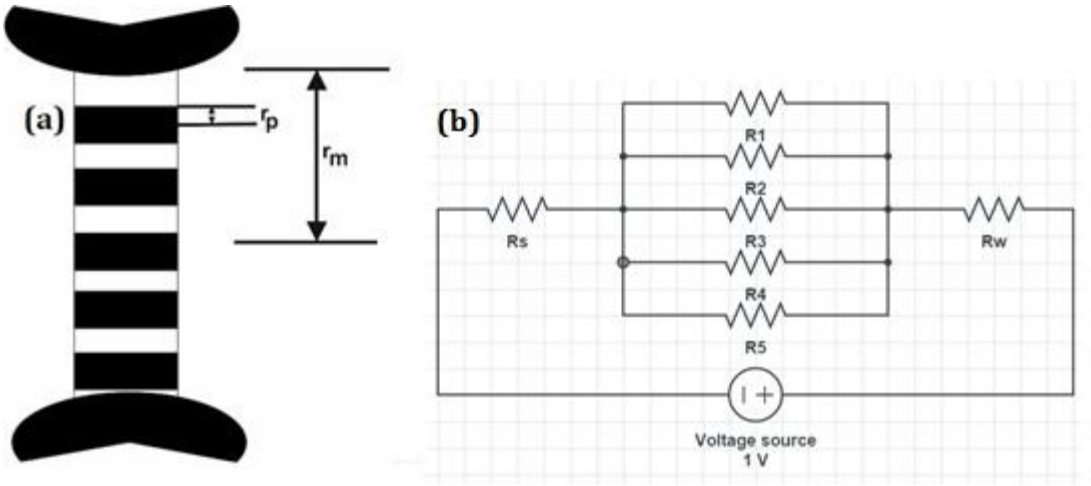

Figure 5.13: (a) Representation of membrane pores used for the conductometric method. (b) Electrical representation of the membrane pore structure.

Where r_p is the radius of the pores in the membrane and r_m is radius of the membrane exposed to the electrolyte solution. The above membrane can be represented electrically as shown

above. The resistance R_1 offered by a single pore of length l and cross sectional area $A_p=\pi r_p^2$ where r_p is the radius of the pores in the membrane is given by

$$R_1 = \rho \frac{l}{Ap} \qquad \textit{Equation 5.3}$$

here ρ is the specific resistance of the electrolyte used.

The resistance offered by the total number of pores 'N' parallel to each other is

$$R_t = R_s + R_w + \frac{R}{N} \qquad \textit{Equation 5.4}$$

R_6 and R_7 are negligible compared to R/N. Hence

$$R_t = \frac{R}{N} = \rho\left(\frac{l}{NAp}\right) \qquad \textit{Equation 5.5}$$

The value of N can be replaced by pore density 'n' and $A=\pi r_m^2$ is the area of the membrane exposed to electrolyte and r_m is the radius of the membrane exposed to the electrolyte.

$$R_t = \rho\left(\frac{l}{nAAp}\right) \qquad \textit{Equation 5.6}$$

Substituting the known values we get

$$r_p{}^2 = \rho\left(\frac{l_m}{n\pi^2 r_m{}^2}\frac{I}{V}\right) \qquad \textit{Equation 5.7}$$

Porosity is defined as the ratio of volume of void spaces to the total membrane volume.

$$P = \frac{n\pi r_p{}^2 l_p}{\pi r_m{}^2 l_m} \qquad \textit{Equation 5.8}$$

Where l_p is the length of the pore and l_m is the length (thickness) of the membrane. Since $l_p=l_m$.

$$P = \frac{n r_p{}^2}{r_m{}^2} \qquad \textit{Equation 5.9}$$

Substituting P into Equation 5.7

$$P = \frac{\rho l_m G}{r_m{}^4} \qquad \textit{Equation 5.10}$$

Where G=I/V is the conductance (mho or Siemens 'S')

Equation 5.10 is the general equation for determining the porosity of a track etch membrane. The equation also has an unknown variable ρ which can be cancelled out by taking a ratio between two membranes where one membrane is of known porosity (P_k) and the second membrane of unknown porosity (P_u).

$$P_k = \frac{\rho l_{mk} C_k}{r_{mk}{}^4} \qquad \textit{Equation 5.11}$$

And

$$P_u = \frac{\rho l_{mu} C_u}{{r_{mu}}^4} \qquad \textit{Equation 5.12}$$

Where the subscripts 'k' and 'u' stands for known and unknown parameters of the membrane.

$$P_u = P_k \frac{l_{mu} C_u}{l_{mk} C_k} \qquad \textit{Equation 5.13}$$

Substituting the experimentally determined value of the conductance, the known porosity and thickness of the reference membrane, and the known thickness of the membrane under investigation, the porosity value of the membrane under investigation can be determined.

5.5.2 Experimental determination of porosity by electrical measurements

In order to use the above mentioned method, a measurement set up (Figure 5.14) was constructed from Tektronix PWS4205 Bench Power Supply 0-20V, a multimeter, a camera to record the multimeter's current readings, Ag/AgCl electrodes and 0.8mm Ag electrodes were used for measurements and sodium chloride was used as an electrolyte for all measurements. Ag/AgCl electrodes were prepared by taking clean Ag electrodes of length 5cm and placing them in a 1M Ferric Chloride solutions for about 10mins. Solutions of sodium chloride electrolyte of various concentrations (10μM-1M) in DI water were tested in order to select an appropriate electrolyte concentration for the measurements.

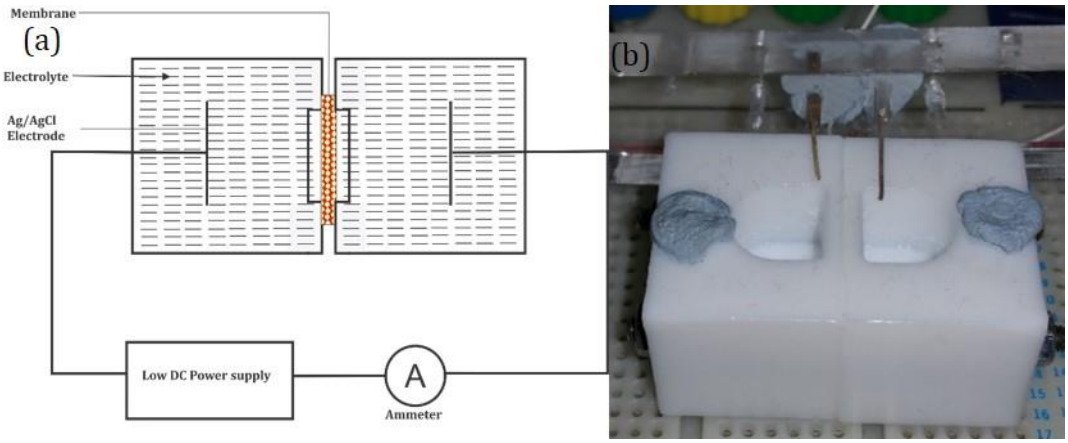

Figure 5.14: (a) Schematic diagram of the experimental setup for the conductometric measurements of porosity of the membranes. (b) Chambers for electrolyte solution, with sandwiched membrane, and Ag/AgCl electrodes.

A track etch membrane with 1μm pore size was clamped between two aqueous chambers. The chambers were made from Delrin and had a circular opening of 5mm in diameter. Each chamber was filled with 100mM NaCl solution (~1mL volume) such that approximately 20mm^2 of each side of the membrane was in contact with the electrolyte solution. One Ag/AgCl electrode was inserted into each chamber and a low voltage of 0.1V was applied to the electrodes. The resulting current value was recorded until a relatively stable current was observed, as shown in Figure 5.15. At this point the polarity of the electrodes was reversed and

the current was again monitored until the current stabilised. Then, to avoid depletion of the Ag/AgCl electrodes, the electrodes were replaced with a new pair of electrodes, the voltage was changed to a higher value and the current measurements were repeated. In this manner current values for potentials of 0.1V, 0.2V, 0.3V. 0.4V and 0.5V were obtained.

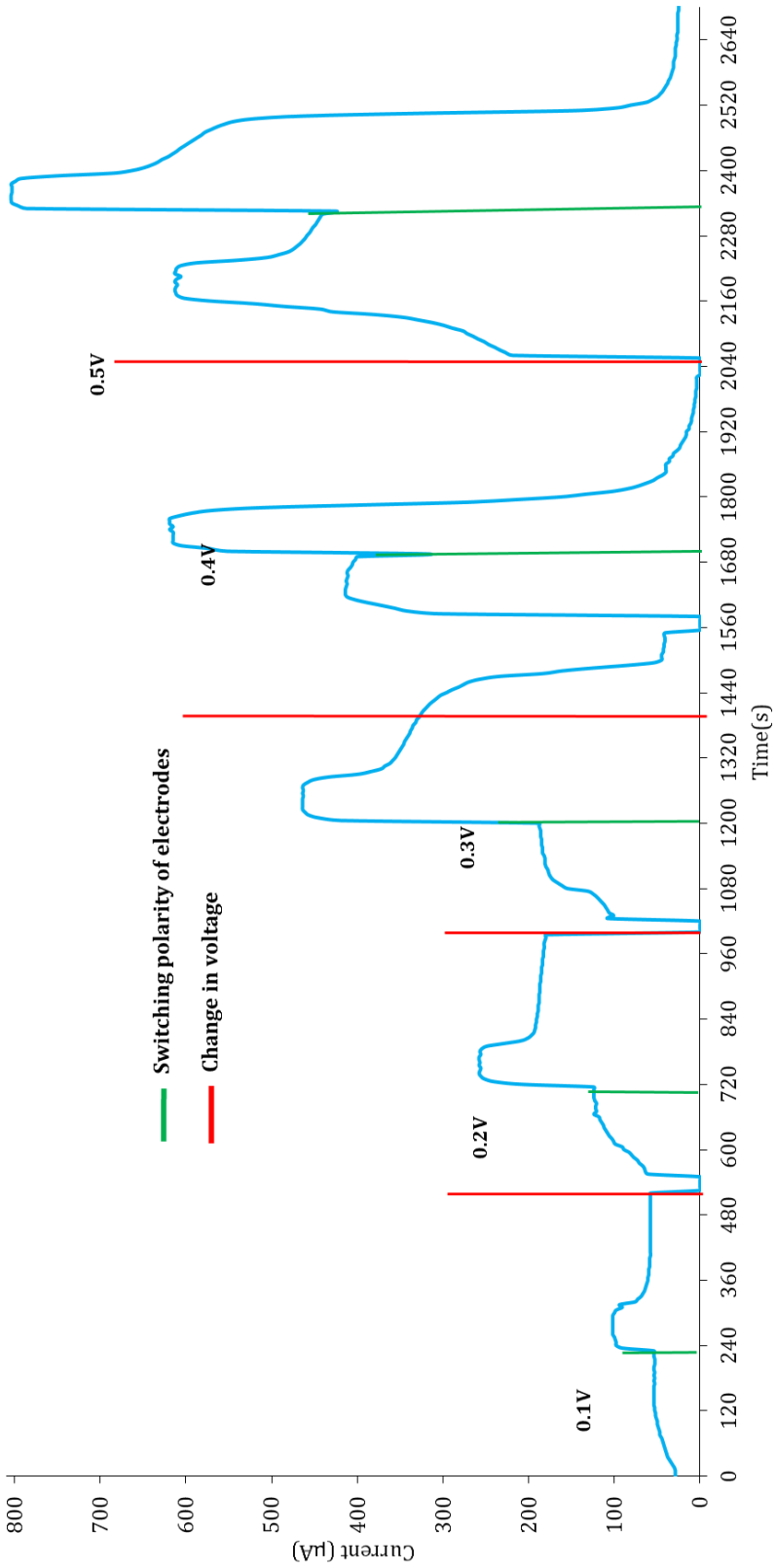

Figure 5.15: Live electrical measurements using membranes of 1 µm pore size. Stable current is not measured instantaneously especially at low voltages.

From the data shown in Figure 5.15, it can be noticed that the current increases slowly towards a stable current regime when a low voltage is applied, while at higher voltages the stable current regime is reached quickly. When the polarity of the electrodes is reversed by switching the power supply leads, the current value, for each applied potential, increases substantially, immediately reaching a stable value. This effect might be due to the relaxing of the concentration polarization at the surface of the membrane surface or in the pores. For each potential, high current values cannot be maintained for a prolonged period of time; the eventual reduction in current with time, observed for each applied potential, is due to depletion of the Ag/AgCl electrodes.

Track etch membranes with a pore size of 50nm were used as a reference membrane for the conductometric determination of porosity for the UF membranes. First, different electrolyte concentrations were measured to identify a suitable current range for an applied potential of 1V. The electrodes were replaced with a new pair for each solution with a different NaCl concentration. From Figure 5.16 it can be observed that the current value for low electrolyte concentrations (10µM-1mM) is very small (~1µA), while for higher concentrations such as 1M the current value can only be maintained for a short time due to electrode depletion. Hence an electrolyte concentration of 10mM, which provided a relatively stable current for a satisfactory period of time, was chosen for subsequent experiments with other track etched membranes and with the UF membranes.

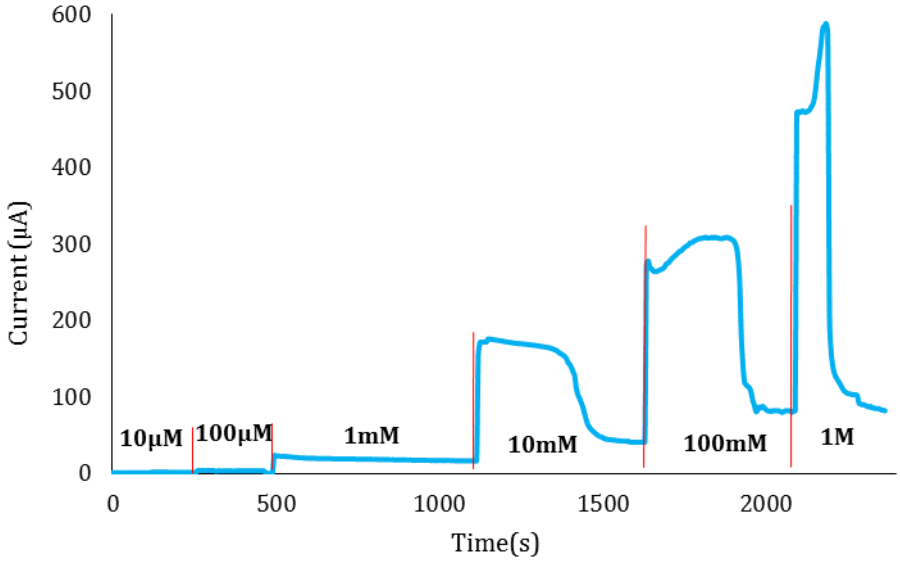

Figure 5.16*:* Live recording of V-I relationship for different electrolyte concentrations for a membrane with 50nm pore size for a constant applied voltage (1V).

To verify the electrical conductance method for the determination of porosity, track etch membranes with 400nm pores but with different, but known, porosity and thickness were employed. The membrane designated as A has a nominal porosity of 0.5% while membranes B and C have a nominal porosity of 12.56%. Membranes A and B have a thickness of 12µm while the thickness of membrane C is 23µm. The values of pore size, pore density and thickness of

the membranes were provided by the supplier and porosity was estimated from them. The V-I relationship for these three membranes was determined and is shown in Figure 5.17. It is obvious from the figure that the conductance measured for membrane A is lower than the other membranes of higher porosity and at the same time the conductance of thicker membrane C is lower than A. This clearly shows that porosity and thickness of the membrane are important factors which would determine movement of ions across the membrane. This agrees with the results obtained by Ravish et al (121) which shows the importance of porosity in electrical conduction.

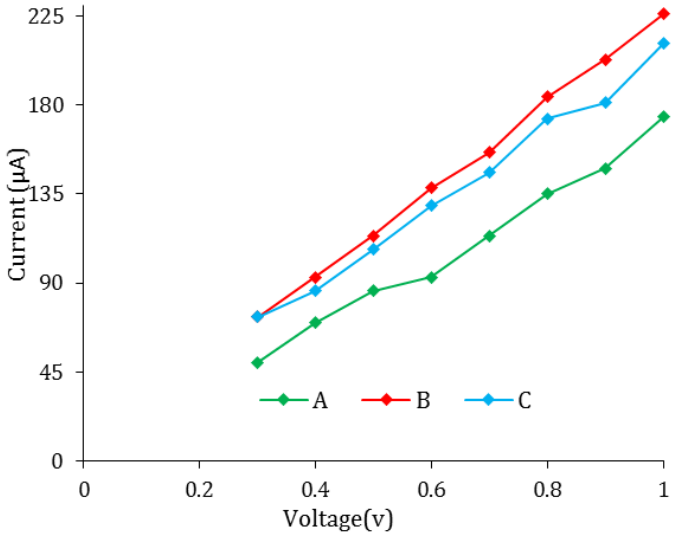

Figure 5.17: Electrical measurements in 10mM NaCl solution for membranes of pore size 400nm track etch membranes and different pore density. A- pore density-$4x10^6/cm^2$, membrane thickness-12µm, B-pore density-$1x10^8/cm^2$, membrane thickness-12µm and C-pore density-$1x10^8/cm^2$, membrane thickness-23µm.

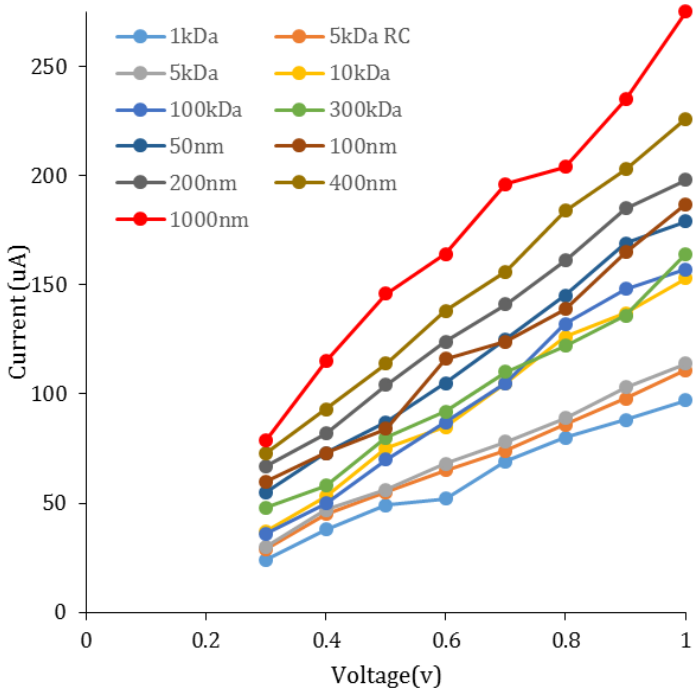

Figure 5.18: Electrical measurements of current using the conductometric method with 10mM NaCl solutions for track etch membranes of known porosity and ultrafiltration membranes of unknown porosity. Membranes with larger pores and high porosity give a higher conductance (V/I).

The electrical measurements were next performed with a larger set of membranes, including the ultrafiltration membranes of unknown porosity. The experimentally determined V-I relationships are shown in Figure 5.18. The slope of these V-I curves give the average electrical conductance of each membrane, which is shown in Figure 5.19, where the membranes are ordered with respect to their (expected) pore diameter.

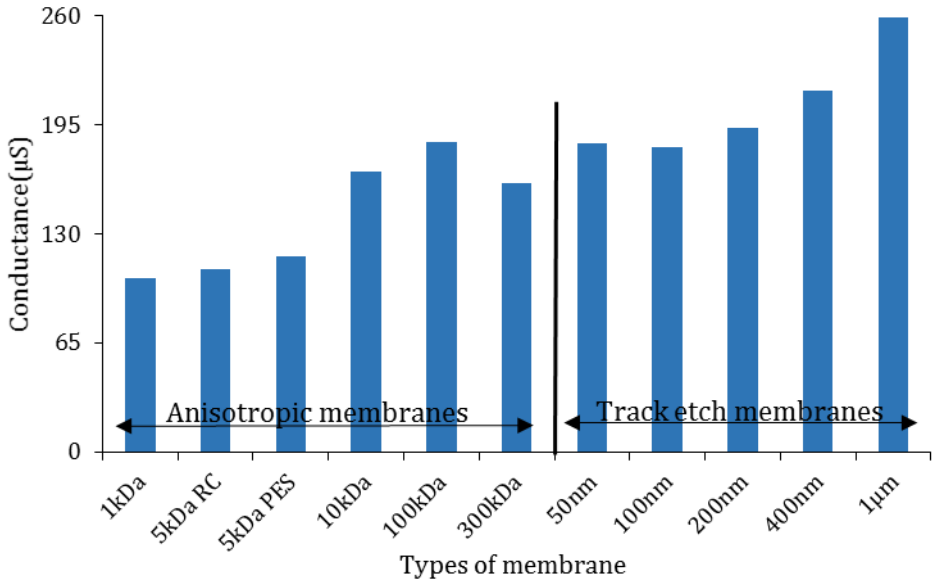

Figure 5.19: Conductance values obtained from electrical measurements in 10mM NaCl solution for anisotropic ultrafiltration and isotropic track etch membranes.

Table 5.4: Conductance and porosity value obtained by electrical measurements for different UF membranes.

Membranes	**Conductance(µS)**	**Membrane Thickness(µm)**	**Porosity (%)**
1kDa	103.69	20	0.53
5kDa RC	108.93	20	0.56
5kDa PES	116.31	20	0.59
10kDa	166.95	20	0.85
100kDa	184.86	20	0.95
300kDa	160.24	20	0.82
50nm	183.57	25	-

From the conductance values obtained for the ultrafiltration membranes (see Table 5.4), together with the conductance value of the reference membrane (the track etch membrane with 50nm pore size), the porosity of the UF membranes was then calculated as outlined in section 5.6.1 (Equation 5.13). The thickness of the ultrafiltration membranes was taken as 20µm, i.e. the thickness of the support layer was not taken into account and the tortuosity of the UF membranes was assumed to be 1, representing a cylindrical pore geometry. The values of the conductance measured, along with the values of the reference 50nm membrane, the porosity of the UF membranes were obtained. The membrane thickness used in the calculation

corresponds to the actual thickness of the membrane excluding the underlying support material. The thus obtained porosity values are also listed in Table 5.4. Comparing the conductance values and substituting the known parameters in Equation 5.13, it was noted that the porosity values varies around 10% from the specifications of the membranes. Similar variations were noted by Kumar et al their work (123). The optically measured values of the pores were found to be 15% higher than the values determined using similar method. This variations is attributed to the fact that all the pores may not be cylindrical as expected. There is also a possibility of finding overlapped pores. Besides this, the specifications are normally based on microscopic images which gives a measure of the pores on the surface but the equation determines the porosity using conduction measurements through the pores entire length.

Although the above mentioned method is applicable to track etch membrane where the pores are cylindrical, it can be applied to UF membrane in crude approximation to obtain the electrical porosity of the membrane. As opposed to the track etch where the pores are cylindrical and tortuous value is 1, in the UF membrane the pores are full of twist and turns and the tortuous values varies in between 1-2.

The average porosity of the UF membranes obtained by using this method is around 0.5-0.9%

5.5.3 Experimental determination of porosity diffusion

Another method of determining the porosity of the UF membrane is by using the transport mechanism of the solute. Cuperus et al. (99) noted that attempts to correlate membrane structure with membrane performance had little success, except for dialysis performance, where diffusion is the main mechanism. Track etch membranes of known porosity and the UF membranes of unknown porosity were used in static dialysis experiments. A simple device (depicted in Figure 4.8) capable of holding around 100µL of sample (NaCl-150mM) was sealed with a membrane and placed on a bulk phase of 200mL DI water. The diffusion of salt across each of the investigated membranes into the water phase resulted in a gradual increase of water phase conductivity as measured with a water-phase immersed conductivity meter probe (see section 4.5). Examining Figure 5.20, it can be noticed that the UF membranes gave a sequential increase in the rate with the 1kDa membrane showing a slow increase compared to the other UF membranes: 10, 100 or 300kDa. Among the UF membranes, the 300kDa membrane showed a high salt removal rate from the sample as follows from the rapid increase of the conductivity of the water phase. Also from Figure 5.20, the 5kDa membranes with and without the fibrous support were tested and gave near-identical conductivity values at each time point, indicating that the fibrous support layer of the ultrafiltration membranes does not

contribute to the salt dialysis performance of these membranes. This was expected because, as mentioned in section 5.4, the pores in this support layer are ~50µm wide.

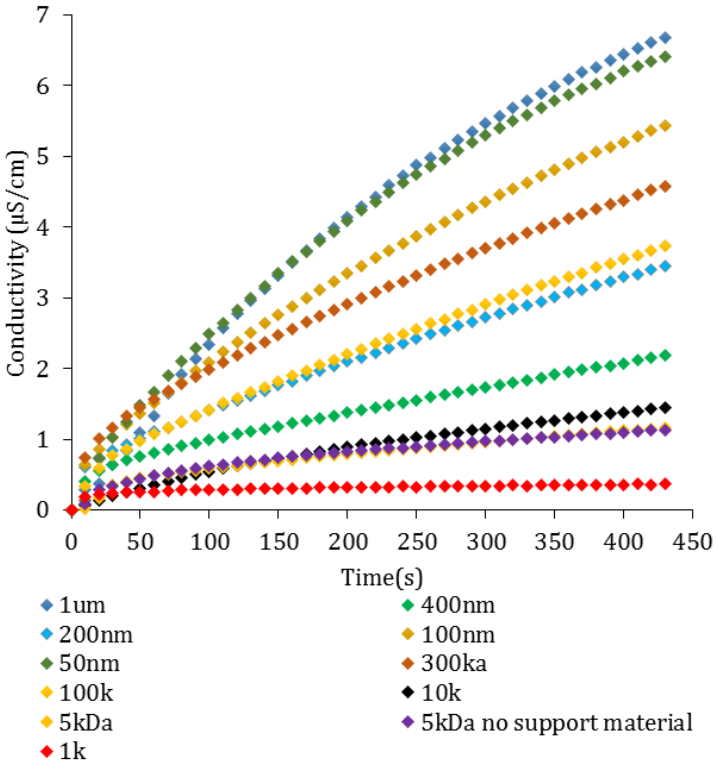

Figure 5.20: Static diffusion measurements for different track etch and UF membranes. The conductivity of the bulk water phase increases with time, indicating a gradual increase in salt concentration of the 200mL volume water phase by salt diffusion over the membrane from a 100µL volume of 150mM NaCl solution.

Membranes of similar MWCO but composed of different polymer species showed similar conductivity values over time, and hence a similar rate of salt concentration increase in the water phase, as shown in Figure 5.21 for a regenerated cellulose membrane and a polyethersulfone membrane with a nominal MWCO of 5kDa.

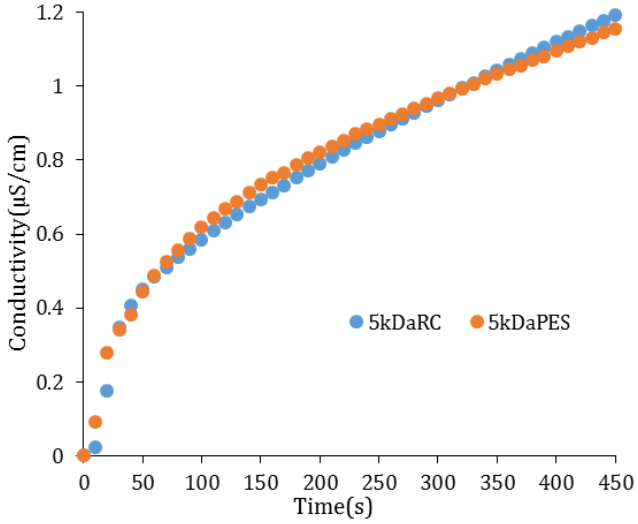

Figure 5.21: Static diffusion measurements for two UF membranes with the same nominal MWCO of 5kDa, composed of polyethersulfone or regenerated cellulose. The conductivity of the bulk water phase increases with time in a near-identical manner. The retentate phase is 100µL 150mM NaCl and the dialysate phase is 200mL DI water.

Examining the results of the track etch membranes in Figure 5.20, the rates of conductivity increase and hence the diffusion rates of the salt ions over these membranes, vary in time and are also different for different membranes. For each membrane, a decrease in the rate of salt diffusion over time is expected because the salt concentration gradient between the sample and the water phase decreases. However, comparing the different track etch membranes, it would be expected that the membranes with larger porosities result in a proportionally larger diffusion rate, but this is not evident from the data. For example, membranes with 50nm pores and membranes with 1µm pores in Figure 5.20 showed an identical increase in conductivity although the porosity of these membrane varies by 10 fold.

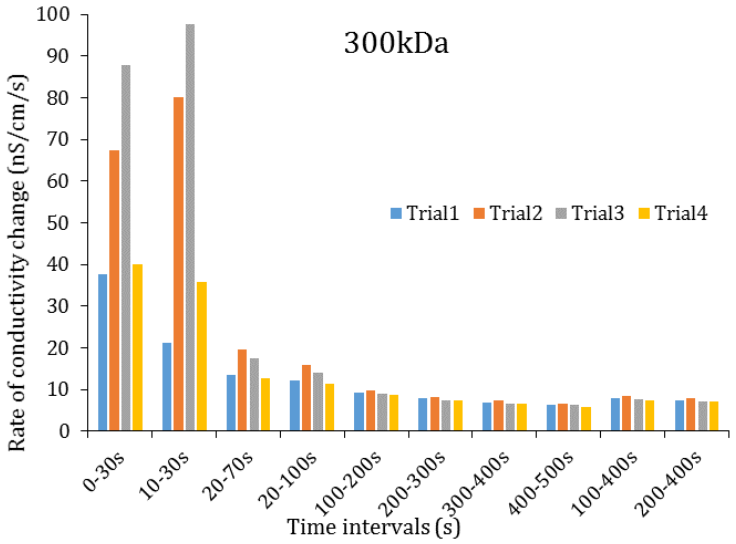

Figure 5.22: Rate of conductivity change for UF RC membranes-300kDa for different time intervals. Initial rate of conductivity change varies considerably in comparison to the later rate.

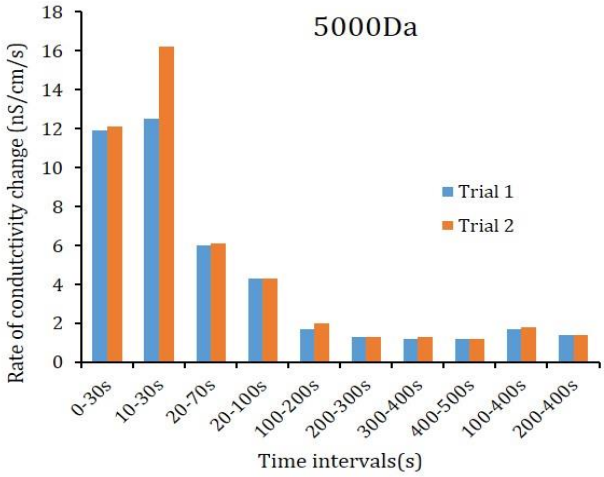

Figure 5.23: Rate of conductivity change for UF RC membranes-5000Da for different time intervals. Initial rate of conductivity change varies considerably in comparison to the later rate.

The values of conductivity measured in the linear range of the measurements are of our interest since the rate of change of conductivity would be ideal for calculations. Comparing the rates of conductivity change for membranes of known porosity with unknown membranes (track etch membrane's) , it is possible to determine the porosity of the unknown membranes.

From the Figure 5.20, it is possible to isolate the rates of salt removal at various time intervals for different membrane as shown in Figures 5.22 and 5.23.

The rate of change in conductivity for various UF membranes at different time intervals are noted and compared with the 50nm track etch membrane of known porosity (ϵ-1.18%). UF membranes of MWCO-1, 5, 10, 100, 300kDa made from regenerated cellulose were selected. Different rates of conductivity change for different membranes can be seen in Table5.5. It can be noticed that the trend in rate changes is common for all the membranes.

Table 5.5: Rates of conductivity change for different time intervals for different membranes.

Time intervals	**Rates of conductivity change for regenerated cellulose UF membranes (µS/cm/s)**					**Track etch membrane**
	1kDa	**5kDa**	**10kDa**	**100kDa**	**300kDa**	**50nm**
0-30s	0.0074	0.0119	0.0066	0.0255	0.0674	0.0367
10-30s	0.0023	0.0125	0.0067	0.0219	0.08	0.0448
20-70s	0.0009	0.006	0.0054	0.0112	0.0196	0.0029
20-100s	0.0008	0.0043	0.005	0.01	0.016	0.0216
100-200s	0.0003	0.0017	0.0035	0.0078	0.0099	0.0166
200-300s	0.0002	0.0013	0.0026	0.007	0.0083	0.0121
300-400s	0.0002	0.0012	0.0022	0.0064	0.0073	0.0089
400-500s	0.0001	0.0012	0.0026	0.0059	0.0067	0.0071
100-400s	0.0002	0.0017	0.0027	0.0071	0.0084	0.0123
200-400s	0.0002	0.0014	0.0024	0.0067	0.0078	0.0104

Comparing the known values of porosity of the 50nm track etch membrane with the different rates of conductivity change from the table above, average porosity of the UF membranes is calculated.

Table 5.6: Porosity calculated from conductivity measurements for different membranes.

Membrane	**Calculated Porosity (%)**
1kDa	0.08
5kDa	0.43
10kDa	0.46
100kDa	1.1
300kDa	1.84
50nm	1.18

From the above table, the porosity of the UF membranes is very small as expected. This corresponds to the surface porosity of the membranes in the skin layer.

5.6 Summary

In this chapter membrane fabrication technologies and membrane morphology have been discussed. Of the membranes employed in this thesis, the microfiltration membranes with larger pores (≥50nm diameter) were fabricated with the track etch method, while the ultrafiltration membranes were made with the phase inversion method. Track etch membranes have well defined cylindrical pores that span the membrane whereas phase inversion membranes consist of a very thin (~200nm) skin layer that contains the smallest pores, with a thicker sub-layer underneath where the irregularly shaped pores are larger. Phase inversion membranes are functionally characterised by the molecular weight of the smallest globular proteins or polymers that are retained by these membranes (MWCO value), rather than by their pore diameter as is the case for the track etch membranes, because the pores in the skin layer are difficult to image, both because of their small size and because of the very small thickness of this top layer. Electron microscopy of the membranes was carried out. SEM imaging revealed the expected track etch membrane morphology and the expected support layer/sub-layer/skin layer ultrastructure of the phase inversion ultrafiltration membranes. TEM imaging confirmed the morphology of track etch membranes and of the sub-layer of phase inversion membranes, but did not succeed in visualising the pores in the skin layer because the required slice could not be obtained with an ultramicrotome. Problems with other methods of determining the porosity of UF membrane is discussed which clearly shows the difficulty in accurately measuring the porosity. Cuperus et al (117) observed the same condition as in the very low porosity of the skin frustrates the accurate determination of the pore size distribution. Conductometric method of porosity determination was formulated from ohm's law which provided a porosity for the UF membrane to be around 0.5-0.9%. Though this method is a crude approximation by not taking into account the tortuous nature of the membrane, the porosity values obtained matches reasonably well with the values obtained by diffusion. Based on dialysis experiments, the membranes were estimated to have porosity of around ~0.1-2%. The values of porosity found using the two methods, matches well with the values of porosity reported for UF membranes (99; 117). Cuperus et al (99) highlighted that the porosity of UF anisotropic membrane is between 0.1-10% and Chen et al (124) from their research on cellulose acetate membrane confirmed the porosity values (ϵ~0.5-0.8%) for UF membranes by osmometry. From all the values obtained the porosity of UF membranes is taken as ϵ~0.5% for all future calculations and reference in this report.

Chapter 6: Mass transfer across the membrane

This Chapter describes experiments to determine the suitability of ultrafiltration membranes for dialysis of salt ions from a protein containing test sample. Salt transfer over the membrane is quantified with conductivity measurements. The salt removal characteristics of different devices for static, quasi-dynamic and dynamic counter-flow dialysis with planar ultrafiltration membranes are then extensively evaluated. For the counter-flow dialyser geometry, a large range of sample and water flow rates is employed and the post-dialysis sample salt concentration is measured for each combination of flow rates. The theoretical desalting performance of this device is subsequently estimated with mass transfer theory, and performance limiting factors, with a focus on the membrane itself, are discussed. Finally, some dialysis experiments are carried out with a hollow fibre membrane.

6.1 Quantification of salt concentrations.

Quantifying the mass transfer of a given species over a membrane defines the performance of that membrane under specific operating conditions of a dialysis device. For salt solutions, mass transfer of the ions can be quantified by conductivity measurements.

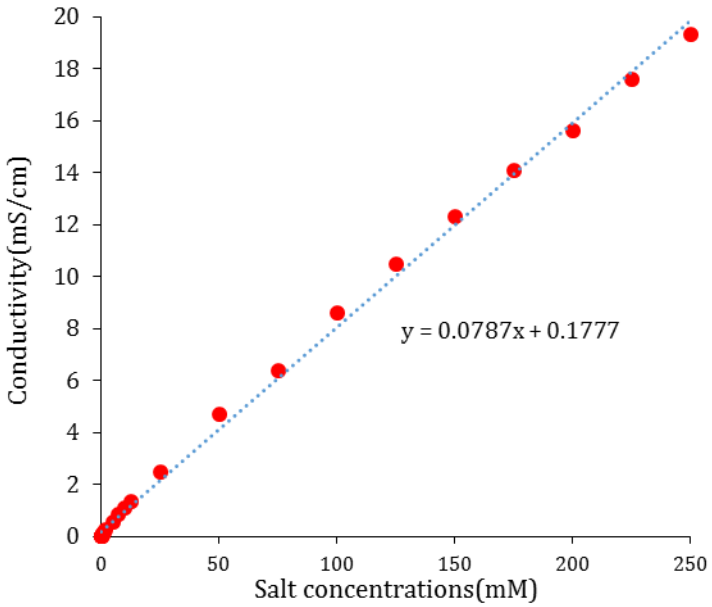

Figure 6.1: Calibration plot (conductivity vs. concentration) for the bench top YSI3200 conductivity meter and the handheld Horiba B-173 conductivity meter.

To correlate conductivity meter readings with the salt concentrations, reference solutions with a wide range of NaCl concentrations in DI water were prepared, and the conductivity of each solution was measured with the Horiba handheld conductivity meter (Section 4.3.2). The obtained data were plotted as a conductivity versus NaCl concentration curve (Figure 6.1) and the parameters of a linear fit were subsequently used to correlate measured conductivity

values of dialyzer retentate or dialysate phases with actual salt concentrations. The smallest salt concentration that can be measured with the Horiba handheld conductivity meter is 10µM below which measurements are impossible. This is because, using the conductivity meter DI water measures a minimum conductivity of 1µS/cm ≈ 10µM in its native state. Similarly, the device has an upper range of 20mS/cm ≈ 250mM above which measurements are possible by diluting the samples. The range mentioned (10µM—250mM) above is the limitation of the device. Although such samples are not used in this research, measurements of such samples can still be made by diluting the samples using DI water. When using the plot to extrapolate the concentration, small range that fits the conductivity value within the plot is taken into consideration.

6.2 Static Dialysis.

Salt diffusion through the ultrafiltration membranes was measured under static dialysis conditions as described in section 4.5. The test sample (100µL of 150mM NaCl + 2 mg/mL fluo-BSA) was kept in a sample chamber made of acrylic and placed in a beaker containing 200mL DI water as the dialysate phase. The primary aim of this experiment was to check the possibility of salt dialysis with a membrane meant for ultrafiltration. The performance test of the ultrafiltration membrane for the use of dialysis can be seen from the initial experiments with the static set of experiment. The conductivity of the water phase at the start of the experiment read 0.55µS/cm, which is the value measured for DI water. Over time, an increase in the conductivity of the water phase was measured with the immersed YSI 3200 conductivity cell, as shown in Figure 4.8 for the 5kDa MWCO RC membrane. The experiment was performed with a static water phase and also with a water phase that was stirred with a rotating magnetic stirrer bar

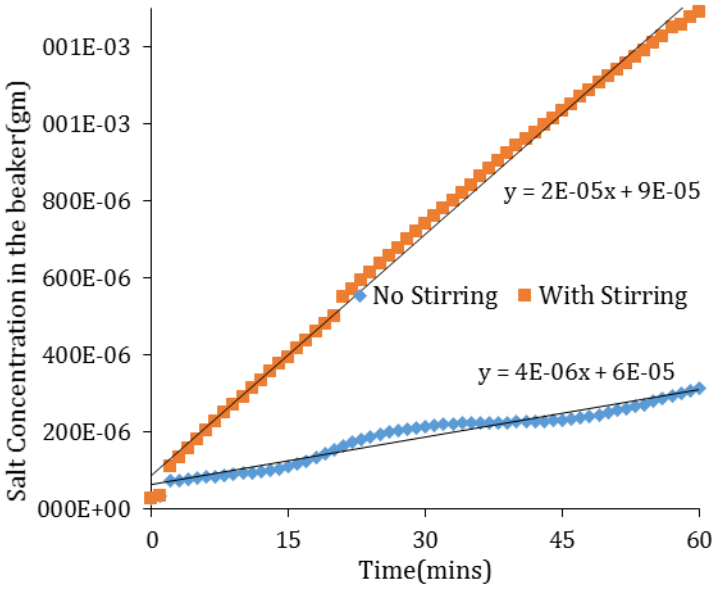

Figure 6.6.2: Salt concentration of a 200mL water phase, converted from conductivity readings of an immersed conductivity cell, exposed to a static test sample of 100µL of 150mM NaCl and 2mg/mL fluo-BSA through a 5kDa MWCO RC ultrafiltration membrane, with and without stirring of the water phase.

Figure 6.2 clearly shows that salt ions transfer from the test sample into the water phase, while visual inspection verified that the fluo-BSA proteins were retained in the acrylic sample chamber. For the duration of the experiment, the salt concentration in the water phase increased linearly with time, at a rate of approximately 4µg/min for a static water phase and 20µg/min for a stirred water phase. Stirring is expected to increase the salt gradient over the membrane by continuously diluting the water layer close to the membrane, hence facilitating cross-membrane diffusion of the salt ions.

When keeping all the experimental parameters, the active surface area of the membrane, the volume of the water phase, the speed of water stirring, etcetera constant, the rate of diffusion is expected to depend on the sample volume. This was investigated by filling the same acrylic test chamber with either 500µL, 250µL, 50µL or 25µL of the test sample and measuring the conductivity of the stirred water phase over time.

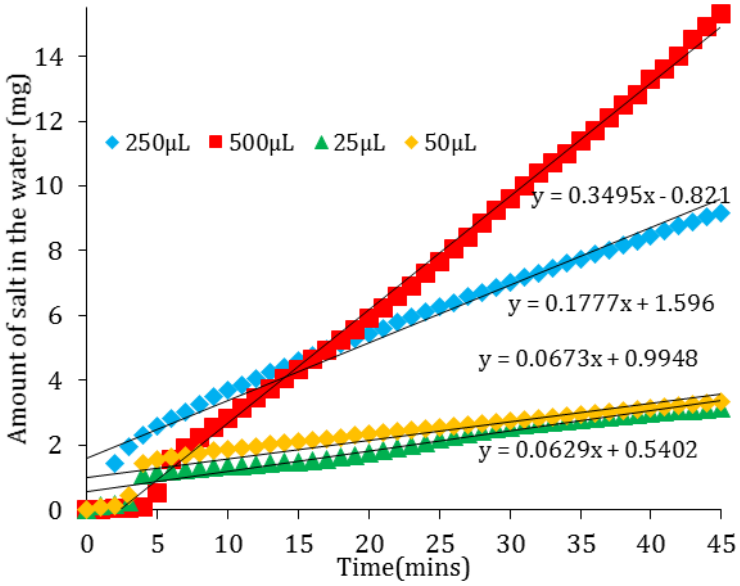

Figure 6.3: Amount of salt in a stirred 200mL water phase exposed to different volumes of a static test sample through a 5kDa MWCO membrane with an active area of 132mm².

Table 6.1: Rate of salt removal as a function of sample volume, calculated from Figure 6.3.

Volume of the sample(µL)	Rate of salt removal (µg/min)
500	349.5
250	177.7
50	67.3
25	62.9

Figure 6.3 and Table 6.1 shows that for the 5kDa RC membrane, more salt diffuses from the test sample into the water phase when the active membrane area is the same but the volume of the test sample is larger. The rate of salt removal from the sample chamber is similar for the

smaller sample volumes (60-70µg/min for sample volumes of 25 and 50µL) while it is substantially higher for the larger sample volumes of 250 and 500µL.

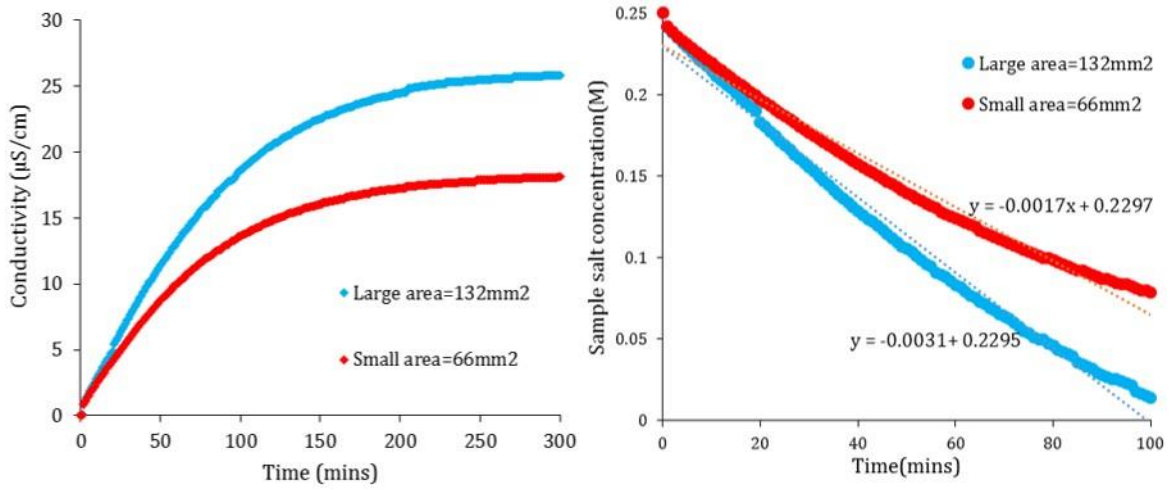

Figure *6.4*: Influence of different surface area of the membrane on diffusion rate. (a) Increase in the conductivity measurements in the dialysate phase over a period of time for device with 2 different membrane area and (b) Decrease in the concentration of the salt in the sample calculated from plot (a). The rate of conductivity increase in the dialysate phase or Salt removal in the sample phase is more for device with bigger membrane area (132mm^2).

The influence of the active surface area of the membrane on the rate of diffusion of salt ions across the membrane was also investigated. Two different acrylic sample chambers, one with an active membrane area of 66mm^2 and another one with an active membrane area of 132mm^2, were filled with 200µL of the test sample. In both chambers, the sample covered the active membrane area completely. The conductivity of a stirred 200mL water phase was recorded over a long period of time, with the result shown in Figure 6.4a. It is apparent that the rate of salt transfer over the membrane decreases substantially after approximately one hour. It can also be concluded that the membrane with the larger active area enables a higher initial rate of salt removal and enables a larger amount of salt to transfer across the membrane, hence resulting in a lower salt concentration in the sample, as shown in Figure 6.4b. The initial rate of salt removal from the sample for the active membrane area of 132mm^2 is approximately 18µg/min or 3.1mM/min, while for the area of 66mm^2 the rate is approximately 9.2µg/min or 1.7mM/min. Hence the 2-fold smaller membrane area gives a 1.8-fold decrease in the rate of salt concentration reduction of the test sample. These experiments confirm that a larger active membrane area enables more efficient dialysis of salt ions from the sample to the water phase.

6.3 Stop and flow dialysis.

All the above experiments were carried out with a static sample and a bulk water phase, at least 400 times larger in volume than the sample phase that was not refreshed. Figures 6.2 and 6.3 show that within the first few minutes of the dialysis experiments, the rate of salt ion transfer over the membrane is high, illustrating that dialysis is most efficient at a high concentration gradient. In order to maintain such a high concentration gradient between the water and the

sample phase, it is necessary to continuously supply fresh DI water to the dialysate side of the membrane.

6.3.1 Rectangular channel dialyser

Initial experiments with a static sample and a quasi-dynamic water phase were performed with the devices shown in Figure 4.9 in Section 4.6, which consist of a rectangular sample chamber and a rectangular water channel of millimetre dimensions. The aim of these experiments was to estimate the optimal refreshing rate, or flow rate, of the water phase. First, the test sample (150mM NaCl and 2mg/mL fluo-BSA) was inserted in the sample channel and DI water was flown into the water channel. The device was then left undisturbed for about 10 minutes, during which the water phase was static. Subsequently, the contents of the water channel (450µL volume) were flushed out and collected in an eppendorf tube. Fresh water was then flown into the water channel once again and the process was repeated several times, with each new 450µL post-dialysis water phase aliquot collected in a separate eppendorf tube. This stop-and-flow experiment was repeated twice, once with a water phase stop time of 5mins and once with a stop time of 3mins. The conductivity of the collected water phase aliquots was then measured and the salt concentration of the sample was estimated by subtracting the amount of salt present in the water phase aliquots from the amount of salt originally present in the sample. The results of the three experiments with different stationary water phase durations are presented in Figure 6.5 as the remaining salt concentration in the sample versus time.

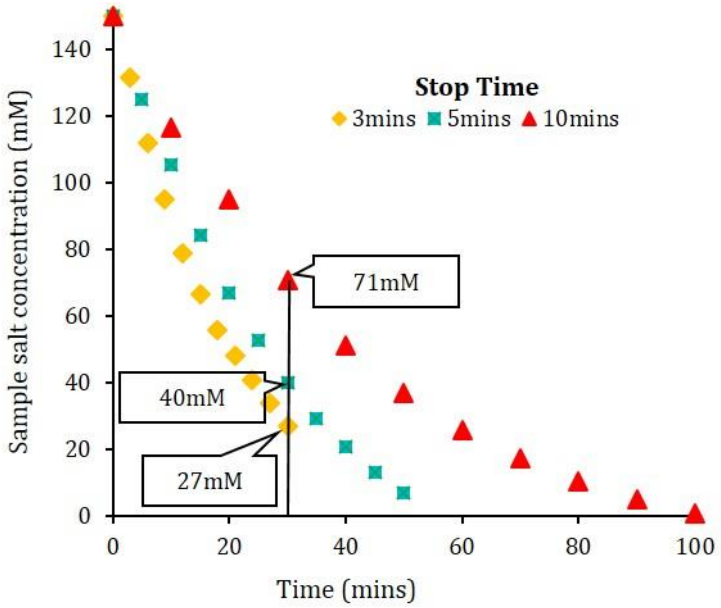

Figure 6.5: Stop and flow experiment using rectangular channels with a static sample and a periodically refreshed water phase. A 5kDa MWCO RC ultrafiltration membrane is separating the two channels

The first conclusion from the data in Figure 6.5 is that with longer time, it is possible to desalt the sample effectively, from 150mM to 0.916mM NaCl. The second conclusion is that the desalting of the sample is faster with more frequent refreshing of the water phase. Table 6.2

lists the salt concentration of the sample, calculated from the conductivity of the post-dialysis water phase aliquots, after 30mins of dialysis. We see that with the most frequent refreshing of the water phase (every 3mins; total dialysate volume 4.5 mL) the sample had desalted to 27mM while refreshing at a slower rate of every 5mins (total volume 3.0 mL) the sample had a concentration of about 40mM NaCl. The sample salt concentration was higher again, 71mM, in case of refreshing every 10mins, with a total water phase volume of 1.5 mL. Having 460µL of water in contact with the membrane for 10 minutes, with fresh DI water supplied at this point, etcetera, is in a crude approximation equivalent to a continuous water phase flow rate of 460µL/10mins, or approximately 50µL/min. Likewise, 460µL/5mins corresponds to ~100µL/min and 460µL/3mins to ~150µL/min. Hence it can be deduced that with a higher flow rate of the water phase in the dialysate channel, desalting of the sample by dialysis is more efficient.

Table 6.2: Sample salt concentration after 30mins of dialysis over a 5kDa MWCO membrane, with the water phase being refreshed every 3mins, 5mins and 10mins. The data are from Figure 6.5. The total water phase volume and equivalent flow rates are also given.

Water phase refreshing time point (mins)	**Sample salt Concentration after 30mins (mM)**	**Total volume of water passed through the water channel (mL)**	**Equivalent continuous water flow rate (µL/min)**
3	27	4.5	153
5	40	3	92
10	71	1.5	46

Although this dialyser design with straight rectangular channels enabled efficient desalting of the static sample at higher equivalent water phase flow rates, the relatively large width of the channels could lead to sagging of the membrane, with sample spreading over a larger area of the membrane, as mentioned in section 4.6. To maximise the membrane surface area in a controlled manner, the channels were narrowed and elongated, with a spiral geometry being preferred over a more densely packed serpentine geometry because of laser micromachining performance (section 4.6).

6.3.2 Spiral design

The spiral channel design has a sample channel of 200µm height and 1.76mm width, while the water channel is 4mm deep and 2.86mm wide. Both channels have a length of approximately 75mm, giving a sample channel volume of 26 µL and a water channel volume of ~750µL. The quasi-dynamic stop and flow experiments described in the previous section were also performed with this spiral channel geometry, but with a larger range of water refreshment times. First, the sample chamber was filled with 26µL of the test sample using a syringe pump,

and the sample channel inlet and outlet port were then sealed with blu-tag. The water chamber was then filled with DI water, which was left stationary for a given amount of time, after which it was refreshed and again left stationary for the same amount of time, etcetera. This experiment was repeated several times, with water refreshment times of 30, 15, 10, 7.5, 5, 2.5 and 1minute, which in a crude approximation are equivalent to a continuous water phase flow rate of 25, 50, 75, 100, 150, 400 and 750µL/min, respectively. The salt concentration of the sample was calculated from the conductivities of the water phase aliquots and is shown in Figure 6.6 as a function of time for the different frequencies of water phase refreshment.

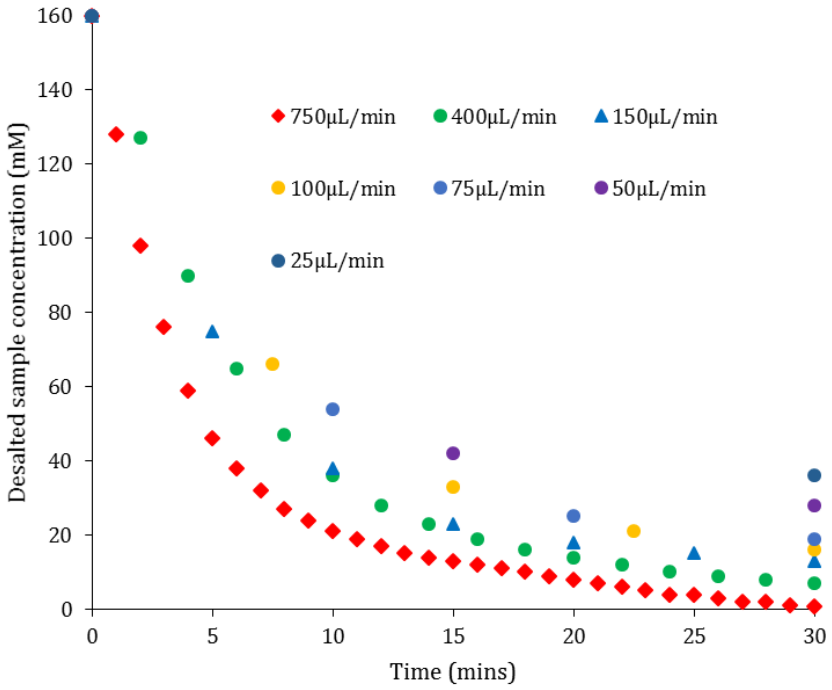

Figure 6.6: Stop and flow experiment using spiral channels with a static sample and a periodically refreshed water phase. A 5kDa MWCO ultrafiltration membrane is separating the two channels.

Figure 6.6 shows that more frequent refreshing of the water phase leads to quicker desalting of the sample. Longer water phase stop times systematically result in slower salt removal from the sample. It is also apparent, from a decrease in slope of the concentration-time curves in Figure 6.6 with time, that the rate of salt removal is higher at the start of the dialysis experiment then towards the end of the experiment. For all water phase refreshment rates, the rate of salt removal was calculated for the first 3.75mL of water, i.e. for the initial dialysis performance, to pass through the sample (Table 6.3).

The data in Table 6.3 demonstrate that even if the same amount of water (3.75mL, i.e. the spiral dialyser has been filled five times with fresh DI water) has flown through the channel, the rate of salt removal from the sample depends strongly on the amount of time the water phase has been stationary. For example, when the water channel contents were refreshed every minute (750µL/min equivalent continuous flow rate), the salt concentration of the sample was reduced at a rate of 23.3mM/min during the initial 5minutes, while when the water was

refreshed every 5mins (150μL/min equivalent continuous flow rate) the salt concentration was reduced at a significantly lower rate of 6.8mM/min.

Table 6.3: The rate of salt removal at different refreshing rates, for the same volume of dialysate or water.

Water phase refreshing time point (mins)	Equivalent continuous water flow rate (μL/min)	Time taken to have 3.75mL of water to pass through the water channel (mins)	Rate of salt removal from the sample (mM/min)
1	750	5	23.3
1.875	400	9.3	14.7
2.5	300	12.5	12.9
5	150	25	6.8
7.5	100	37.5	4.5
10	75	50	4.5
15	50	75	4.3

Table 6.4 Rate of removal of salt from the sample during earlier and later 5minute periods, for different refreshing rates.

	Water phase refreshment time (equivalent continuous flow rate)		
	1min (750μL/min)	2.5mins (300μL/min)	5mins (150μL/min)
Dialysis time range	Rate of salt removal from the sample (mM/min)		
0-5mins	23.3	18.3	17.6
5-10mins	4.2	6.6	7.4
10-15mins	1.5	2.8	3
15-20mins	1	1.4	1.5
20-25mins	0.8	0.6	0.6
25-30mins	0.5	0.4	0.4

For the three highest water phase refreshment rates (1, 2.5 and 5mins water phase stationary time), the rate of salt concentration decrease of the sample was calculated for specific time segments of the dialysis experiments. Table 6.4 shows a clear trend: the salt transfer from the sample into the water phase is fastest at the initial stage of the dialysis experiment, and then gradually slows down. This is because the salt concentration gradient between the sample and

the water phase becomes smaller with decreasing salt concentration of the sample, and hence mass transfer from the sample to the water phase becomes less efficient. A slower water phase refreshment rate results in a lower initial rate of salt removal but in a higher rate of salt removal at later stages of the dialysis because of a larger amount of salt left in the sample and hence a larger salt concentration gradient.

With this knowledge of the flow rates of water and device, it is possible to now design a counter flow device which could effectively desalt the sample. And by customizing the flow rates of water and introducing a flow in the sample chamber and tweaking it, it is possible to desalt the sample to any desired concentrations.

6.3.3 Effect of non- laminar flow in water channels.

From the previous section 6.3.2, it can be concluded that the dialyser with spiral channels is capable of achieving good desalting of a microvolume (~30µL) test sample under stop-and-flow refreshment of the water phase. The water flow in the water channel is expected to be laminar but it was highlighted in section 3.2 that a turbulent, non-laminar, flow will result in more efficient mass transfer over the membrane. To determine whether the dialysis performance of the spiral channel dialyser could be further improved, a spiral channel was fabricated with chevrons/grooves (Figure 4.2 in section 4.2.2), which are expected to cause turbulent flow. As with the experiments before, the sample was stationary and water was flown through the channels at 750µL/min in each case. Three different types of water channels were tested and the results can be seen in Figure 6.7

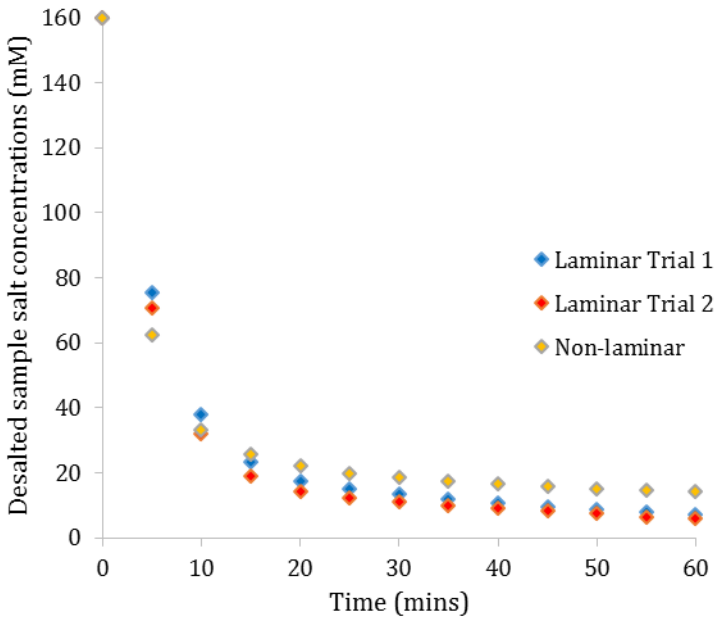

Figure 6.7: Stop and flow Experiment using a spiral channel with static sample and refreshing buffer in differently structured water channels.

The water channel design with chevrons did not improve the sample desalting performance of the dialyser and hence this was not implemented. Having established that the spiral dialyser with long channels of millimiter depth and width is able to efficiently remove salt ions from a stationary sample under stop-and-flow conditions with frequent refreshment of the water phase, subsequent experiments were carried out with a continuous flow of both the water and the sample phase.

6.4 Dynamic counter-flow dialysis

The dialyser with spiral sample and water phase channels was operated with a continuous flow of water and a continuous flow of sample, in opposite directions, as shown in section 4.7 and in Figure 6.8. Sample and water flow were regulated with syringe pumps as outlined in section 4.7.1. The sample from the device was pushed into the outlet tube which forms the inlet tube for the in-line Horiba conductivity meter. In order to wet the entire surface of the sensor on the conductivity cell, it is necessary to collect about 20µL of the post-dialysis sample. Additionally, the sample inlet and the outlet tube to the device consume about 5µL of the sample each. With 26µL being the internal sample channel volume, the total amount of sample required is about 36µL. The in-line conductivity meter makes it possible to directly measure the sample conductivity, rather than inferring the sample salt concentration from the conductivity of water phase aliquots as in the previous sections where the sample was static. The performance of the counter-flow dialysis device was tested for a large range of flow rates, 0.5-50µL/min for the sample phase and 10-750µL/min for the water phase.

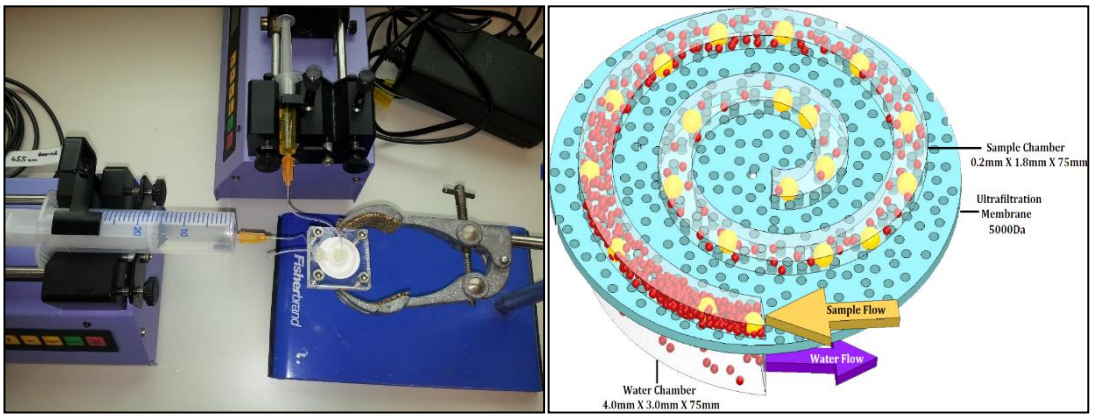

Figure 6.8: Experimental setup (left) and schematic diagram (right) for counter-flow dialysis.

Table 6.5 shows the post-dialysis salt concentrations of the test sample (originally 150mM NaCl and 2mg/mL fluo-BSA, with a conductivity equivalent to a sample of 170mM NaCl due to the presence of salts in the lyophilized BSA powder) for all the 110 combinations of sample and water flow rate. For each sample flow rate, the desalting of the sample improves with a faster water flow, while for each water flow rate, sample desalting improves with a slower sample

flow. These trends are systematic and clearly relate to the optimal conditions for dialysis, a large salt concentration gradient over the membrane and a long sample-water contact time. The best desalting of the sample (99.88% salt removal) occurs at low sample flow rates (0.5-1µL/min) with a high water flow rate (750µL/min). However, the salt concentration of the post-dialysis sample can be tuned to any value inbetween ~200µM and 170mM with the appropriate combination of sample and water flow rate. This control of the desalting efficiency is important for various assays. For example, samples for nanoFET applications should have a salt concentration of ~1mM whereas samples for mass spectrometry can have a salt concentration of ~10-30mM. These targets can easily be achieved with this microvolume counter-flow dialysis platform.

Table 6.5: Desalted sample concentrations(M), calculated from conductivity readings of the post-dialysis sample, for different sample and water flow rate combinations in the dialysis device with a spiral channel geometry. The membrane is a 5kDa MWCO ultrafiltration membrane.

Sample conductivity 13.8mS/cm and the corresponding salt concentration 170mM										
Sample volume in the device-26µL										
Water Volume-750µL										
Time 1µL of sample is in contact with water (s)	3120	1560	600	300	210	156	78	48	39	31
Sample flow rate (µL/min) →	0.5	1	2.5	5	7.5	10	20	30	40	50
750	197E-06	314E-06	7E-03	31E-03	052E-03	66E-03	95E-03	115E-03	126E-03	157E-03
600	204E-06	416E-06	7E-03	38E-03	054E-03	74E-03	99E-03	121E-03	146E-03	157E-03
500	243E-06	433E-06	7E-03	40E-03	057E-03	77E-03	102E-03	127E-03	156E-03	160E-03
400	286E-06	535E-06	8E-03	43E-03	066E-03	77E-03	104E-03	134E-03	157E-03	161E-03
300	301E-06	636E-06	8E-03	46E-03	072E-03	78E-03	108E-03	132E-03	157E-03	163E-03
200	293E-06	687E-06	9E-03	46E-03	073E-03	79E-03	109E-03	136E-03	158E-03	164E-03
150	310E-06	806E-06	9E-03	47E-03	077E-03	82E-03	117E-03	131E-03	158E-03	165E-03
100	328E-06	857E-06	14E-03	47E-03	78E-03	87E-03	118E-03	139E-03	157E-03	165E-03
50	476E-06	001E-03	15E-03	48E-03	79E-03	91E-03	123E-03	142E-03	160E-03	167E-03
25	627E-06	3E-03	17E-03	51E-03	79E-03	96E-03	131E-03	149E-03	161E-03	168E-03
10	973E-06	11E-03	28E-03	52E-03	83E-03	97E-03	140E-03	152E-03	165E-03	168E-03
Water Flow rate (µL/min) ↑										

Best Desalting 0-1mM Good Desalting 1-10mM Considerable Desalting 10-50mM

Satisfactory Desalting 50-100mM Poor Desalting >100mM

Table 6.5 also highlights for each sample flow rate how long 1µL of a sample is in contact with the water phase, through the membrane, disregarding intra-channel diffusion. This ranges from 31s for the highest sample flow rate of 50µL/min to 52min for the lowest sample flow rate of 0.5µL/min. Dialysis times and required water volumes, etcetera, for the more relevant lower sample flow rates are presented in Table 6.6.

Compared to conventional dialysis, this counter-flow microvolume dialyser consumes a much smaller volume of the sample (36µL) and also less DI water (at most 60mL) while still giving a well desalted sample. If required, this sample volume could be further decreased by defining the sample channel with an alternative fabrication method. Although the desalting of the sample is highly efficient at low flow rates of the samples, from Tables 6.5 and 6.6 it can also

be seen that the efficiency of desalting can remain fairly constant upon further increasing the water flow rate.

Table 6.6: Expanded desalted sample concentrations (M) at low flow rates of the sample. With slow sample flow rate and high water flow rate, it can be observed that the sample is exposed to a large amount of water facilitating increased removal of salt.

			Total amount of water required (mL)		Total amount of water required (mL)		Total amount of water required (mL)
Sample flow rate →		0.5 µL/min		1 µL/min		2.5 µL/min	
Total sample required for collecting 20 µL of the sample outside the dialysis cell		36 µL		36 µL		36 µL	
Time taken to obtain 20 µL of sample outside the device		80 mins		40 mins		15 mins	
Time 1 µL of sample is in contact with water (mins)→		52 mins		26 mins		10 mins	
	750ulmin	197E-06	60	314E-06	30	007E-03	11.25
	600ul/min			416E-06	24	007E-03	9
	500ul/min			433E-06	20	007E-03	7.5
	400ul/min			535E-06	16	008E-03	6
	300ul/min	301E-06	24	636E-06	12	008E-03	4.5
	200ul/min	293E-06	16	687E-06	8	009E-03	3
	150ul/min	310E-06	12	806E-06	6	009E-03	2.25
	100ul/min	328E-06	8	857E-06	4	014E-03	1.5
	50ul/min			001E-03	2	015E-03	0.75
	25ul/min			003E-03	1	017E-03	0.75
	10ul/min			011E-03	0.750	028E-03	0.75
	↑	↑		↑		↑	
	water flow rate	salt conc.		salt conc.		salt conc.	

Best Desalting 0-1mM Good Desalting 1-10mM Considerable Desalting 10-50mM

The percentage of salt removed from the sample is plotted in Figure 6.9 for the highest water flow rate and the lowest sample flow rate. This percentage is calculated from the post-dialysis salt concentration and the input salt concentration as:

$$Removal\ of\ salt = \left(1 - \frac{C_{out}}{C_{in}}\right) x100\% \qquad \textit{Equation 6.1}$$

Where C_{out} is the output sample concentration and C_{in} is the input sample concentration (170mM)

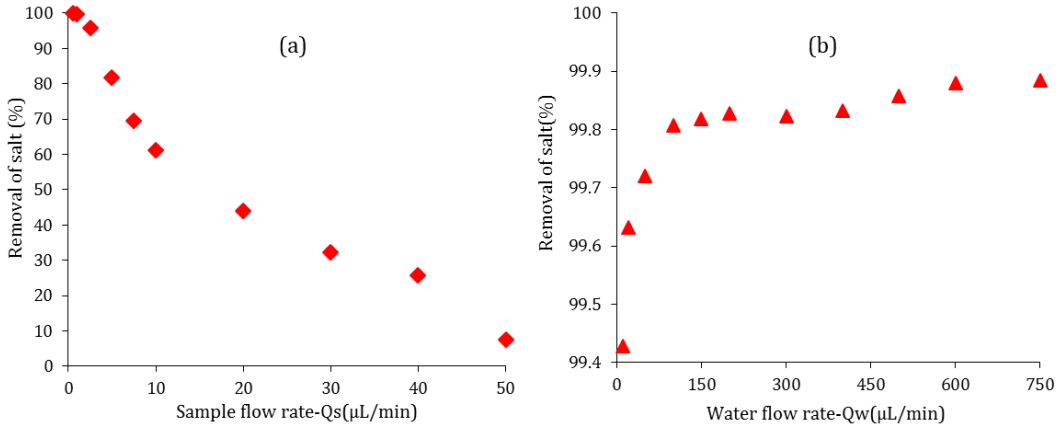

Figure 6.9: Removal of salts for various flow conditions. (a) Removal of salt at constant water flow rate (750µL/min) and varying sample flow rates and (b) Removal of salt at constant sample flow rate (0.5µL/min) and varying water flow rate.

Figure 6.9a shows that at a water flow rate of 750µL/min, the desalting is very sensitive to the sample flow rate, with the highest percentage of salt removed (~99.8%) being achieved at a sample flow rate of 0.5-1µL/min. Figure 6.9b shows that for a sample flow rate of 0.5µL/min the extent of desalting improved from ~99.4% to ~99.8% for water flow rates up to ~200µL/min. Further increasing the water flow rate, from 200 to 750µL/min, only resulted in an additional ~0.1% of salt removal. This suggests that beyond a certain flow rate, the dialysis performance of the device is limited by the device itself and not by the choice of flow regime. The limiting factor is likely to be the ultrafiltration membrane. The membrane properties do influence the effectiveness of diffusion as mentioned in section 3.3. The membrane thickness, the pore size / MWCO value, the pore density and the tortuous nature of the pores can all be expected to influence diffusion over the membrane.

6.5 Analysis of desalting efficiency.

In order to understand the performance of the counter-flow dialyser better, the mass transfer equations discussed in section 3.3 were used to predict the desalting efficiency of the dialyzer and to identify the limiting factors. Mass transfer is given by Equation 3.12 on page 33 as

$$M = \frac{(C_{sin} - C_{win})\left[1 - e^{-kS\left[\frac{1}{Q_s} - \frac{1}{Q_w}\right]}\right]}{\left(\frac{1}{Q_s}\right) - \left(\frac{1}{Q_w}\right)e^{-kS\left[\frac{1}{Q_s} - \frac{1}{Q_w}\right]}}$$

where M is the total mass transfer rate (mol/s), k is the overall mass transfer coefficient, A is the overall mass transfer area of the membrane sheet (m^2), $Q_s=Q_a$, $Q_w=Q_b$ are the volume flow rates in the retentate phase (sample) and dialysate phase (water), $C_{a,i}=C_{sin}$, $C_{a,e}=C_{sout}$, $C_{b,i}=C_{win}$, $C_{b,e}=C_{wout}$ are the concentrations at the inlet and outlet of the dialyzer.

In order to calculate the mass transfer, it is crucial to determine the overall mass transfer coefficient of the system. In order to calculate the overall mass transfer coefficient (k), it is necessary to calculate the individual mass transfer coefficient in the sample channel, water channel and the membrane. From equation 3.10 on page 32

$$\frac{1}{k} = \frac{1}{k_s} + \frac{1}{k_m} + \frac{1}{k_w}$$

Where k_s- mass transfer coefficient in the sample channel (m/s),

k_m- mass transfer coefficient in the membrane(m/s),

k_w- Mass transfer coefficient in the water channel (m/s)

the formula for obtaining the value of k_s and k_w is the same with their corresponding flow rates of the sample and water and their appropriate channel dimensions. The mass transfer coefficient is given by equation 3.8 from page 32

$$k_s = k_w = 0.816\left(\frac{6QD^2}{W_c{H_c}^2 L_c}\right)^{\frac{1}{3}}$$

Where *Q*- feed flow rate (m^3/s), *D*- diffusion coefficient (m^2/s), W_c-Width of the channel(m), *Hc*- Channel height (m),*Lc*- Length of the channel(m)

In case of water channels, k_w will have W_c=2.82mm, H_c=4mm, and Q_w varies from10-750µL/min. while in k_s, W_c=1.76mm, H_c=200µm and Q_s=0.5-50µL/min. The length of the channel remains constant at 75mm on both sides of the membrane. The diffusion co-efficient is assumed to be $1.29x10^{-9}m^2/s$ in both sample and water channel.

The mass transfer coefficient of a membrane is given by equation 3.9 from page 32

$$k_m = \frac{D_c\varepsilon}{\tau t}$$

Dc- the diffusivity of the solute in the membrane is assumed as $1.29x10^{-9}m^2/s$ (125) and t-thickness as 20µm as discussed in section 5.4. The membrane mass transfer coefficient is fixed since it is obtained by substituting the constant and assumed values. From equation 3.9, it follows that the limiting factors for km are the porosity of the membrane, the tortuous nature of the membrane pores and the membrane thickness. The porosity ε for an ultrafiltration membrane ranges from 0.3 to 0.73 and is taken as 0.5%, as discussed in sections 5.3 and 5.6. The tortuosity τ values varies between 0 and 2 and is assumed to be 2 [108]. From the above values, we can calculate the mass transfer coefficient of the membrane (k_m) as $1.667x10^{-7}m/s$. Using all the known and assumed values, the overall mass transfer coefficient k and overall mass transfer rate M can be obtained. Table 6.7 lists *k* and *M* values for sample phase flow rates ranging from 0.5 to 50µL/min and for water phase flow rates ranging from 10 to 750 µL/min.

Table 6.7: Overall mass transfer coefficient-k (m/s) and the overall mass transfer rate M (moles/s) at different flow rates for the cross-flow dialysis device with the parameters described in the main text.

	Overall mass transfer coefficient for various flow rates of the sample and water –k (m/s)									
Sample flow rate (µL/min)	0.5	1	2.5	5	7.5	10	20	30	40	50
10µL/min	3.8E-07	3.9E-07	4.1E-07	4.2E-07	4.2E-07	4.3E-07	4.3E-07	4.4E-07	4.4E-07	4.4E-07
20µL/min	4.3E-07	4.5E-07	4.7E-07	4.8E-07	4.9E-07	4.9E-07	5E-07	5.1E-07	5.1E-07	5.1E-07
50µL/min	5E-07	5.2E-07	5.5E-07	5.7E-07	5.8E-07	5.9E-07	6E-07	6.1E-07	6.1E-07	6.1E-07
100µL/min	5.6E-07	5.9E-07	6.3E-07	6.6E-07	6.7E-07	6.8E-07	6.9E-07	7E-07	7.1E-07	7.1E-07
150µL/min	5.9E-07	6.3E-07	6.7E-07	7E-07	7.1E-07	7.2E-07	7.4E-07	7.5E-07	7.5E-07	7.6E-07
200µL/min	5.9E-07	6.3E-07	6.7E-07	7E-07	7.1E-07	7.2E-07	7.4E-07	7.5E-07	7.5E-07	7.6E-07
300µL/min	6.2E-07	6.6E-07	7.1E-07	7.4E-07	7.6E-07	7.7E-07	7.9E-07	8E-07	8.1E-07	8.2E-07
400µL/min	6.4E-07	6.9E-07	7.4E-07	7.7E-07	7.9E-07	8E-07	8.3E-07	8.4E-07	8.5E-07	8.5E-07
500µL/min	6.5E-07	7E-07	7.5E-07	7.9E-07	8E-07	8.2E-07	8.4E-07	8.5E-07	8.6E-07	8.7E-07
600µL/min	6.6E-07	7.1E-07	7.7E-07	8E-07	8.2E-07	8.4E-07	8.6E-07	8.8E-07	8.9E-07	8.9E-07
750µL/min	6.8E-07	7.3E-07	7.9E-07	8.3E-07	8.5E-07	8.6E-07	8.9E-07	9E-07	9.1E-07	9.2E-07
	Overall mass transfer for various flow rates of the sample and water –M (moles/s)									
10µL/min	1.4E-09	2.7E-09	4.9E-09	6.2E-09	6.8E-09	7.2E-09	7.7E-09	7.9E-09	8E-09	8.1E-09
20µL/min	1.4E-09	2.7E-09	5.3E-09	7.2E-09	8E-09	8.5E-09	9.1E-09	9.7E-09	9.9E-09	1E-08
50µL/min	1.4E-09	2.8E-09	5.8E-09	8.2E-09	9.5E-09	1E-08	1.2E-08	1.2E-08	1.2E-08	1.1E-08
100µL/min	1.4E-09	2.8E-09	6.1E-09	9.1E-09	1.1E-08	1.2E-08	1.3E-08	1.4E-08	1.5E-08	1.5E-08
150µL/min	1.4E-09	2.8E-09	6.2E-09	9.4E-09	1.1E-08	1.2E-08	1.4E-08	1.5E-08	1.6E-08	1.6E-08
200µL/min	1.4E-09	2.8E-09	6.2E-09	9.4E-09	1.1E-08	1.2E-08	1.4E-08	1.5E-08	1.6E-08	1.6E-08
300µL/min	1.4E-09	2.8E-09	6.3E-09	9.8E-09	1.2E-08	1.3E-08	1.5E-08	1.6E-08	1.7E-08	1.7E-08
400µL/min	1.4E-09	2.8E-09	6.4E-09	1E-08	1.2E-08	1.3E-08	1.6E-08	1.7E-08	1.7E-08	1.8E-08
500µL/min	1.4E-09	2.8E-09	6.4E-09	1E-08	1.2E-08	1.3E-08	1.6E-08	1.7E-08	1.8E-08	1.8E-08
600µL/min	1.4E-09	2.8E-09	6.5E-09	1E-08	1.2E-08	1.4E-08	1.6E-08	1.8E-08	1.8E-08	1.9E-08
750µL/min	1.4E-09	2.8E-09	6.5E-09	1E-08	1.3E-08	1.4E-08	1.7E-08	1.8E-08	1.9E-08	1.9E-08
Water flow rate (µL/min)										

In Figure 6.10, these *k* and *M* values are also plotted as a function of the sample phase flow rate, for the different water phase flow rates, which visualises some important trends.

From the Figure 6.10, it is apparent that the overall mass transfer coefficient and mass transfer rate are very low at low flow rates (Q_s-0.5-1µL/min) of the sample. The values of *k* and *M* increase as the sample flow rate increases to 5µL/min, but beyond this flow rate, the *k* and *M* values remain fairly constant. Another important finding is that the value of the *k* and *M* depend on the flow rate of the water phase. A higher water flow rate causes an increase in the *k* and *M* values, but this increase is larger for lower water flow rates (<300µL/min) than for higher flow rates (>300µL/min). With flow rates of the water phase >750µL/min, it might be possible to reach a point beyond which no distinct change would be observed. This confirms the limiting conditions of the device as discussed earlier.

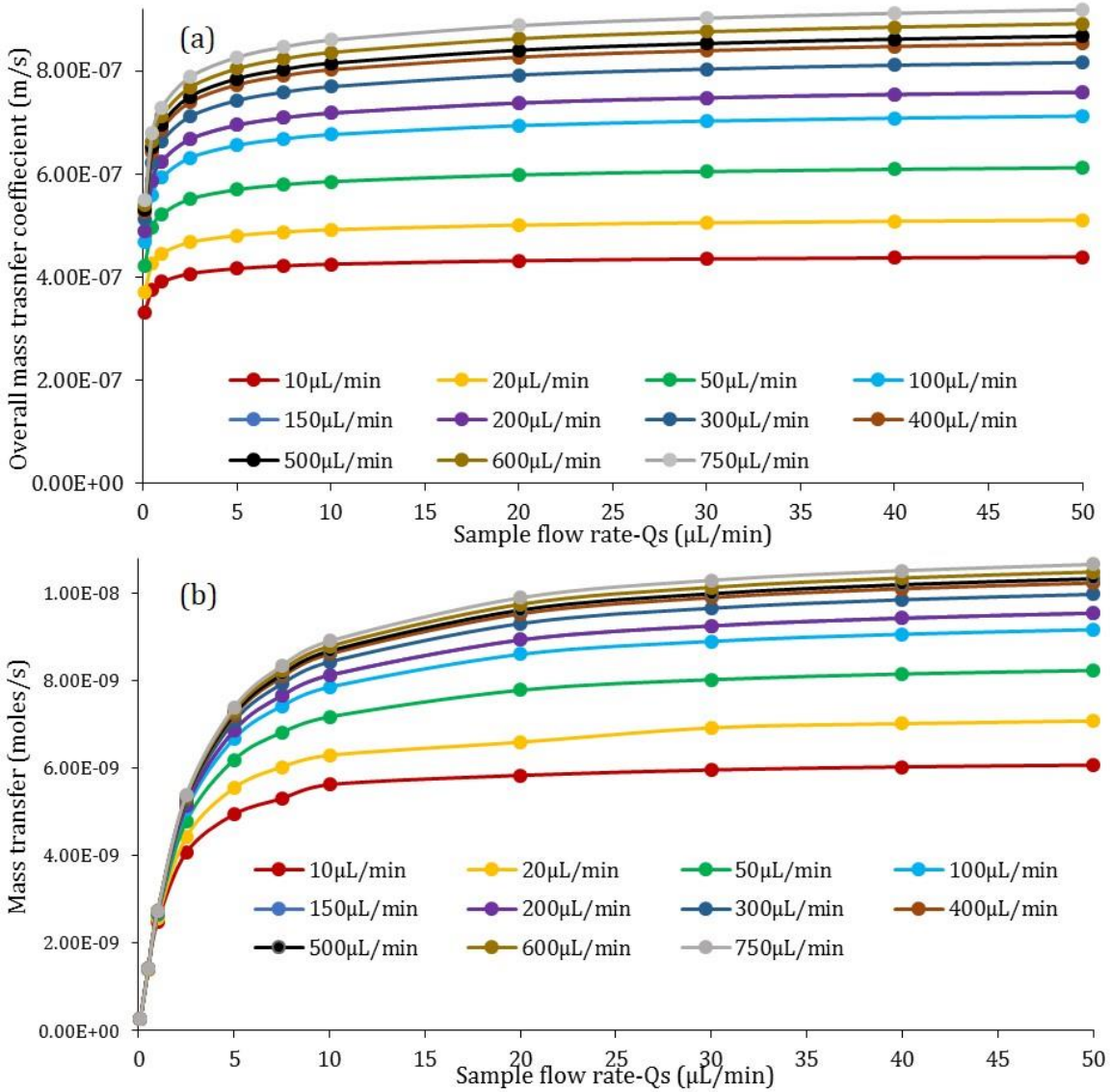

Figure 6.10: (a) Calculated overall mass transfer coefficient k (m/s) for various sample and water flow rates (b) Calculated mass transfer M (moles/m) for various sample and water flow rates.

Figure6.10 represents the mass transfer and the mass transfer coefficient for the system highlighting the important conditions of system limited by flow rates or channel dimensions. The results shown in figure 6.10 are obtained from predictions method using the mass transfer equations which are then used to compare it with the experimental results from the experimental work as demonstrated below

Using the obtained values for the overall mass transfer, it is possible to predict the desalting efficiency of the cross-flow dialyzer for various flow rates. From Table 6.5 & 6.6, we can find that 1µL of the sample will be in contact with the water phase across the membrane for different lengths of time for different sample flow rates. For example, with a sample flow rate of 0.5µL/min, 1µL of the sample will take 52mins to flow through the sample channel, remaining all the time in contact with fresh water because the counter flow arrangement is used. The initial sample salt concentration of 170mM equates to 0.17µmoles/µL. Hence 26µL (the volume of the sample channel) of sample originally contains 4.42µmoles of NaCl. For a

sample flow rate of 0.5µL/min and a water flow rate of 750µL/min, Table 6.7 indicates that the calculated mass transfer rate is 1.41×10^{-9}moles/s for this combination of flow rates. During the 52mins required for the 26µL sample to traverse the sample channel, the amount of NaCl transferred from the sample to the water phase would hence be 4.39µmoles. This implies that 99.3% of the salt would be removed from the sample and that the post-dialysis salt concentration of the sample would be 68µM.

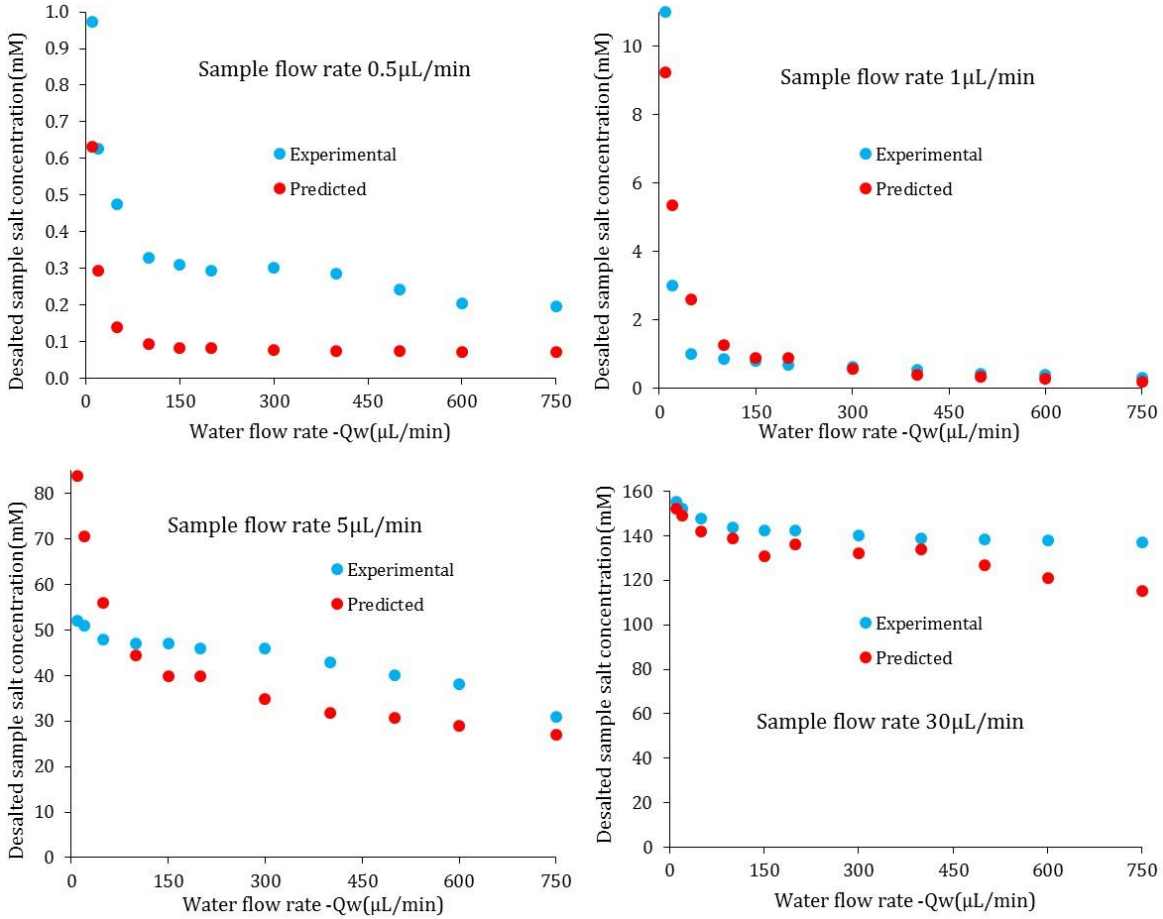

Figure 6.11: Comparison between the post-dialysis sample salt concentration as determined by conductivity measurements and the theoretical salt concentration as calculated with the mass transfer equations. Results for various other sample flow rates can be found in Appendix I.

In this manner, the predicted post-dialysis salt concentration of the sample was calculated for a large number of sample and water flow rates, and the results are plotted in Figure 6.11, together with the experimentally obtained salt concentrations from post-dialysis conductivity measurements. An important conclusion from Figure 6.11 is that the estimated and the experimentally determined salt concentrations are very close, with the largest variation (~3 times lower sample salt concentration predicted than experimentally measured) observed for the lowest sample flow rate of 0.5µL/min, where post-dialysis salt concentrations are below 1mM. For sample flow rates of 1, 30 and 50µL/min, the theoretical and experimentally determined sample salt concentration versus water phase flow rate curves almost overlap, suggesting that the mass transfer theory is appropriate for the cross-flow dialyser and that the approximated values for the membrane thickness, the porosity and the pore tortuosity are

reasonable. The porosity of 5kDaRC membrane can be back-tracked from the experimental results to 0.52 % assuming a known value of diffusion coefficient, tortuosity and membrane thickness as before.

6.5.1 Limiting conditions

In order to further understand the limiting conditions of the device, we analyse the individual cases of the variables in the mass transfer equations. The mass transfer coefficient of the membrane is given by Equation 3.9 on page 32 as

$$k_m = \frac{D_c \varepsilon}{\tau t}$$

6.5.1.1 Membrane thickness (t)

The mass transfer coefficient of the membrane (k_m) is inversely proportional to the thickness of the membrane. In Figure 6.12, k_m values have been plotted for a range of membrane thicknesses, for different membranes that are commercially available. It can be noted clearly that membranes that are thin (20µm) provide high mass transfer coefficient compared to the thick (180µm) membranes.

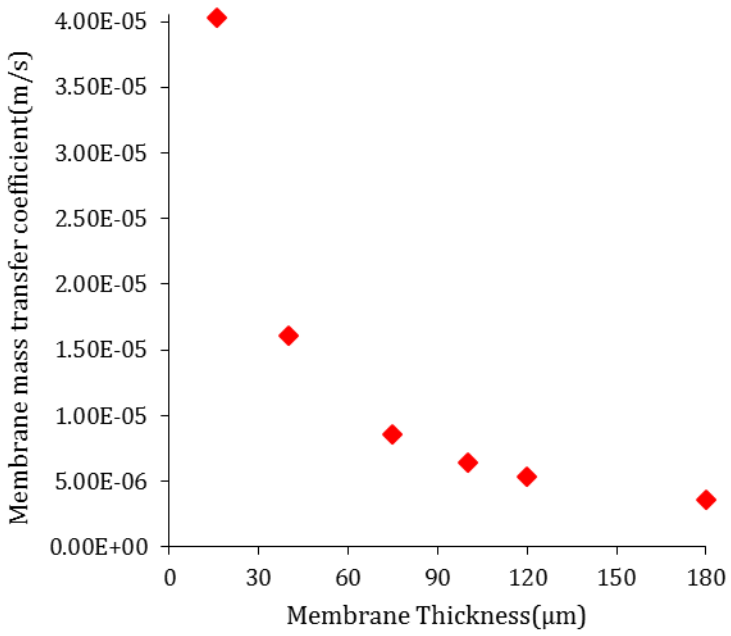

Figure 6.12: Mass transfer coefficient of the membrane calculated for a range of membrane thicknesses assuming porosity as 0.5% and tortuosity as 2 and D_c-1.29x10^{-9}m^2/s.

In case of the UF membranes that are used in this chapter, of which the structure was discussed in section 5.3, the overall thickness is around 180µm of which ~160µm forms the supporting layer and ~20µm forms the membrane. In the analysis described in section 6.5, 20µm thickness of the membrane itself was used. Alternative options are to use the thickness of the skin layer

(~200nm) only, or the total thickness of membrane and supporting layer (~180µm). The predicted desalted concentration varies considerably depending on the thickness used in the analysis as shown in Figure 6.13.

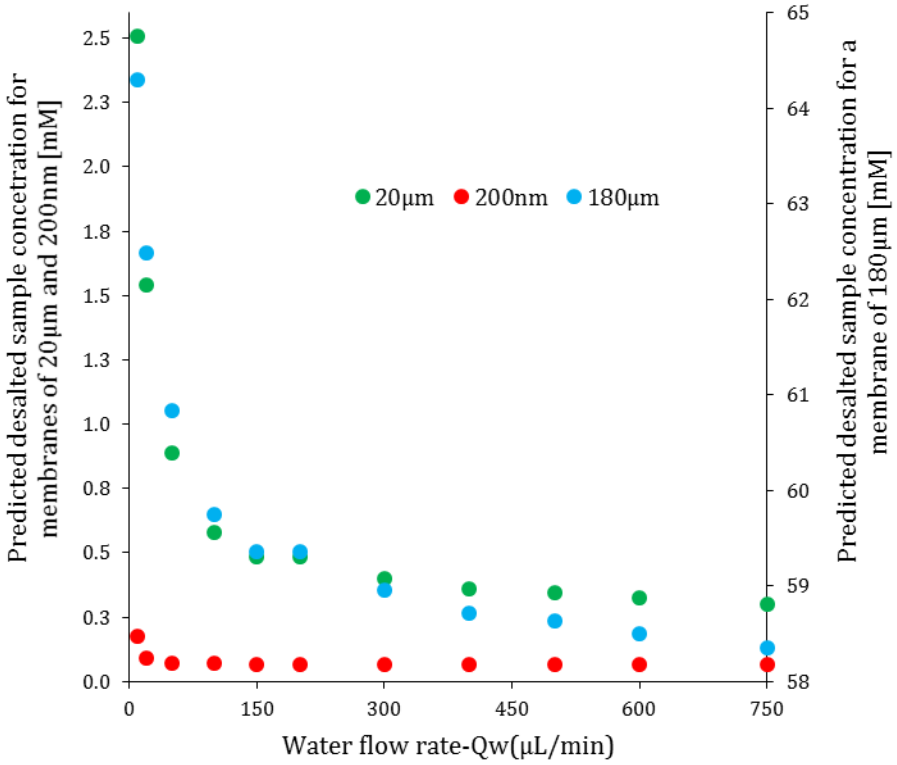

Figure 6.13: Prediction of desalting efficiency at Qs-0.5µL/min for different Qw. The prediction has been calculated for different membrane thickness conditions such as the membrane with the whole support layer (blue), membrane without the support layer (orange) and skin layer of the membrane (grey).

From Figure 6.13, at high Q_w the predicted sample concentration after dialysis for a membrane of 180µm is quite high 58mM whereas for a membrane of 20µM is around 300µM which is close to the value observed experimentally. This confirms the assumption of the membrane thickness to be around 20µm.

6.5.1.2 Porosity of the membrane (ε).

The mass transfer coefficient in the membrane (k_m) is directly proportional to the porosity of the membrane (Equation 3.9). From the earlier Chapter 5, the porosity of different UF membranes can be noted from the literature and experimental work to be around ~0.5% (section 5.6). Figure 6.14 shows that the mass transfer in a membrane of low porosity (<0.5%) is quite low. Hence a membrane with low porosity such as the 1kDa membranes should have low mass transfer which would give reasonably low desalting results for the same flow conditions compared using 5kDa UF membranes.

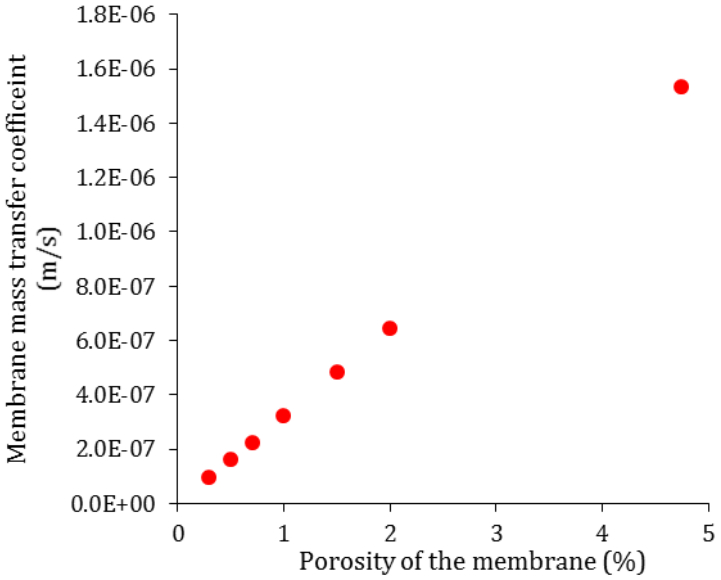

Figure 6.14: Variation in mass transfer coefficient and predicted desalted salt concentration for varying porosity of the membranes.

6.5.1.3 Tortuosity of the membrane (τ)

Tortuosity refers to the twist and turns in the membrane pores that an ion or molecule experiences when moving from one side of the membrane to the other side. Typically the values ranges from 0-20 in case of UF membranes. Using different values of the tortuosity while keeping the remaining parameters constant, it is possible to membrane mass transfer coefficient as shown in Figure 6.15. It can be observed that with high tortuosity value (τ=2), the k_m is low since the time taken for the ions to move from one side of the membrane to the other is long. This clearly shows that membranes that are less tortuous in nature would facilitate in better mass transfer of the solute.

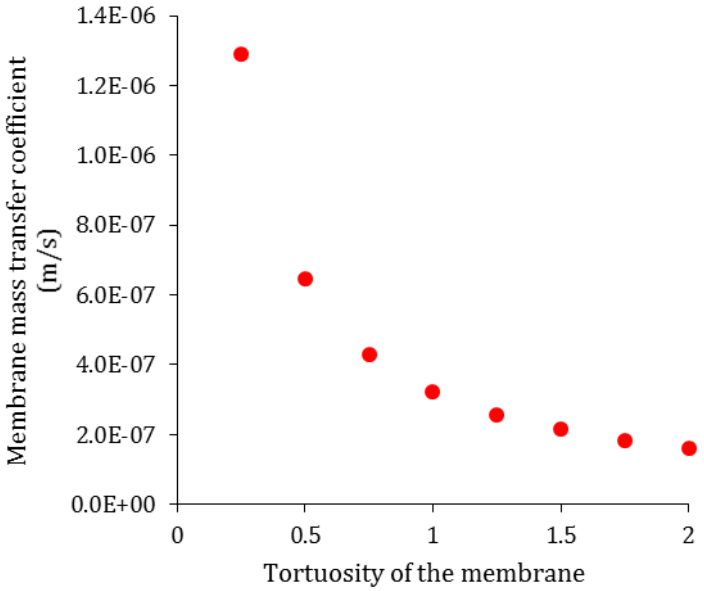

Figure 6.15: Variation in the membrane mass transfer coefficient for different values of tortuosity. The mass transfer is low in membranes which are highly tortuous in nature.

6.6 Hollow fibre membrane test for improved surface area

A robust way to establish the effect of membrane thickness and porosity experimentally is to use membranes of different thickness and different porosity. However these values are similar for all the planar ultrafiltration membranes of the relevant MWCO range. Instead, a hollow fibre membrane was used for comparison purposes. The desalting efficiency of the cross-flow hollow fibre membrane dialyser described in section 4.7 was characterized using a sample of 1M NaCl. The regenerated cellulose hollow fibre membrane of I.D. 200μm and O.D. 216μm will have a membrane thickness of 8μm. With the hollow fibre membrane enclosed in an eppendorf tube, the 1M salt solution was flown through the fibre at flow rates between 0.5 and 10μL/min while the water phase passed through the eppendorf tube, in the opposite direction, at a flow rate of either 0.1 or 1 mL/min. The post-dialysis salt concentration of the sample was determined from conductivity measurements, with the results shown in Table 6.8.

Table 6.8: Desalted sample concentrations obtained with a hollow fiber membrane based dialyzer for different flow rates of the sample and the water phase. The sample originally has a high salt concentration of 1M NaCl.

	Post-dialysis sample salt concentration (mM)	
Water Flow rate μL/min →	0.1	1
0.5	12	1.3
1	25	12
5	330	227
10	550	450
Sample flow rate μL/min ↑		

The post-dialysis salt concentration varied between 1.3 and 550mM, with both slower sample flow rate and higher water flow rate giving lower salt concentrations. At the lowest sample flow rate of 0.5μL/min and the highest water flow rate of 1mL/min, this hollow fibre membrane dialyzer is capable of reducing the salt concentration of the sample from 1M down to 1.3mM, i.e. 99.87% of the salt was removed from the sample by diffusion over the membrane.

The desalting performance of this cross-flow hollow membrane dialyser exceeds the performance of the cross-flow dialyser with planar ultrafiltration membranes between laser micromachined spiralling sample and water channels due to several factors. The hollow fibre membrane offered a much higher surface area with respect to the sample volume, with the membrane surrounding the sample rather than being on one side of the sample channel only. In the planar sandwiched membrane, 26μL of the sample is in contact with 750μL of water across a supported-layer membrane of 180μM in thickness (~20μm effective thickness),

whereas in the hollow fibre membrane, 1-1.5μL of the sample is in contact with 2000μL of water across a membrane of 8μm in thickness. The low volume is due to the small inner diameter of the membrane. However, another important parameter that has to be taken into account for its high salt dialysis effectiveness is the MWCO of the membrane. The hollow fibre membrane has a higher MWCO (13000Da) hence the pores in the membrane will be larger than the pores present in the planar ultrafiltration membranes with a MWCO of 1000 or 5000Da. It is also possible that the pore density of the hollow fibre membrane is higher, but this was not characterized because the MWCO of 13kDa was considered too high for the intended application of salt removal from protein samples without loss of protein species, and hollow fibre membrane with a smaller MWCO could not be obtained. Further experiments with this hollow fibre membrane were therefore not carried out.

6.7 Summary

In this chapter salt removal from a test sample of 150mM NaCl and 2mg/mL fluo-BSA through ultrafiltration membranes of 5kDa MWCO was investigated and optimized with different devices for static, quasi-dynamic and dynamic counter-flow dialysis. For the counter-flow dialyser geometry, the theoretical desalting performance was also estimated with mass transfer theory.

Using a membrane-enclosed acrylic sample chamber floating on a bulk water phase, conductivity measurements of the water phase indicated gradual transfer of salt ions from the sample to the water phase while visual observation showed that the fluorescently labelled BSA proteins were retained in the sample, indicating that the ultrafiltration membranes are suitable for dialysis applications. The salt removal rate was faster (20 instead of 4μg/min) when the water phase was stirred, which will result in dilution of the solution close to the membrane, reducing the local salt concentration and increasing the salt concentration gradient over the membrane. With stirring, a larger sample volume of 500μL resulted in a higher rate of salt removal (350μg/min) than for a sample of ~50μL volume (63μg/min). Furthermore, the rate of salt removal was nearly twice as fast when the membrane area was increased from 66 to 132mm2.

Next, the performance of dialysers with millimetre scale sample and water channels was explored. With a static sample and a periodically refreshed ('stop and flow') water phase in the water channel, desalting of the sample was more efficient with more frequent refreshment of the water phase. A spiral channel geometry was then implemented to maximize the membrane area with which the sample is in contact. With a static sample and a continuous water flow rate of 750μL/min (the highest possible flow rate) a sample salt concentration of 200μM was achieved, while lower flow rates resulted in a higher post-dialysis sample salt concentration.

The spiral dialyser was then operated in a fully dynamic dialysis mode, with counter-flow of both the sample and water phase. The dialysis performance was extensively characterized, using a wide range of sample and water flow rates. With a sample flow rate of 0.5μL/min and a water flow rate of 750μL/min, the most efficient desalting of the sample was achieved, down to ~200μM (99.88% of salt removed). Significantly, any salt concentration between this value and the original salt concentration of the sample can be obtained by selecting the appropriate combination of sample and water phase flow rates.

It was observed that at low sample flow rates of 0.5-1μL/min, salt dialysis from the sample is not significantly enhanced by increasing the flow rate beyond ~200μL/min. Mass transfer theory for cross-flow dialysis was applied to the spiral dialyser device geometry to gain insight in the theoretical desalting efficiency under various flow conditions. Predicted performance was in good agreement with the actual measurements and the calculations suggested that a significant increase in dialysis efficiency would require a different membrane, of smaller thickness or with a larger porosity (or a different device geometry, with a larger membrane surface to sample volume ratio). This was then tentatively explored by performing cross-flow dialysis with a hollow fibre membrane, with which a sample of 1M NaCl could be desalted to a concentration of 1.3mM (99.87% of salt removed).

In the next Chapter, the developed spiral cross-flow dialyser is used to reduce the salt concentration of samples with a higher, serum-like, protein concentration, of samples with a mixture of proteins, and of blood serum samples and the effect of specific residual salt concentrations on the quality of mass spectrometry measurements is determined.

.

Chapter 7: Counter-flow dialysis of protein samples and serum

The previous Chapter concerned the development of a counter-flow dialyser with microvolume sample and water channels, with a focus on a test sample consisting of 150mM NaCl and 2mg/mL fluo-BSA and a 5kDa MWCO ultrafiltration membrane. These experiments showed that under optimal flow conditions the salt concentration in the sample could be reduced to ~200μM while the fluorescent protein was retained. In this Chapter, the performance of the counter-flow dialyser was investigated for higher protein concentrations, for mixtures of proteins and also for blood serum. The tuneable desalting capability of the counter-flow dialyser is exploited to obtain protein samples with specific salt concentrations, which are then used for mass spectrometry measurements that illustrate the signal enhancement obtained for various extents of sample desalting

7.1 Counter flow dialysis using protein samples.

Human blood serum contains about 60-80mg/mL of protein, of which 40-50mg/mL is human serum albumin (HSA). To investigate whether such a high protein concentration has an effect on salt removal by dialysis, a sample containing 50mg/mL of BSA and 150mM NaCl was used. Experiments were conducted as described in Section 6.4, under dialysis conditions (Qs-0.5μL/min and Qw-10-750μL/min) that were optimal for salt removal from the test sample with 50mg/mL fluo-BSA. The post-dialysis salt concentration of the sample, calculated from conductivity measurements of the retentate phase, is shown in Figure 7.1, together with the results for a sample that only contained 150mM NaCl.

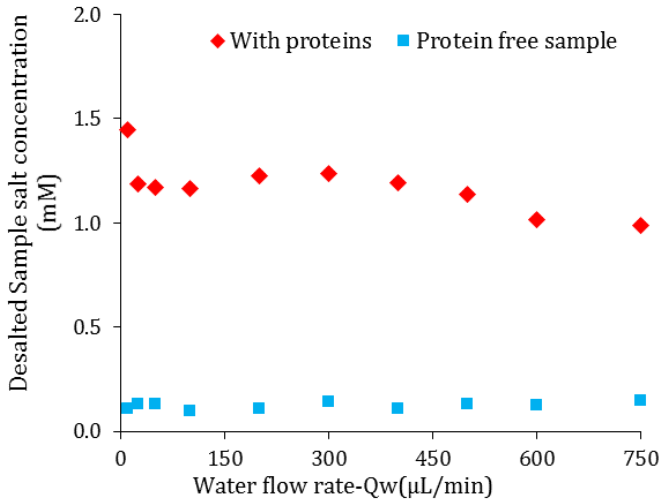

Figure 7.1: Post-dialysis salt concentration of a sample originally consisting of 50mg/mL BSA and 150mM NaCl, and of a sample originally consisting of 150 mM NaCl without proteins. Counter-flow dialysis was performed with a 5kDa MWCO ultrafiltration membrane and a sample flow rate of 0.5μL/min.

For water phase flow rates >20µL/min, the salt concentration of the post-dialysis sample was ~1.2mM. Although this presents efficient desalting, a lower value of ~0.1mM was obtained for the protein-free sample while ~0.2mM was obtained for the test sample containing 2mg/mL fluo-BSA (Table 6.5). In order to check whether the post-dialysis salt concentration, or more accurately the post-dialysis conductivity of the retentate phase is correlated with the protein concentration in the sample, samples with different BSA concentrations, ranging from 0 to 50mg/mL were dialysed using Q_s-0.5µL/min and Q_w-750µL/min.

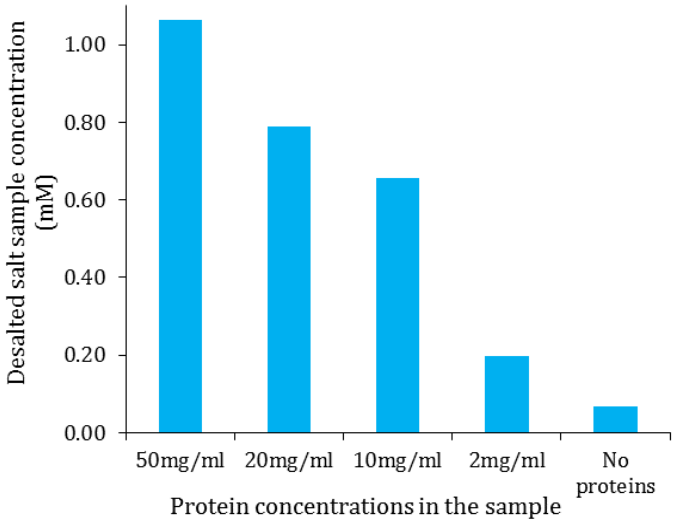

Figure 7.2: Post-dialysis salt concentration of samples of 150mM NaCl and various concentrations of BSA. Counter-flow dialysis was performed with a 5kDa MWCO ultrafiltration membrane, a sample flow rate of 0.5µL/min and a water flow rate of 750µL/min.

The conductivity of the sample phase after dialysis was measured and converted to the salt concentration values depicted as a bar chart in Figure 7.3. Because samples with an original BSA concentration of 10 and 20mg/mL are desalted, respectively, to ~0.65 and 0.8 mM salt, it appears that an increasing concentration of BSA leads to a small, but measurable, decrease in the desalting efficiency. Although lyophilized protein powders tend to contain salt, it was estimated that dissolving the BSA used in this work to a concentration of 50mg/mL would only introduce ~2mM of co-lyophilised salt into the solution. Given that all samples contained 150mM NaCl, this is not expected to give rise to a significant increase in the post-dialysis sample salt concentration. It is hence more likely that the proteins themselves contribute to the conductance of the aqueous solution, implying that the salt concentration as derived from these conductance measurements with the use of a calibration curve of NaCl solutions (see for example Figure 6.1) is slightly overestimated. Hopfer et al (126) also reported that a change in the plasma protein concentration can cause a change in the conductivity of the solution. However, the main conclusion from these experiments is that solutions with a protein concentration comparable to the protein concentration in blood serum can be efficiently desalted by the developed microvolume counter-flow dialyser.

It is also of interest to establish whether the desalting performance of the dialyser changes over time. This was tested by carrying out counter-flow dialysis of the 50mg/mL BSA and 150mM

NaCl sample continuously for 16 hours, with periodical measurement of the post-dialysis sample phase conductivity. The bar chart in Figure 7.2 shows that during the first four hours the sample salt concentration, as determined from conductivity readings, was about 985µM, gradually increasing to 1.13mM for the final 12-16 hour time period. It can hence be concluded that the dialysis performance of the device is very stable, with only a minor decrease in desalting efficiency over time.

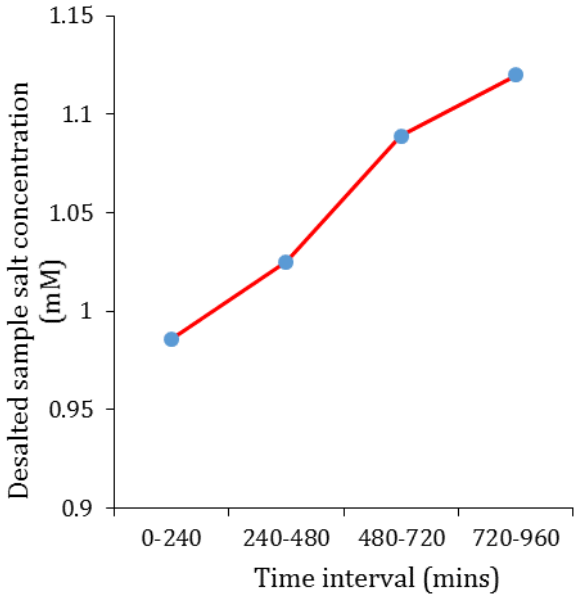

Figure 7.3: Post-dialysis salt concentration of a solution of 50µg/mL BSA and 150mM NaCl, calculated from the post-dialysis conductivity of the sample phase at specific time points. Counter-flow dialysis was performed continuously for a period of 16 hours, with a 5kDa MWCO ultrafiltration membrane, a sample flow rate of 0.5µL/min and a water flow rate of 750µL/min.

Aliquots of the sample phase and post-dialysis water phase, taken at various time intervals, were also measured with UV-VIS spectroscopy. It was experimentally determined that the UV-VIS spectrometer (Perkin Elmer Lambda650) could detect BSA at a concentration of 5nM or higher by the aromatic residue absorbance at 280nm. Water phase samples were measured undiluted but, due to the smaller volumes, the sample phase aliquots were diluted 50-fold in deionized water. An absorbance signal at 280nm could not be detected for any of the water phase aliquots, confirming that the 5kDa MWCO membrane is not permeable to the BSA molecules, which are present at a concentration of 0.75mM (50mg/mL) in the original sample. However, the absorbances measured for the 50-fold diluted post-dialysis protein sample aliquots were approximately 5% lower than those of the pre-dialysis diluted sample aliquots. Although more measurements would have to be performed to confirm that these are not measurement artifacts, it could be the case that a fraction of the proteins that are flowing through the dialyser are retained within the device.

It is possible that membrane fouling occurs to some extent, with protein molecules adsorbing to the membrane material, potentially leading to a reduction in the effective porosity of the membrane. For ultrafiltration membranes it may be important that the skin layer faces the

sample and not the support layer. The ultrafiltration dialysers described in this work always have the sample flowing along the skin layer and the water flowing along the support layer. As an exception, the orientation of the membrane was switched and the UV-VIS spectroscopy experiment described above was repeated. It was found that this resulted in a more pronounced reduction of the absorbance of the post-dialysis protein sample with respect to the pre-dialysis sample. This suggests that the contact of the sample with the micrometer-size pores of the supporting layer and perhaps also the submicrometer pores of the sublayer (see sections 5.3.2 and 5.4) leads to increased membrane fouling. This coincided with a decrease in desalting efficiency over time, which could be caused by a decrease in the effective porosity of a partially protein-clogged membrane.

7.2 Dialysis using different UF membranes

Earlier experiments were carried out on the 5kDa UF membrane for various samples of different protein concentration. In order to widen the applications of the dialysis device built, UF membranes of various MWCO- 1, 5, 10kDa were used.

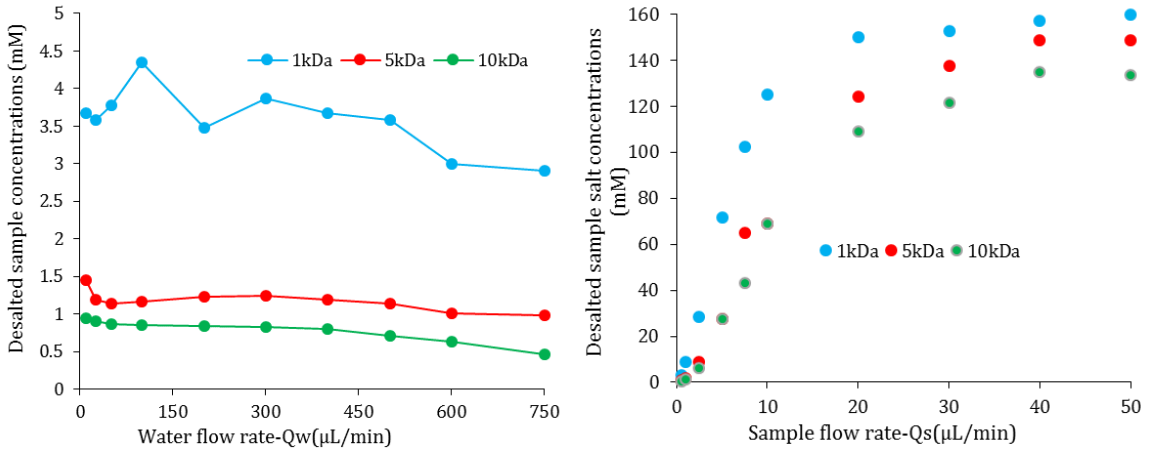

Figure 7.4: Counter-flow dialysis of a sample of 50mg/mL BSA and 150mM NaCl using different UF membranes. (a) Post-dialysis Desalted samplesalt concentration of the sample for Qs-0.5µL/min and varying water flow rates and (b) Desalted sample concentrion for varying sample flow rate and Qw-750µL/min.

The use of the membrane with a MWCO of 1kDa resulted in less efficient desalting for all flow conditions, whereas the 10kDa MWCO resulted in somewhat better desalting than the 5kDa membrane. For example, at Qs-0.5µL/min and Qw-750µL/min, with the 10kDa, 5kDa and 1kDa MWCO membranes, post-dialysis salt concentrations of respectively 452µM, 1.1mM and ~3mM were obtained. These relatively small differences in desalting efficiency are likely related to differences in the porosity of these membranes. As noted in section 5.6.2, the porosity of the 1kDa membrane (ε-0.08%) is lower than that of the 5kDa (ε-0.43%) and 10kDa membranes (ε-0.46%). The choice of the membrane pore size is dictated by the nature of the sample and the type of experiment that is performed with the dialysed sample. For salt removal

from a protein solution, the pores of a 1kDa MWCO membrane are unnecessary small while a 10kDa MWCO membrane is expected to be permeable to the smallest protein species.

7.3 Desalting of blood serum

Human blood serum purchased from Sigma Aldrich was used as the sample in the counter-flow dialyser. The concentration of human serum albumin (HSA) is 40-50mg/mL and the total concentration of all serum proteins is 60-80mg/mL, hence the serum is different from the 50mg/mL BSA and 150mM NaCl sample used in the previous sections because of the wide variety of proteins and other molecules, while the concentration of the majority protein albumin and the ionic strength is similar. The conductivity of human serum was measured before dialysis and was found to be equivalent to a solution of 132mM NaCl. The serum was dialyzed at the highest water flow rate, Qw-750µL/min, using the 5kDa MWCO UF membrane at various sample flow rates. The post-dialysis salt concentration of the serum, estimated from conductance measurements and a NaCl solution calibration curve, is shown in Figure 7.5.

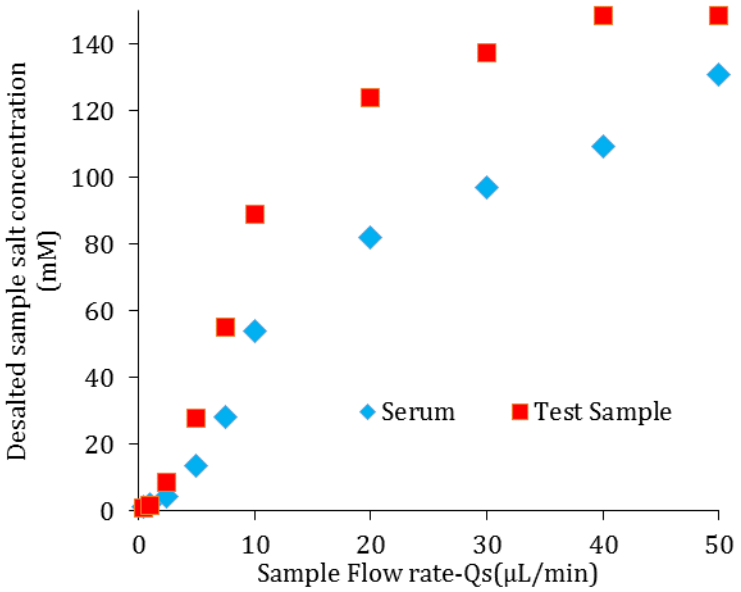

Figure 7.5: Post-dialysis salt concentration human blood serum and of a test sample originally consisting of 50mg/mL BSA and 150mM NaCl. Values, determined for several sample flow rates, are calculated from conductivity readings and a calibration curve of NaCl solutions. Counter-flow dialysis was performed with a 5kDa MWCO ultrafiltration membrane and a water flow rate of 750µL/min.

The data show that despite the complex composition of serum, the post-dialysis conductivity at low sample flow rates is just as low as that of the protein test sample of 50mg/mL BSA and 150mM NaCl, demonstrating efficient desalting of the serum. At sample flow rate(Q_s)-0.5µL/min and water flow rate (Q_w)-750 µL/min, post dialysis of serum showed salt concentration of 1.5mM while the test protein sample showed 1.3mM. At higher flow rates, the post-dialysis conductivity of the serum is consistently lower than that of the BSA+NaCl sample, which is most likely due to the lower initial conductance of the serum. It is also clear that the extent of desalting of the serum can be regulated by the choice of sample flow rate.

7.4 Gel electrophoresis analysis

Protein retention in the sample phase was investigated by on-chip gel electrophoresis with an Agilent 2100 Bioanalyzer system, for serum and for a protein sample dialysed using a 5kDa or a 10 kDa MWCO UF membrane, Qw-750µL/min and Qs-0.5µL/min. Post-dialysis serum samples were diluted 5-fold in order to obtain reasonable variations in gel electrophoresis band intensity, while the post-dialysis protein samples of BSA (66kDa) and cytochrome c (12kDa) and the post-dialysis water phases were applied without dilution. BSA (50mg/mL) was used as an upper marker while cytochrome c (10mg/mL) was used as the lower marker for the test sample. For the gel electrophoresis results depicted in Figure 7.6, diluted post-dialysis serum samples were in lanes 2 and 4 while lanes 3 and 5 contained the corresponding post-dialysis water phase aliquots. Lanes 1 and 6 were used as controls, with lane 1 showing the protein ladder provided with the Agilent Protein 230 chip and lane 6 containing a post-dialysis sample of BSA and cytochrome c proteins.

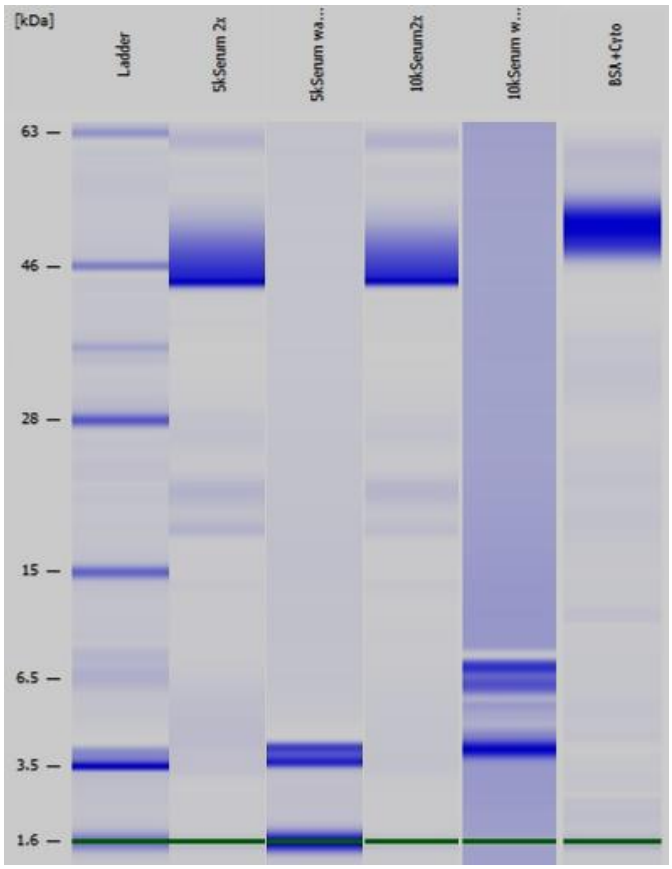

Figure 7.6: Gel electrophoresis results of serum samples and water samples after counter-flow dialysis. Lane (1) protein ladder, (2) 5-fold diluted dialyzed serum using a 5kDa MWCO membrane, (3) water phase obtained from 5kDa membrane after dialysis, (4) 5-fold diluted dialyzed serum using a 10kDa MWCO membrane, (5) water phase obtained from 10kDa membrane after dialysis, and (6) sample containing BSA and cytochrome c proteins.

Lane 2 shows that there are no protein bands above 5kDa in the post-dialysis water phase of the serum sample dialysed with the 5kDa MWCO membrane, while lane 5 shows that there are no protein bands above 10kDa when a 10kDa MWCO membrane was used. Given that the detection limit of this gel system is about 10µg/mL it can be concluded that the 5kDa and 10kDa

membranes are indeed permeable to proteins that are smaller than these MWCO specifications and are not permeable to proteins with a molecular weight larger than these MWCO values. The lanes that contain the serum sample or the BSA/cytochrome c sample show an intense band that migrates with an apparent molecular weight of ~50kDa which is attributed to albumin. Because this is by far the most abundant protein in serum and because the Bioanalyser instrument adjust the imaging conditions according to the most intense band, other protein bands are difficult to observe. However, it is clear that albumin is retained in the sample phase and was not able to diffuse over the membranes into the water phase. Determination of the protein composition of the post-dialysis sample and water phase by gel electrophoresis thus indicates that the ultrafiltration membranes perform according to their MWCO specifications, also for the complex biological sample that is human serum.

7.5 Response to variations in the sample flow rates

The effect of varying the flow rate of the sample and/or water phase can be studied by continuously recording the conductivity of the post-dialysis sample stream. Rather than collecting the sample as it exits the dialyser into small (~50µL) aliquots that are each measured with a conductivity meter, the conductivity meter was connected to the sample (or water) outlet of the dialyser. This enables a 'live recording' of the post-dialysis conductivity, which is convenient to establish how the conductivity changes when the sample or the water flow rate is changed. Initially the conductivity sensor was calibrated with a calibration solution with a conductivity of 1.41mS/cm and then DI water was passed through until a conductivity of 1µS/cm was measured, which is the lowest value that the conductivity meter can measure.

A sample consisting of 50mg/mL BSA and 100mM NaCl was then flown through the counter-flow dialyser with periodic changes in the sample flow rate. The salt concentration of the post-dialysis sample phase, calculated from the conductivity recording, is presented in Figure 7.7 as a function of time, with the timing of the sample flow rate changes indicated in the Figure.

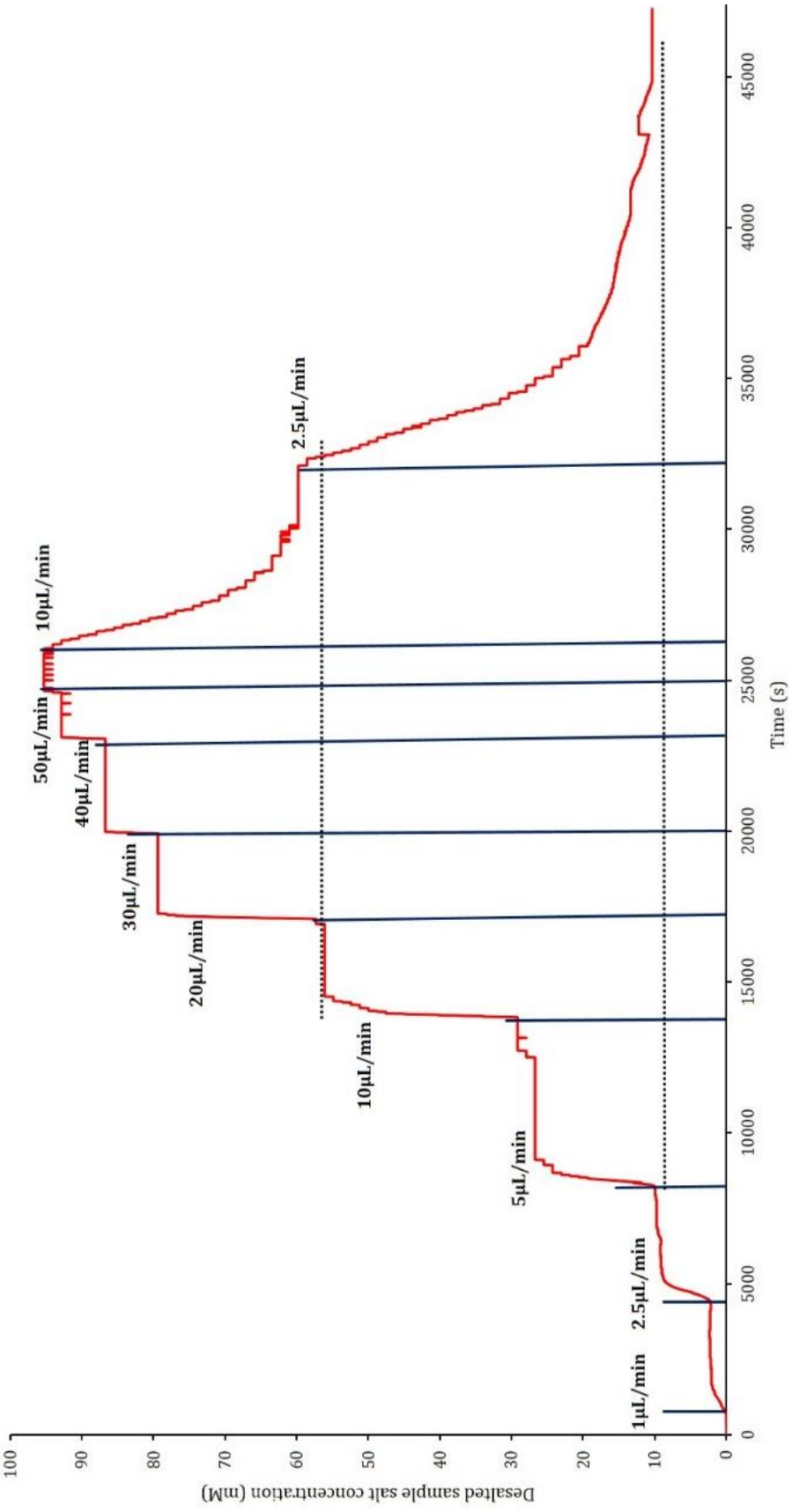

Figure 7.7: Continuous recording of the conductivity, presented as a salt concentration, of the post-dialysis sample stream for a sample of 50mg/mL BSA and 100mM NaCl. The water flow rate is kept constant at 750µL/min while the sample flow rate is periodically changed, as indicated by the annotated blue lines. Counter-flow dialysis was performed with a 5kDa MWCO membrane.

Starting with a low sample flow rate, it is observed that increasing the sample flow rate leads to a new stable conductivity value after a period of time (up to ~20min) during which the salt concentration gradually increases. As shown in Figure 7.8, for the higher sample flow rates, where the salt dialysis is relatively inefficient, this period of time is reduced.

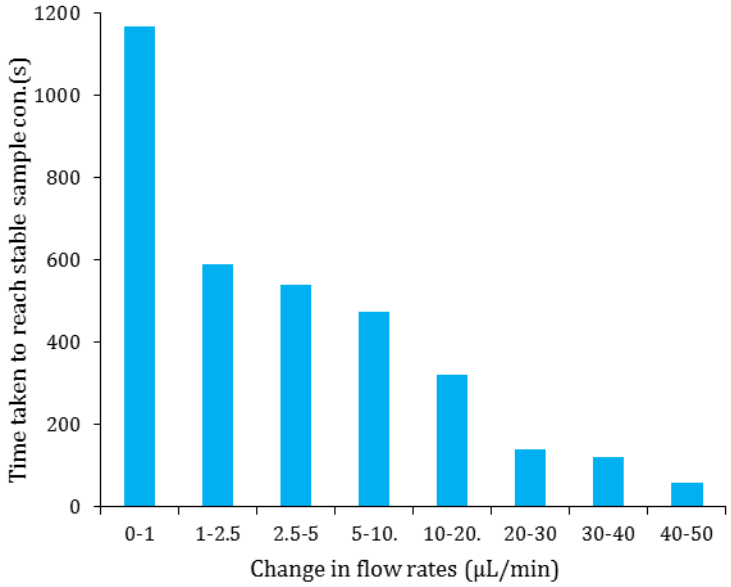

Figure 7.8: Time taken to reach a stable new post-dialysis sample concentration in the conductivity sensor well for various changes in the flow rates (e.g. "1-2.5" refers to a flow rate change from 1 to 2.5µL/min), determined from the data in Figure 7.7

It is important to note that the sensor surface of the conductivity meter plays an important role in the recording set up. Approximately 50µL of the sample is required at the sensor surface/well (shown in Figure 4.6) for accurate measurements. For larger changes in the post-dialysis salt concentration it takes more time for the entire solution in the well to reach the new, higher, salt concentration. Likewise, when sample flow rate is decreased from 50µL/min to 2.5µL/min, the time taken to reach a new stable conductivity reading is quite long (~1hr), reflecting the amount of time to dilute the post-dialysis sample in the conductivity well. In other words, with Qs-50µL/min desalted sample salt concentration was measured to be 100mM. So the sensor would have 50µL of sample which has a salt concentration of 100mM. With Qs reduced to 20µL/min, the output salt concentration is ~60mM. So the gradient between the two stable points is the time taken by a post-dialysis sample of 60mM to dilute a sample of 100mM to 60mM. The gradient of change increases when sample flow rate is reduced further, which can be observed when sample flow rate is reduced to 2.5µL/min. The limiting case for this gradient is the volume required to wet the entire sensor surface on the conductivity meter.

The rate of the salt concentration change (µM/s) in the well of the conductivity meter was extracted from Figure 7.7 and is shown in Figure 7.9 for each sample flow rate transition. The rate of salt concentration change increased significantly up to a sample flow rate of 10µL/min, after which this rate remained fairly constant until the sample flow rate was reduced. When sample flow rate changes from 0-1µL/min, the rate of concentration change is around ~2µM/s. at the same time when sample flow rate changes from 5-10µL/min, the rate is 72µM/s. As noted above, the rate of salt concentration change is expected to be lower when the difference between the new and the previous sample output salt concentration is larger. These rates

would all be increased when a smaller-volume well would be designed for the conductivity sensor, especially with a lamellar flow over the conductivity sensor.

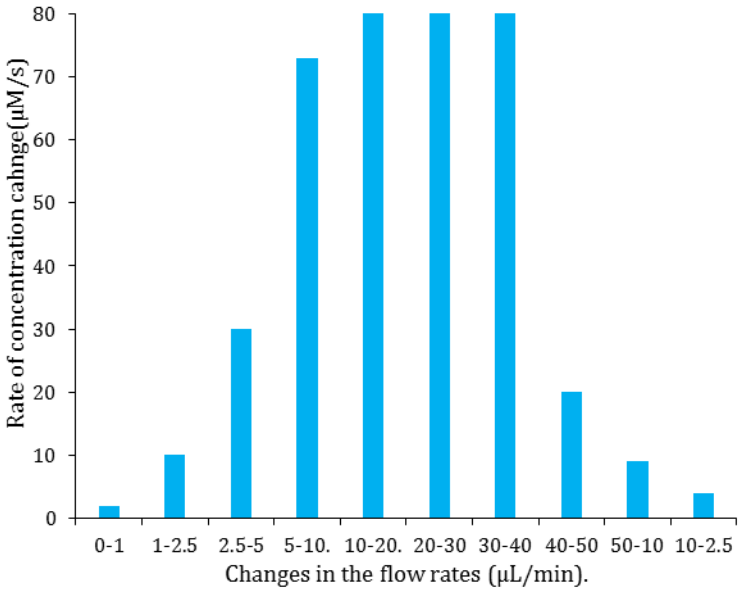

Figure 7.9: Rate of change of the post-dialysis salt concentration in response to a change in sample flow rate (e.g. "1-2.5" refers to a flow rate change from 1 to 2.5µL/min), determined from the data in Figure 7.7

Next, to observe how the conductivity of the post-dialysis water phase varies with changes in Qs and Qw, another conducitivity meter was connected to the dialyser, at the outlet of the water channel. The benchtop conductivity meter used for this had a modified conductivity cell which requires around 750µL of sample for accurate measurements. For a sample of 50mg/mL BSA and 100mM NaCl, the salt concentration of the post-dialysis sample phase and of the post-dialysis water phase was measured simultaneously while the flow rates were changed, and the results are shown in Figure 7.9. It is clear that any change in flow rate affects the conductivity of the sample phase as well as that of the water phase. Initially Qw was kept constant at 750µL/min and Qs was increased from 1 to 2.5 to 5µL/min, which resulted in an increase of the salt concentration in both the sample and the water phase. The sample phase conductivity was increased because a faster sample flow rate reduces the extent of salt diffusion from the sample into the water phase. The conductivity of the water phase also increased, but not to the same extent, probably because a faster sample flow rate implies contact with a larger sample volume. On the other hand, when Qs is kept constant at 1µL/min, decreasing Qw from 750 to 300 to 100µL/min results in a minor increase in the post-dialysis sample salt concentration but a large increase in the post-dialysis water phase salt concentration.. With a decrease in Qw the amount of time water is in contact with the sample across the membrane is longer, which would enable more salt to diffuse into the water phase.

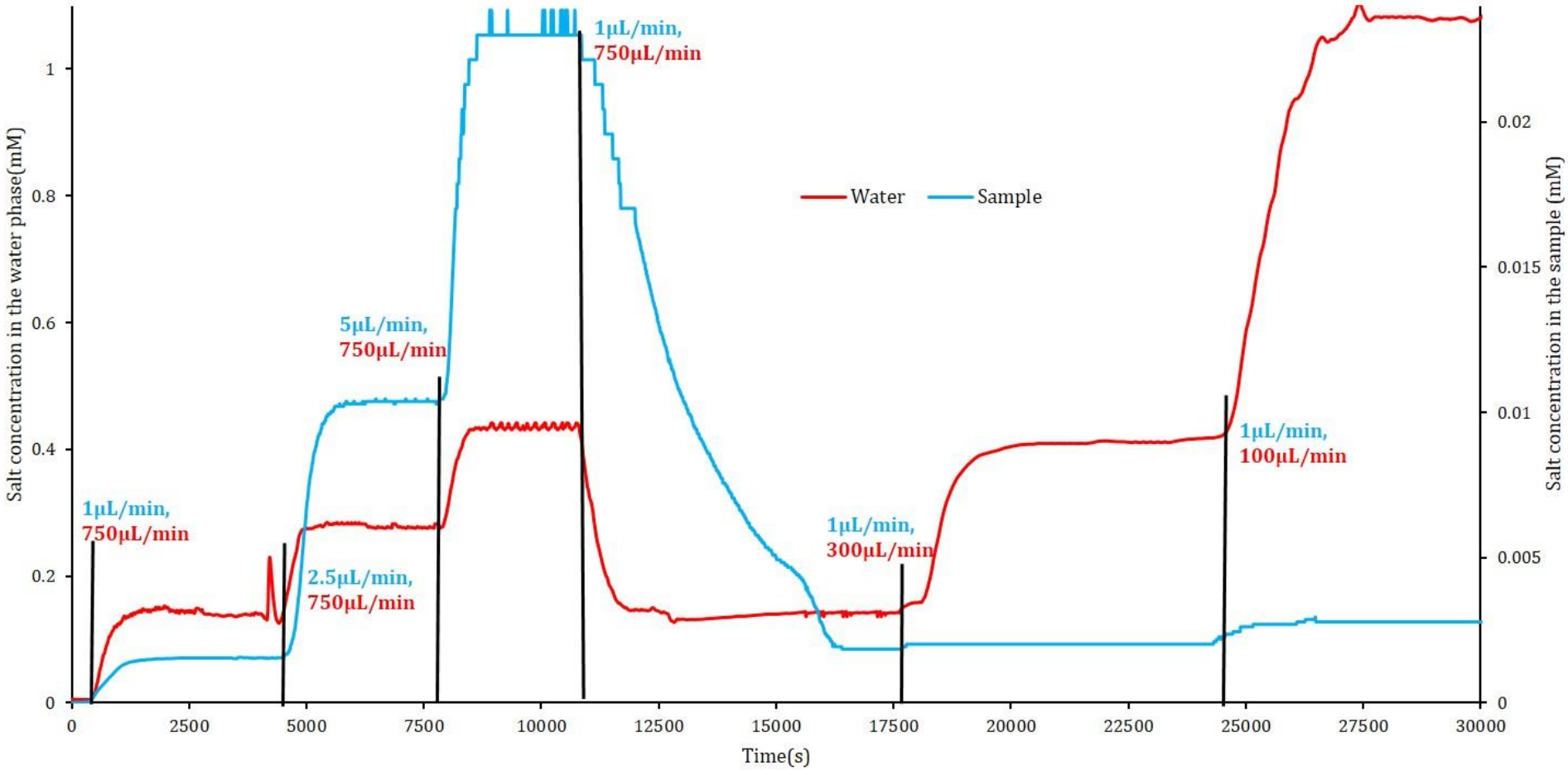

Figure 7.10: Continuous recording of the conductivity, presented as a salt concentration, of the post-dialysis sample stream and the post-dialysis water stream for a sample of 50mg/mL BSA and 100mM NaCl. The water flow rate is initially kept constant at 750µL/min while the sample flow rate is increased from 1 to 5 µL/min, after which the sample flow rate is kept constant at 1µL/min and the water flow rate is reduced to 100µL/min, as indicated by the annotated black lines. Counter-flow dialysis was performed with a 5kDa MWCO membrane.

The rate of the salt concentration change in the flow chamber of the conductivity meters is shown in Figure 7.11. When a flow rate is changed in such a way that the output salt concentration changes significantly, it takes a longer time until a new stable conductivity value is obtained. As mentioned above, this time could be reduced by developing smaller conductivity flow chambers.

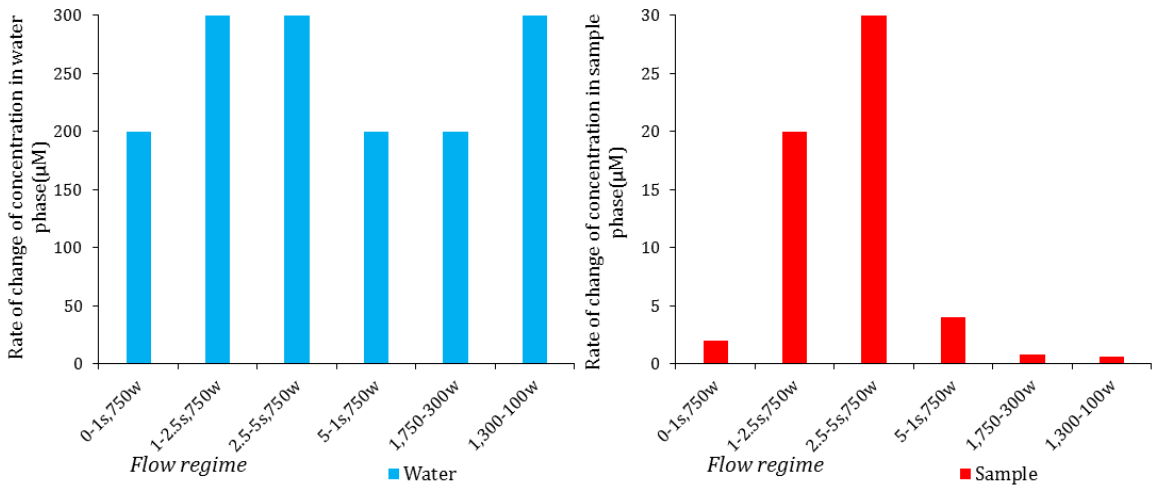

Figure 7.11 Rate of change of the salt concentration in the water phase (blue bars) and in the sample phase (red bars), upon changing either the water or the sample flow rate, calculated from the data in Figure 7.10.

The continuous monitoring of the output sample channel and the output water channel clearly illustrates that the extent of sample desalting can be tuned by regulation of the sample and the water flow rate, and that increasing the water flow rate beyond ~300μL/min only leads to a marginal improvement in sample desalting. This relates back to the analysis of the dialysis efficiency in the previous chapters, especially section 6.5.

7.6 Summary

Desalting of samples of higher protein concentration, a mixture and serum samples were well investigated by means of counter-flow dialysis using the set up discussed in the previous chapter. The influence of salt removal for using membrane of different molecular weight cut-off was elaborated from which it can be inferred that membranes with low MWCO removes lower salt than membranes with higher MWCO for similar flow conditions. The retention properties of these membrane were evaluated using gel electrophoresis. Tuneable desalting has been achieved as demonstrated by controlling the flow rate of the sample and water. The salt dialysis performance was characterized in Chapter 6 with NaCl solutions that contained a low concentration, 2mg/mL, of fluorescently labelled albumin to visually verify that this protein did not diffuse through the membrane into the water phase. In this chapter , solutions with a higher protein concentration, protein mixtures and also blood serum were investigated the performance the counter-flow dialyser with a protein content more typical for biological

samples. Under optimal sample and water flow conditions the conductivity of the post-dialysis sample phase only increased marginally for higher albumin concentrations. If the proteins themselves do not contribute to the conductivity, which may not be the case, a 50mg/mL BSA and 150mM NaCl solution, contains only 1.1mM salt after dialysis. If the proteins do contribute to the conductivity, the actual salt concentration will be less. For the same sample, the counter-flow dialyser can be operated continuously for at least 16 hours with only a minor reduction (~1%) in desalting efficiency, which may be related to protein adsorption to the 5kDa MWCO membrane. Desalting was slightly more efficient (~0.8mM salt) with a 10kDa MWCO membrane and somewhat less efficient (~3.5mM salt) with a 1kDa MWCO membrane, which probably reflects differences in membrane porosity as established in Chapter 5. Continuous monitoring of the conductivity of the post-dialysis sample and water phases revealed the response to changes in flow rate, which in terms of the conductivity measurements themselves is presently limited by the volume of the flow cells on top of the conductivity sensors. Dialysis of human serum resulted in a very similar dependence of post-dialysis sample conductivity to the sample flow rate as observed for the 50mg/mL albumin with 150mM NaCl solution, indicating that a complex biological solution can also be efficiently desalted. Preliminary gel electrophoresis experiments indicated for serum dialyzed with 5kDa or 10kDa MWCO membranes that larger proteins are not present in the water phase and hence that these ultrafiltration membranes perform according to the specifications of the supplier.

Chapter 8: Application of counterflow dialysis in Mass Spectrometry

As outlined in Chapter 2, mass spectrometry is an important bioanalytical technique but is not compatible with physiological salt concentrations because an excess of electrolyte ions leads to a large number of different salt adducts (e.g. $[M + iH + jNa + kK]^{(i+j+k)+}$) for each charged biomolecular species, causing signal broadening and a reduced intensity of the $[M + nH]^{n+}$ species. To determine the effect of various distinct salt concentrations on the quality of the mass spectrum, a protein sample containing 10mg/mL cytochrome c (0.8mM) in phosphate buffered saline (PBS) was dialysed with the counter-flow dialyser (see section 6.4) with a 5kDa MWCO UF membrane under various flow conditions. Table 7.1 lists the desalting conditions and shows the post-dialysis salt concentration of the samples, estimated from conductivity measurements.

Table 8.1: Salt concentration of the 10mg/mL cytochrome c solution in PBS, before (Cytc150) and after dialysis under various flow conditions.

Sample abbreviation	**Sample flow rate used for desalting Q_s(µL/min). Q_w=750µL/min**	**Sample salt concentration (mM)**
Cyctc150	0	~150
Cyctc0.5	0.5	~1.3
Cyctc5	5	~31
Cyctc10	10	~95

Mass spectrometry of these samples, mixed with methanol and formic acid to enhance protonation, was then performed by Mr Neville Wright of the Biomolecular Facility (Center for Biological Sciences, University of Southampton) as described in section 4.8. Myoglobin served as a calibration protein for the mass spectrum analysis and while the cytochrome c signals were used to assess the quality of the mass spectrum. The obtained mass spectra are depicted in Figures 7.12 and 7.13.

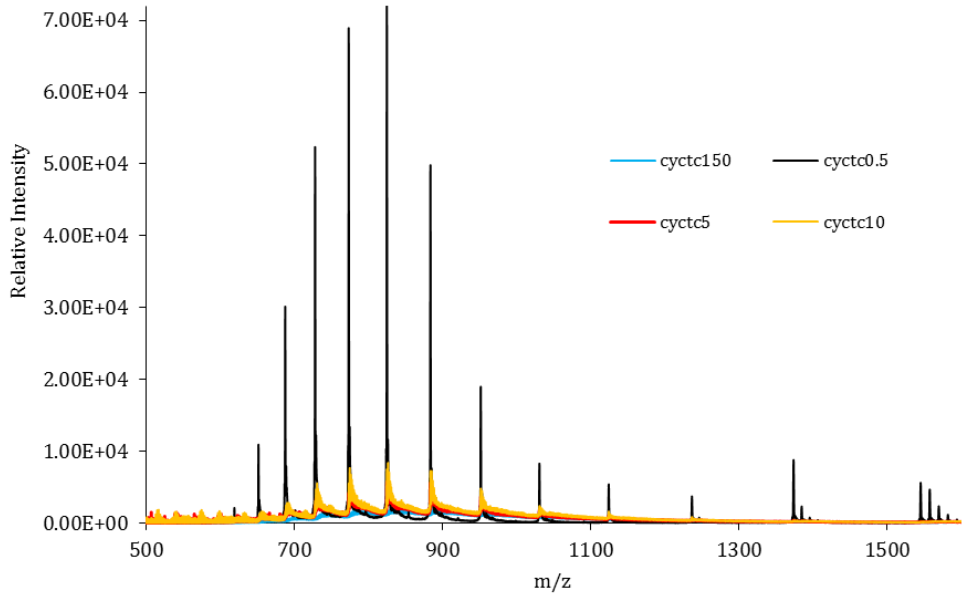

Figure 8.1: ESI m/z spectra of cytochrome c solutions with different salt concentrations. The sample abbreviations are explained in Table 7.2.

Figure 7.12 clearly shows that the m/z spectrum of the sample with the lowest salt concentration (Cyctc0.5=1.3mM) has the most intense signals, giving well-resolved $[M + nH]^{n+}$ peaks for cytochrome c. The dialysed samples with a salt concentration of ~31 and ~95mM give approximately 10-fold less signal intensity and also suffer from significant peak broadening by the salt adduct species, whereas in the spectrum of the non-desalted Cytc150 sample the $[M + nH]^{n+}$ positions are hardly distinct from the salt adduct background signal. This is emphasized by scaling all mass spectra to the same maximum intensity as the Cytc0.5 spectrum (Figure 7.13)

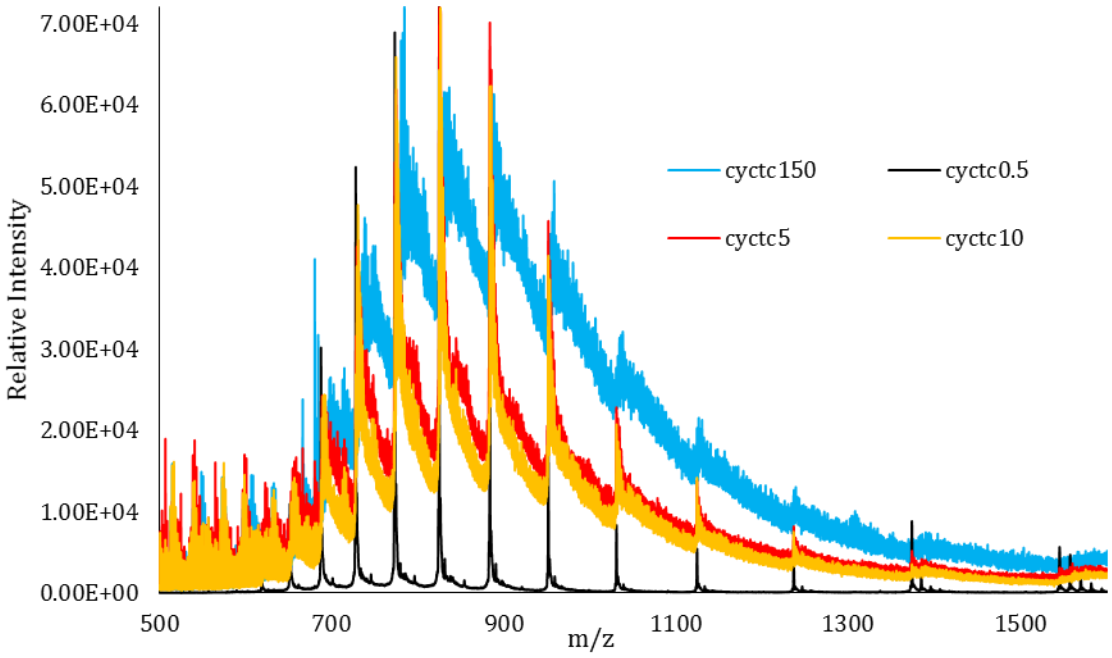

Figure 8.2 ESI m/z spectra of cytochrome c solutions with different salt concentrations. The relative intensity axis only applies to the cytc0.5 sample; the intensity of the other spectra have been normalized with respect to the maximum intensity of the cytc0.5 spectrum.

The fact that the high-salt content Cytc10 and Cytc150 samples still give a m/z spectrum with some discernible features illustrates that nano-electrospray mass spectrometry is the most salt tolerant method of all the mass spectrometry techniques. However, the m/z spectrum needs to be deconvoluted to obtain the mass spectrum which gives the mass of the original non-ionized protein species. These mass spectra of the four different cytochrome c samples are shown in Figure 7.14a, while Fig 7.14b shows the spectra of the samples normalized to the maximum intensity of the Cytc0.5 sample.

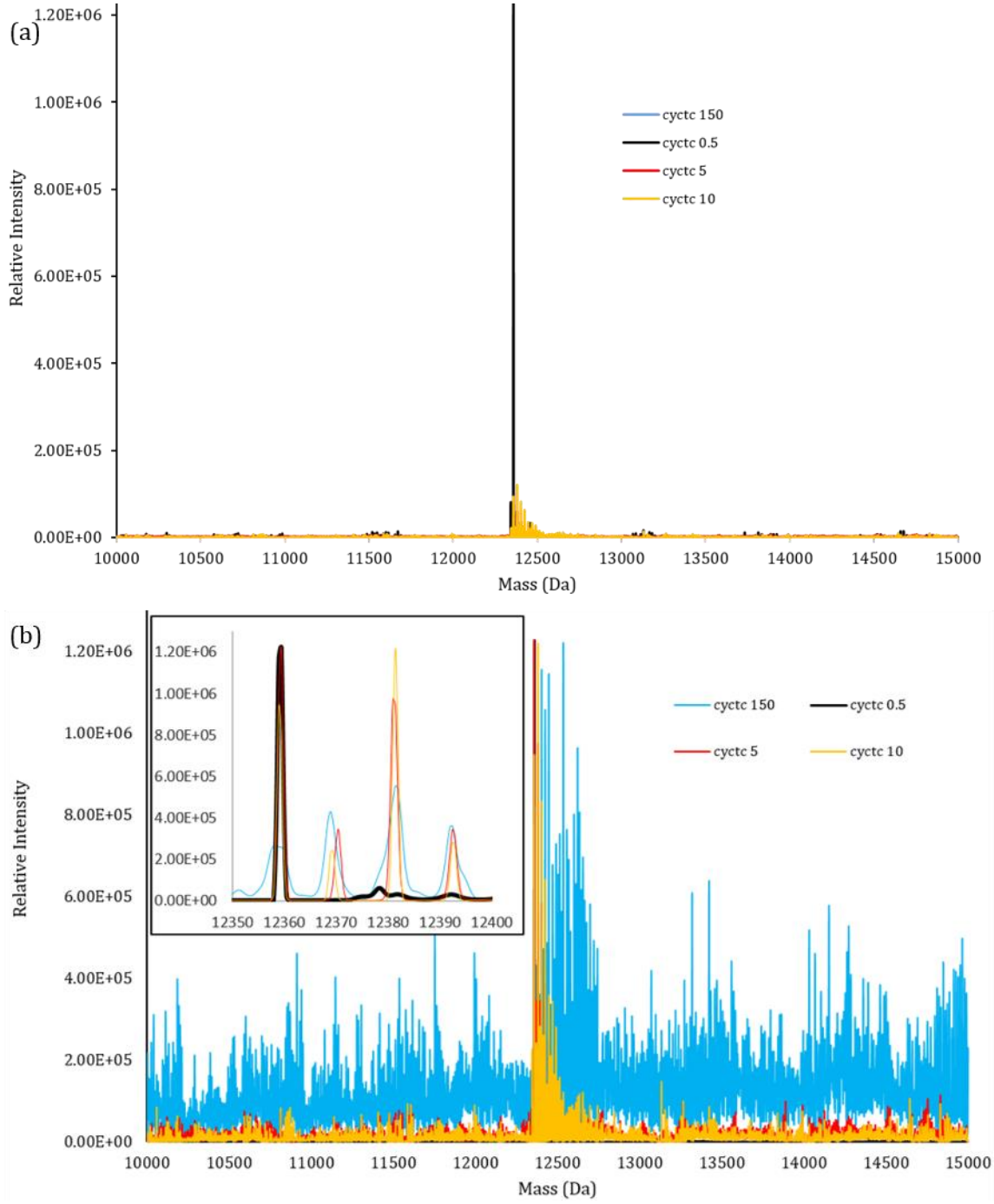

Figure 8.3: (a) ESI mass spectra of cytochrome c solutions with different salt concentrations, obtained by deconvolution of the m/z spectra. Deconvulted data obtained from the mass spectrometer for samples containing cytochrome c. (b) Intensity-normalized mass spectra; the relative intensity axis only applies to the cytc0.5 sample. Inset: Expanded view of the mass values close to the molecular weight of cytochrome c. The sample abbreviations are explained in Table 7.2.

As can be seen from these mass spectra, the molecular weight of cytochrome c can readily be determined in the case of the Cytc0.5 sample as 12358Da, which has been desalted to a salt concentration of 1.3mM. The Cytc5 sample with ~31mM salt gives a more complex mass spectrum but the most intense peak indicates the correct mass of the protein. For the sample with 95mM salt this is almost, but not quite, the case as well. However, for the non-desalted cytochrome c sample the mass spectrum consists of a large number of peaks spread over quite a wide range of mass values and hence the correct molecular weight of the protein cannot be identified. The above data indicate that the deconvolution procedure is complicated by the presence of salt adduct species in the m/z spectrum. With high salt concentrations, presence of peaks between the peaks would be masked as in the case of a complex samples where there are more than a single protein. Figure 7.12 and 13 clearly exhibits this phenomenon in the range where m/z is between 1300 and 1700. Hence, for biological samples that consist of a wide range of different proteins with similar molecular weights, the mass spectrometry is more demanding and the salt content of the samples is expected to be more critical.

Therefore another protein sample was prepared which also contained lysozyme, which is only 2kDa heavier than cytochrome c.

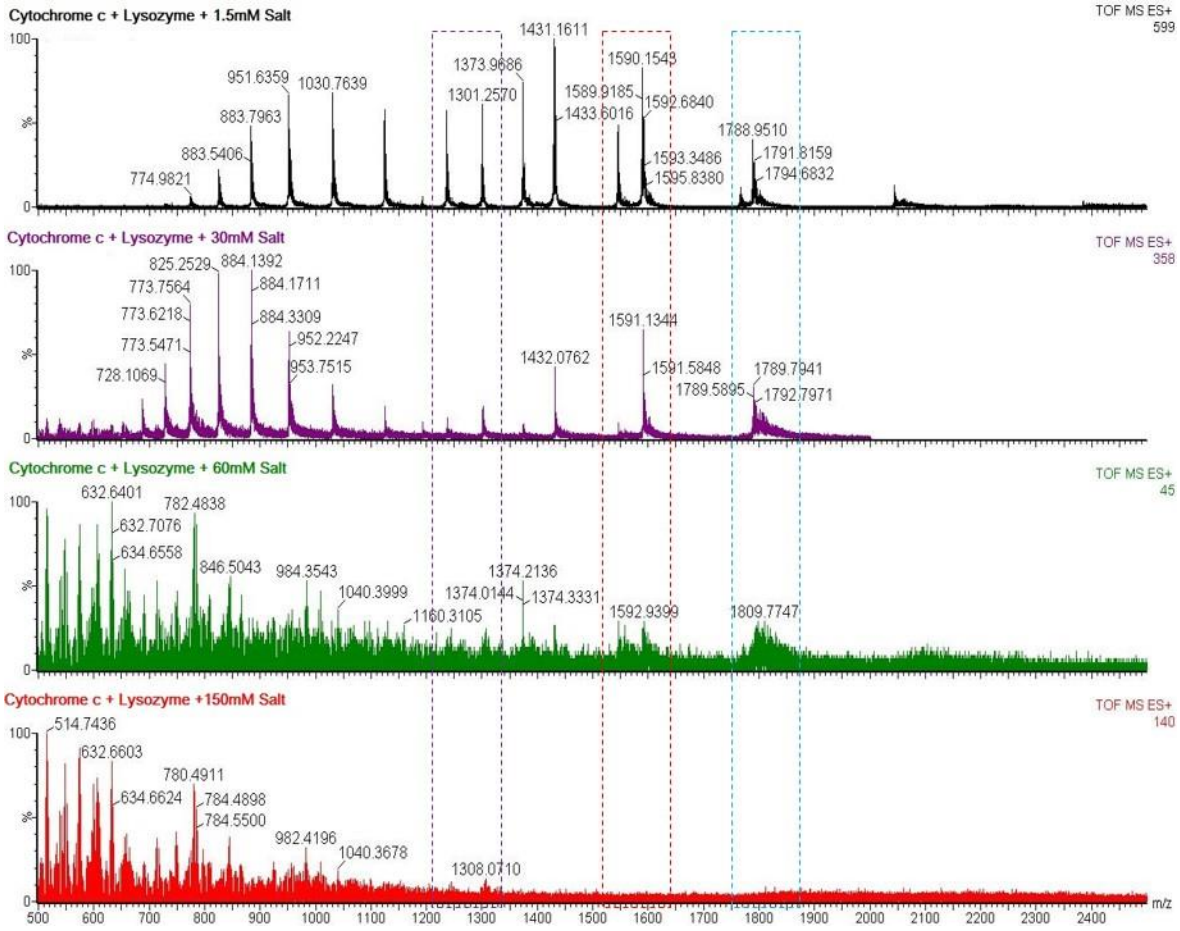

Figure 8.4 ESI m/z spectra of protein samples containing cytochrome c and lysozyme with different salt concentrations as indicated in the panels. All spectra are scaled to the intensity of the strongest signal.

This sample was prepared in the same way as the previous protein sample of cytochrome c and lysozyme was also present at 10mg/mL (0.7mM). Counter-flow dialysis was employed to reduce the original salt content of 150mM to 60, 30 or 1.5mM. Mass spectrometry of the original and the desalted samples was then performed by Mr Neville Wright.

The m/z spectra in Figure 7.15 show that for the sample with the lowest salt concentration of 1.5mM, many well resolved signals with high intensities are present in the ~800-1700 region of the spectrum. For the sample with 30mM salt, the same signals can be recognized in the m/z spectrum but due to salt adducts the relative intensity of many peaks has been severely reduced. It is noteworthy that the m/z signals for cytochrome c, which are expected to cluster around a value of 900 (see Figure 7.13), are less reduced than the signals for lysozyme, which are most likely clustered around a value of 1500. This reflects different salt adduct formation tendencies of these two proteins. At 60mM and 150mM salt, signal intensities are almost reduced to baseline level due to the occurrence of more salt adduct species (e.g. $[M + iH + jNa + kK](i+j+k)^{n+}$) for each $[M + nH]^{n+}$ species. Unfortunately, the deconvoluted mass spectra were not made available, but it is expected that only the two protein samples with the lower salt concentration would correctly identify the molecular weight of cytochrome c and lysozyme. Because desalting of protein samples to a residual salt content of ~1mM may have adverse effects on biomolecular structure and biomolecular interactions, the capability of the developed counter-flow dialyser to determine the extent of salt removal by the selection of the sample and water flow rates enables the analysis of protein samples at the highest salt concentration that still gives good mass spectrometry results.

Finally, a trial experiment was performed with human serum, a sample that is considered to be inaccessible to mass spectrometry without extensive sample pre-treatment.

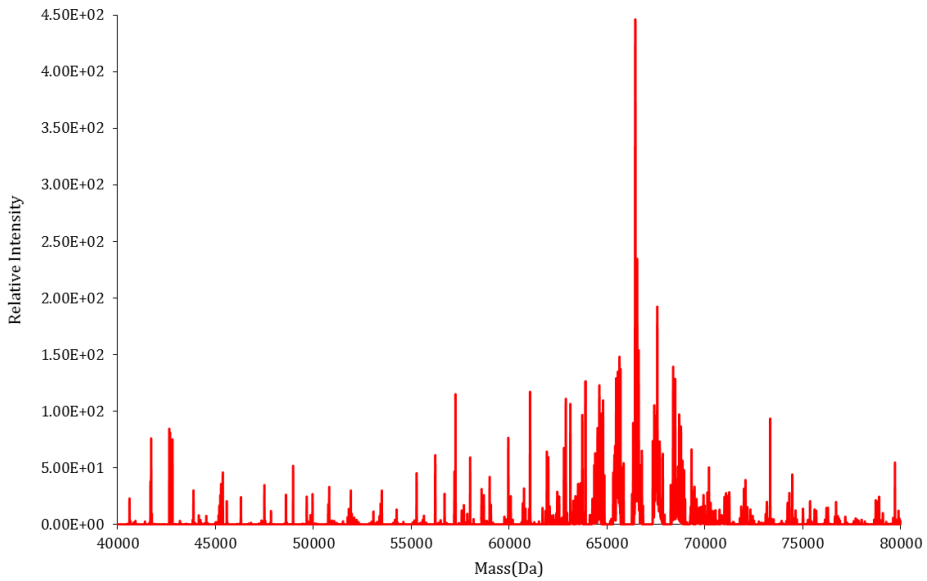

Figure 8.5: ESI Mass spectra obtained for serum samples after desalting containing ~1.5mM of salts. A distinct peak corresponding to the human serum albumin (66kDa) can be noticed.

Human serum was desalted to 1.7mM from its initial concentration of 138mM salt by counter-flow dialysis with Q_s=0.5µL/min and Q_w=750µL/min. The mass spectrum shown in Figure 7.16, obtained by Mr Neville Wright, shows a main signal at ~66.5kDa, corresponding to albumin, which would not be observable without extensive desalting of the serum. However, because the serum concentration of albumin is significantly higher than the concentration of other blood proteins, the albumin signal dominates the mass spectrum. Mass spectrometry analysis of serum samples therefore requires an albumin depletion step, either before or after the desalting step.

8.1 Summary

Mass spectrometry measurements with serum and with solutions containing two or three different proteins illustrated how the quality and hence information content of mass spectra depend on the salt concentration of the sample. It can be inferred that with reduction in the salt concentration in the sample a high quality mass spectrum will be obtained showing unique peaks useful in distinguishing one protein from another. Evaluating the samples obtained from desalting using the microdialyser it can be noticed how the sample has been enriched for better analysis.

Chapter 9: Conclusion and Future Outlook

9.1 Summary

Detection and quantification of molecular biomarkers, biomolecules that are associated with a specific disease or even a specific stage of a disease, promises significant advantages for medical diagnostics, especially for complex diseases such as cancer. Mass spectrometry is an established biomolecular analytical technique, also in the area of proteomics, while nanoscale field effect transistors are being developed as an adaptation of CMOS technology for point-of-care biomolecular sensors. However, both these label-free techniques are incompatible with physiological salt concentrations, in the case of mass spectrometry because of salt adduct formation with concomitant peak broadening and in the case of nanoFET biosensing because of the short Debye length. Desalting of the sample prior to loading in the detection device is hence necessary for these methods.

Conventional desalting protocols require a large sample volume (millilitres), multiple process steps and/or take a long time (tens of hours). This is all disadvantageous for molecular diagnostics, particularly for point of care applications, for which small sample volumes such as a blood droplet obtained by fingerprick and simple and robust one-step assays are preferred. A small number of microvolume desalting devices have been described in the literature and some of these have been commercialized for mass spectrometry sample desalting. However, these devices can only desalt to one specific salt concentration and several designs have not been tested with protein solutions that mimic a biological sample. The main aim of this work was therefore to develop a microvolume dialyser capable of desalting protein samples to any desired salt concentration.

The various methods of desalting were reviewed in Chapter 2. These include size exclusion chromatography, reverse osmosis, dialysis and electrodialysis. It was noted that most literature on miniaturized desalting devices concerned dialysis, where the salt molecules diffuse from a retentate/sample phase over a semi-permeable porous membrane to a dialysate/water phase with a low salt concentration. It was concluded that this was also the most suitable approach for this project, from a fabrication/operation perspective as well as from a desalting performance perspective. It was then established in Chapter 3 that the dialysis performance can be predicted from diffusion and mass transfer theory. This requires knowledge of the dimensions and flow conditions of a dialyser but also of the pore structure (size, shape, 'length' and density) of the membrane.

Previous approaches to microvolume dialysis included planar membranes sandwiched between retentate and microfabricated dialysate channels as well as hollow fibre membranes suspended in a dialysate tube of millilitre volume. As described in Chapter 4, it was possible to define microvolume sample and water compartments by laser ablation of optically transparent acrylic sheets. A method was developed to attach commercially available membranes to a layer that defines a microvolume sample compartment/channel without leakage along the membrane into a (bulk or channel-confined) water phase and without blockage of the membrane pores. A hollow fibre membrane dialyser was also constructed, but this only served as a reference device because hollow fibre membranes with a suitable pore size for desalting could not be sourced. Furthermore, handheld 'dip stick' conductivity meters were customized with flow cells that enable microvolume conductivity measurements, from which the salt concentration in the sample and the water phase can be derived.

Membranes of different materials and with a wide range of pore sizes were introduced in Chapter 5. Track etch membranes of polyethylene terephthalate with pore sizes from 50 to 1000nm were employed as reference membranes because of their known pore size and pore density, and because of their regular shape, also their known porosity. Ultrafiltration membranes prepared by the phase inversion method consisted of either regenerated cellulose or polyether sulfone, with nominal MWCO values of 1, 5, 10, 100 and 300kDa. The expected ultrastructure of the track etch and phase inversion ('ultrafiltration') membranes was confirmed by scanning and transmission electron microscopy. Ultrafiltration membranes consist of a ~200nm thick skin layer that contains the smallest pores, underneath which is a ~20µm thick sub-layer, where the irregularly shaped pores are substantially larger, up to hundreds of nanometers. This UF membrane is supported by a fibrous support layer with a mesh size of ~50µm. The porosity of these membranes was determined with an extensive set of electrical porosity and diffusional porosity measurements, using a 50nm track etch membrane of known porosity as a reference. Both methods indicated a porosity of ~0.5%, which matches well with the literature on phase inversion membranes.

The desalting capability of the dialyser configurations described in Chapter 4 was then characterized, primarily with 5kDa MWCO UF membranes which are expected to be permeable to salt ions but not to proteins. The test sample consisted of 150mM NaCl, approximately physiological ionic strength, and 2mg/mL fluorescently labelled bovine serum albumin to visually verify that the sample solution did not leak out of the sample compartment and that this 66kDa protein did not diffuse through the membrane into the water phase. Chapter 6 outlines a systematic approach to maximize the desalting efficiency. First, static dialysis against a bulk water phase showed that the salt concentration of the test sample was gradually reduced while the albumin proteins were contained in the sample compartment. Next, in a dialyser

where also the water phase was confined in a milliscale acrylic chamber, static dialysis was performed with periodic refreshment of the water phase. Although the water content of the channel was ~400-fold smaller than the previous bulk water volume, similar salt removal rates were achieved for high refreshment rates, while lower rates significantly decreased the extent of desalting.

Equivalent continuous flow rates were calculated and experimentally implemented in a dynamic dialyser with a continuously flowing water phase, where the same relationship was observed. To realize desalting of an unspecified sample volume, counter-flow dialysis was then implemented, with enables a continuous sample input and (desalted) output flow. Using a very low sample flow rate (0.5μL/min) and a high water flow rate (750μL/min) the salt concentration of the test sample could be reduced to ~200μM, representing a desalting efficiency of 99.88%. Significantly, by selecting the appropriate combination of sample and water flow rate, any post-dialysis test sample salt concentration down to 0.2mM can be realized, as demonstrated in Table 6.5 for 110 different flow rate combinations. These experimental results were then compared, for a range of flow rates, with predictions based on mass transfer theory, for which knowledge of the UF membrane porosity, measured in Chapter 5, was required. The theoretical desalting performance was in good agreement with the actual measurements, and this analysis indicated that a significant increase in dialysis efficiency is only possible with a membrane of larger porosity and/or a smaller thickness.

Finally, in Chapter 7, the performance of counter-flow dialysis was investigated for samples with a protein content more typical for biological samples and also for human blood serum. Under optimal sample and water flow conditions, the salt content of a 50mg/mL BSA and 150mM NaCl solution could be reduced to ~1mM, while the dialyser could be operated continuously for 16 hours with only a minor reduction (~1%) in desalting efficiency which suggests that significant membrane fouling does not occur. Tuneable desalting with sample enrichment- the novelty of this research has been demonstrated by varying the flow rates and gel electrophoresis. During device operation the flow rates could be changed, as demonstrated by 5-9 flow rate adjustments during ~10-hour dialysis runs, which resulted in the expected change in desalting performance. Significantly, dialysis of human serum resulted in a very similar dependence of post-dialysis sample conductivity to the sample flow rate as observed for the high-concentration albumin sample, indicating that a complex biological solution can also be efficiently desalted, without, as established by gel electrophoresis, loss of proteins larger than the specified MWCO of the membrane.

Subsequent mass spectrometry measurements with serum and with solutions of lysozyme and/or cytochrome c, desalted to a specific extent, showed how the quality and hence information content of mass spectra depend on the salt concentration. This illustrates how this

important bioanalytical technique depends on efficient desalting approaches that do not interfere with the structure or interactions between the biomolecules, including molecular biomarkers, in the sample. The microvolume tuneable counter-flow dialysis method developed in this work not only enables efficient desalting down to ~1mM ionic strength, but also offers the opportunity to retain a specific salt concentration in the sample that strikes a balance between mass spectrometry performance and preservation of intra and inter-biomolecular interactions.

9.2 Recommendations for future work

The counter-flow dialyser developed in this work has been constructed with rapid prototyping methods and materials to establish proof of concept. As raised in section 4.6, the main limitation in achieving a meandering, densely packed, channel geometry is that either the membranes are glued to the acrylic material (and that the glued membrane areas have to be remote from the active areas to avoid clogging of the membrane pores), or that the membrane is tightly secured at its perimeter by mechanical pressure, but not at its centre where the channels are defined. The commercially available ultrafiltration membranes have excellent dialysis properties but are not amenable to traditional microfabrication bonding methods. Future development could therefore focus on designing the two device layers in such a way that the membrane can be sandwiched tightly between the two layers at any position where there are no channels, also at narrow areas that define the walls of a meandering channel. This may necessitate selecting another matrix material than an acrylic sheet and also another fabrication method to create the channel structures.

Traditional microfluidic fabrication strategies, e.g. using photoresist laminates as template for replica moulding would enable a dialyser with shallower channels, but this would only be beneficial in terms of sample throughput if smaller sample volumes can be flown faster through the dialyser because of an increase in desalting efficiency. In terms of measuring the conductivity of the post-dialysis sample and water phase, it would be very convenient to integrate the conductivity sensors with the dialyser, preferable with multiple sensor areas that are positioned at various points within the channels. In terms of depositing the required electrodes, this again relates to the matrix material, but for acrylic screen-printed electrodes may be suitable. Customised electronics for converting electrical signals to conductivity values could be developed and integrated into a dialysis chip holder that also includes fittings for inlet and outlet tubings.

The intended application of the developed counter-flow dialyser is desalting of biological samples, which necessitates few-nanometre or sub-nanometre pore diameters. Although the desalting performance could in principle be improved by fabricating thinner membranes with

higher pore densities, this will be extremely challenging with semiconductor nanofabrication technology and materials (127). However, it may be possible by adjusting the chemical synthesis conditions under which the ultrafiltration membranes are grown. This may be feasible because the counter-flow dialysis procedure does not involve high pressures and structural weakening of the membranes could perhaps be allowed. With a different pore size regime dialysis applications other than desalting could also be explored, for example for continuous-exchange cell-free protein synthesis where optimal synthesis activity needs to be maintained by a continuous removal of by-products and supply of chemical energy molecules and removal of by-products (128).

9.3 Publications arising from this work

Selected results from Chapter 6 have been presented at a national and at an international conference with an associated conference proceeding:

Kalikavunkal, Prameen C. and de Planque, Maurits R.R. (2013) *Cross-flow dialysis for microvolume desalting.* At NanoBioTech 2013, Montreux, Switzerland, 18 - 20 Nov 2013.

Kalikavunkal, Prameen C. and de Planque, Maurits R.R. (2014) *Cross-flow dialysis for microvolume desalting.* At RSC Analytical Research Forum 2014, London, GB, 07 Jul 2014.

Kalikavunkal, Prameen C. and de Planque, Maurits R.R. (2014) *Microvolume tuneable dialysis for mass spectrometry.* At MicroTAS 2015, Gyeongju, South Korea, 25-29 November 2015.

Selected results from Chapter 7 will also be submitted as a late abstract to the *19th International Conference on Miniaturized Systems for Chemistry and Life Sciences (μTAS 2015)*, to be held 25-29 October 2015 in Gyeongju, Korea.

Two full publications will be submitted to international journals, a systematic investigation of salt transport over different membranes under a range of flow conditions, including theoretical analysis (data from Chapter 6), and the results on counter-flow dialysis of human serum and of protein samples and their corresponding mass spectra (data from Chapter 7).

References

1. Nanowire and nanotube transistors for lab-on-a-chip applications. Minbaek Lee, Ku YounBaik, Meg Noah, Young-Kyun Kwon, Jeong-O Leed, Seunghun Hong. 2009, Lab Chip, Vol. 9, pp. 2267-2280.

2. Screening-Limited Response of NanoBiosensors. Pradeep R. Nair, Muhammad A. Alam. 2008, NANO LETTERS, Vol. 8, pp. 1281-1285.

3. The theory and practice of modern nanobiosensors. Pradeep R. Nair, Muhammad A. Alam. s.l. : IEEE, 2008, IEEE, pp. 41-47.

4. A Review on the Electrochemical Sensors and Biosensors Composed of Nanowires as Sensing Material. Umasankar Yogeswaran, Shen-Ming Chen. 2008, Sensors, Vol. 8, pp. 290-313.

5. Applications of mass spectrometry for quantitation of DNA adducts. Hasan Koc, James A Swenberg. 1-2, 2002, Journal of Chromatography B, Vol. 778, pp. 323-343.

6. Isolating single stranded DNA using a microfluidic dialysis device. Yixiao Sheng, Michael T. Bowser. 2014, Analyst, Vol. 139, pp. 215-224.

7. Size selective DNA transport through a nanoporous membrane in a PDMS. Yixiao Sheng, Michael T. Bowser. 2012, Analyst, Vol. 137, pp. 1144-1151.

8. A microfluidic dialysis device for complex biological mixture SERS analysis. Gerardo Perozziello, Patrizio Candeloro, Francesco Gentile, Maria Laura Coluccio, Marco Tallerico, Antonio De Grazia, Annalisa Nicastri, Angela Mena Perri, Elvira Parrotta, Francesca Pardeo, Rossella Catalano, Giovanni Cuda, Enzo Di Fabrizio. 2015, Microelectronic Engineering, Vol. 144, pp. 37-41.

9. Cross polarization compatible dialysis chip. Micha Kornreich, Michael Heymann, Seth Fraden and Roy Beck. 2014, Lab Chip, Vol. 14, pp. 3700-3704.

10. Microfluidic dialysis cell for characterization of macromolecule interactions. Jan Scrimgeour, Jae Kyu Cho, Victor Breedveld and Jennifer Curtis. 2011, Soft Matter, Vol. 7, pp. 4762-4767.

11. Ultrarapid desalting of protein solutions for electrospray mass spectrometry in a microchannel laminar flow device. Konermann, Derek J. Wilson and Lars. 21, 2005, Analytical Chemistry, Vol. 77, pp. 6887-6894.

12. Anil K. Pabby, Syed S.H. Rizvi, Ana Maria Sastre Requena. Handbook of Membrane Separations: Chemical, Pharmaceutical, Food, and Biotechnological Applications. s.l. : CRC Press, 2008. p. 505.

13. Toward a human blood serum proteome: analysis by multidimensional separation coupled with mass spectrometry. Adkins JN, Varnum SM, Auberry KJ, Moore RJ, Angell NH, Smith RD, Springer DL, Pounds JG. 12, 2002, Molecular & Cellular Proteomics, Vol. 1, pp. 947-955.

14. Serum proteomics using mass spectrometry. Brian L. Hood, David E. Malehorn, Thomas P. Conrads, William L. Bigbee. 2009, Methods in Molecular Biology, Vol. 520, pp. 107-128.

15. Quantitative nanoscale field effect sensors. Aleksandar Vacic, Mark A. Reed. 1, 2013, Journal of Experimental Nanoscience, Vol. 9, pp. 41-50.

16. Nanowire sensors for medicine and the life sciences. Fernando Patolsky, Gengfeng Zheng, Charles M Lieber. 1, 2006, Nanomedicine, Vol. 1, pp. 51-65.

17. Carey, Francis. Organic Chemistry. 4. p. 526.

18. Soderberg, Tim. UC Davis ChemWiki. [Online] [Cited:20.11.2015] http://chemwiki.ucdavis.edu/Organic_Chemistry/Organic_Chemistry_With_a_Biological_Emphasis/Chapter_04%3A_Structure_Determination_I/Section_4.4%3A_Mass_Spectrometry.

19. J. Throck Watson, O. David Sparkman. Introduction to Mass Spectrometry: Instrumentation, Applications, and Stratergies for Data Interpretation. 4. s.l. : John Wiley & Sons Ltd., 2007.

20. Effects of buffer loading for electrospray ionization mass spectrometry of a noncovalent protein complex that requires high concentrations of essential salts. Harry J. Sterling, Joseph D. Batchelor, David E. Wemmer, Evan R. Williams. 6, 2010, Journal of the American Society for Mass Spectrometry , Vol. 21, pp. 1045-1049.

21. Life Tecnologies. Pierce™ C18 Tips, 10 µL bed. [Online] [Cited:20.11.2015] https://www.lifetechnologies.com/order/catalog/product/87782#/legacy=www.piercenet.com.

22. Identification of RNA linkage isomers by anion exchange purification with electrospray ionization mass spectrometry of automatically desalted phosphodiesterase-II digests. J.R. Thayer, Nitin Puri, Chris Burnett, Mark Hail, Srinivasa Raoa. 1, 2010, Analytical Biochemistry, Vol. 399, pp. 110-117.

23. Size Exclusion Chromatography Beads. Galleryhip. [Online] [Cited:] http://galleryhip.com/size-exclusion-chromatography-beads.html.

24. Dermot Walls, Sinéad T. Loughran. Protein Chromatography, Methods and Protocols. s.l. : Humana Press, 2011. p. 3.

25. Spectrum Labs. Pore Size Chart. [Online] [Cited:20.11.2015] http://www.spectrumlabs.com/filtration/PoreSize.html.

26. Modular microfluidics for point-of-care protein. L. J. Millet, J. D. Lucheon,R. F. Standaert,S. T. Retterer, M. J. Doktycz. 2015, Lab Chip , Vol. 15, pp. 1799-1811.

27. Cytidine 5'-Monophospho-N-acetylneuraminic Acid or a Related Compound is the Low Mr Factor from Human Red Blood Cells Which Induces Gonococcal Resistance to Killing by Human Serum. Christine A.Nairn, J.A.Cole, P.V.Patel,N.J.Parsons,J.E.Fox, H.Smith. 12, 1988, Microbiology, Vol. 134, pp. 3295-3306.

28. Immobilization of starch phosphorylase from cabbage leaves: production of glucose-1-phosphate. N.Garga, A.Kumar. 2, Brazilian Journal of Chemical Engineering, Vol. 25, pp. 229-235.

29. Lifetechnologies. [Online] Thermo Fisher Scientific Brand. [Cited: 15 6 2015.] https://www.lifetechnologies.com/uk/en/home/life-science/protein-biology/protein-purification-isolation/protein-dialysis-desalting-concentration/zeba-desalting-products.html.

30. Fabrication of fritless chromatographic microchips packed with conventional reversed-phase silica particles. Gaspar A, Piyasena ME, Gomez FA. 20, 2007, Analytical Chemistry, Vol. 79, pp. 7906-7909.

31. Microfluidic Liquid Chromatography System for Proteomic Applications and Biomarker Screening. Iulia M.Lazar, Phichet Trisiripisal, Hetal A.Sarvaiya. 15, 2006, Analytical Chemistry, Vol. 78, pp. 5513-5524.

32. A microfluidic device for detection of single nucleotide Polymorphisms by allele specific single base extention. Jing Zhu, Chunmei Qiu, Mirkó Palla, ThaiHuu Nguyen, Jingyue Ju, Qiao Lin. s.l. : µTAS, 2011, 15th International Conference on Miniaturized Systems for Chemistry and Life Sciences.

33. Agilent. Agilent technologies. Agilent Reverse-phase C-18 columns. [Online] [Cited: 20 4 2015.] http://www.chem.agilent.com/Library/ datasheets/Public/5990-8868en_lo.pdf.

34. Robert Rautenbach, R.Rautenbach, R. Albrecht. Membrane processes. s.l. : John Wiley & Sons Ltd, 1989.

35. Reverse osmosis desalination: Water sources, technology, and today's challenges. Lauren F. Greenleea, Desmond F. Lawlerb, Benny D. Freemana, Benoit Marrotc, Philippe Moulin. 2009, Water research, Vol. 43, pp. 2317-2348.

36. Diffusion dialysis-concept, principle and applications. Jingyi Luo, Cuiming Wu, Tongwen Xu, Yonghui Wu. 2011, Journal of Membrane Science, Vol. 366, pp. 1-16.

37. Ion exchagne resins. Electrosynthesis. [Online] [Cited:21.4.2015.] http://www.electrosynthesis.com/electrodialysis.html.

38. Working principle of Electrodialysis. [Online] [Cited:20.04.2015.] http://glossary.periodni.com/glossary.php?en=electrodialysis.

39. Strathmann, Heinrich. Electrodialysis. [book auth.] W.S.W. Ho and K.K. Sirkar. Membrane Handbook. 1992, pp. 219-255.

40. Diffusion dialysis processes of inorganic acids and their salts: The permeability of different acidic anions. Jingyi Luo, Cuiming Wu, Tongwen Xu, Yonghui Wu. 2011, Separation and Purification Technology, Vol. 78, pp. 97-102.

41. Effect of Increasing Dialyzer Mass Transfer Area Coefficient and Dialysate Flow on Clearance of Protein-Bound Solutes: A Pilot Crossover Trial. Frank J.-G.Luo, Kajal P. Patel, Ilian O. Marquez, Natalie S. Plummer, Thomas H. Hostetter, Timothy W. Meyer. 6, 2009, American Journal of Kidney Diseases, Vol. 53.

42. Increasing Dialysate Flow and Dialyzer Mass Transfer Area Coefficient to Increase the Clearance of Protein-bound Solutes. Timothy W. Meyer, Evonne C. Leeper, Derek W. Bartlett, Thomas A. Depner, Yiming Zhao Lit, Channing R. Robertson, Thomas H. Hostetter. 2004, Journal of the American Society of Nephrology, Vol. 15, pp. 1924-1935.

43. Treatment Methods for Kidney Failure: Hemodialysis. National Kidney and Urologic Diseases. [Online] 20 04 2015.

44. Spectrum Labs. Spectra/Por® Dialysis Reservoirs. [Online] [Cited: 20 04 2015.] http://www.spectrumlabs.com/dialysis/Reservoirs.html .

45. Piercenet. Formation of the nernst diffusion layer near the membrane during dialysis. [Online] [Cited: 20 04 2015.] http://www.piercenet.com.

46. Spectrum Labs. Spectra/Por® Dialysis Kit with Assorted Biotech RC Membranes. [Online] [Cited: 20 04 2015.] http://www.spectrumlabs.com/dialysis/MembraneKit.html.

47. Float dialyzer kit from Spectrum Labs. Spectrum labs. [Online] [Cited: 20 04 2015.] http://www.spectrumlabs. com/dialysis/MicroDialyzerA.html.

48. A microfilter utilizing a polyethersulfone porous membrane with nanopores. Ye Gu, Norihisa Miki. 2007, Journal of Micromechanical and Microengineering, Vol. 17, pp. 2308-2315.

49. Properties of membranes used for hemodialysis therapy. William R. Clark, Dayong Gao. 1, 2002, Seminars in dialysis, Vol. 15, pp. 191-195.

50. A facile microdialysis interface for on-line desalting and identification of proteins by nano-electrospray ionization mass spectrometry. Liangliang Sun, Jicheng Duan, Dingyin Tao, Zhen Liang, Weibing Zhang, Lihua Zhang, Yukui Zhang. 2008, Rapid Communications Mass Spectrometry, Vol. 22, pp. 2391-2397.

51. Online microdialysis-dynamic nanoelectrospray ionization-mass spectrometry for monitoring neuropeptide secretion. Jennifer A. Jakubowski, Nathan G. Hatcher, Jonathan V. Sweedler. 2005, Journal of Mass Spectrometry, Vol. 40, pp. 921-931.

52. Microdialysis Sampling Coupled to Microchip Electrophoresis with Integrated Amperometric Detection on an All-Glass Substrate. David E. Scott, Ryan J. Grigsby, Dr. Susan M. Lunte. 10, 2013, ChemPhysChem,Special Issue: Photo- and Bioelectrochemistry, Vol. 14, pp. 2288-2294.

53. On-Line Microdialysis Sample Cleanup for Electrospray Ionization Mass Spectrometry of Nucleic Acid Samples. Chuanliang Liu, Qinyuan Wu, Amy C. Harms, and Richard D. Smith. 18, 1996, Analytical Chemistry, Vol. 68, pp. 3295-3299.

54. On-line microdialysis of proteins with high-salt buffers for direct coupling of electrospray ionization mass spectrometry and liquid chromatography. S. Canarelli, I. Fisch, R. Freitag. 2002, Journal of Chromatography A, Vol. 948, pp. 139-149.

55. An Integrated Microfabricated Device for Dual Microdialysis and On-Line ESI-Ion Trap Mass Spectrometry for Analysis of Complex Biological Samples. Fan Xiang, Yuehe Lin, Jenny Wen, Dean W. Matson, Richard D. Smith. 1999, Analytical Chemistry, Vol. 71, pp. 1485-1490.

56. On-chip microdialysis system with in-line sensing capabilities. Yi-Cheng Hsieh, Jeffrey D. Zahn. 2005, IEEE, pp. 802-805.

57. On-Chip Microdialysis System with Flow-Through Glucose Sensing Capabilities. Yi-Cheng Hsieh, Jeffrey D. Zahn. 3, 2007, Journal of Diabetes Science and Technology, Vol. 1.

58. Microfiltration platform for continuous blood plasma protein extraction from whole blood during cardiac surgery. Kiana Aran, Alex Fok, Lawrence A. Sasso, Neal Kamdar, Yulong Guan, Qi Sun, Akif Undar, Jeffrey D. Zahn. 2011, Lab Chip, Vol. 11, pp. 2858-2868.

59. A microfilter utilizing a polyethersulfone porous membrane with nanopores. Ye Gu, Norihisa Miki. 2007, Journal of Micromechanical and Microengineering, Vol. 17, pp. 2308-2315.

60. Microfilter Fabricated with PDMS and PES Membrane Applicable for Implantable Artificial Kidney. Ye Gu, Norihisa Miki. 2007, IEEE, pp. 63-67.

61. Analysis of the mass transfers in an artificial kidney microchip. Aissa Ould-Dris, Patrick Paullier, Laurent Griscom, Cécile Legallais, Eric Leclerca. 2010, Journal of Membrane Science, Vol. 352, pp. 116-125.

62. A Microfabricated Dialysis Device for Sample Cleanup in Electrospray Ionization Mass Spectrometry. Naxing Xu, Yuehe Lin, Steven A. Hofstadler, Dean Matson, Charles J. Call, Richard D. Smith. 1998, Analytical Chemistry, Vol. 70, pp. 3553-3556.

63. On-chip protein sample desalting and preparation for direct coupling with electrospray ionization mass spectrometry. Niels Lion, Jean-Olivier Gellon, Henrik Jensen, Hubert H. Giraul. 2003, Journal of Chromatography A, Vol. 1003, pp. 11-19.

64. Silicon-based microdialysis chip with integrated fraction collection. G.L.Subrebost, G.K.Fedder. 2005, Sensors.

65. Microchip Dialysis of Proteins Using in Situ Photopatterned Nanoporous Polymer Membranes. Simon Song, Anup K. Singh, Timothy J. Shepodd, Brian J. Kirby. 8, 2004, Analytical Chemistry, Vol. 76, pp. 2367-2373.

66. Miniaturized one-chip electrochemical sensing device integrated with a dialysis membrane and double thin-layer flow channels for measuring blood samples. Kurita R, Yabumoto N, Niwa O. 8, 2006, Biosensors Bioelectronics, Vol. 21, pp. 1649-1653.

67. Diffusive clearance of small and middle-sized molecules in combined dialyzer flow configurations. Eloot S, De Vos JY, Hombrouckx R, Verdonck P. 3, 2004, Int J Artif Organs, Vol. 27, pp. 205-213.

68. Size selective DNA transport through a nanoporous membrane in a PDMS microfluidic device. Sheng Y, Bowser MT. 5, 2012, Analyst, Vol. 137, pp. 1144-1151.

69. Stein, Wilfred. Transport And Diffusion Across Cell Membranes. s.l. : Academic Press Inc, 1986.

70. The solution-diffusion model: a review. J.G. Wijmans, R.W. Baker. 1-2, 1995, Journal of Membrane Science, Vol. 107, pp. 1-21.

71. Cussler, E. L. Diffusion: Mass Transfer in Fluid Systems. 3. s.l. : Cambridge University Press, 2009. pp. 15-18.

72. ALEVEL NOTES. [Online] [Cited: 20 04 2015.] http://alevelnotes.com/Fluid-Flow/112?tree=.

73. Nam-Trung Nguyen, Steven T. Wereley. Fundamentals And Applications of Microfluidics. s.l. : Artech House, 2006.

74. Lewis, R. I. Vortex Element Methods for Fluid Dynamic Analysis of Engineering Systems. s.l. : Cambridge University Press, 1991.

75. Influence of Crossflow Membrane Filter Geometry and Shear Rate on Colloidal Fouling in Reverse Osmosis and Nanofiltration Separations. Eric M. V. Hoek, Albert S. Kim, Menachem Elimelech. 6, 2002, Environmental Engineering Science, Vol. 19, pp. 357-372.

76. Mass transfer, fluid flow and membrane properties in flat and corrugated plate hyperfiltration modules. I.G.Rácz, J.Groot Wassink, R.Klaassen. 3, Desalination, Vol. 60, pp. 213-222.

77. Increasing dialysate flow and dialyzer mass transfer area coefficient to increase the clearance of protein-bound solutes. Meyer TW, Leeper EC, Bartlett DW, Depner TA, Lit YZ, Robertson CR, Hostetter T. 7, 2004, J Am Soc Nephrol, Vol. 15, pp. 1927-1935.

78. Effect of increasing dialysate flow rate on diffusive mass transfer of urea, phosphate and β2-microglobulin during clinical haemodialysis. Jai P. Bhimani, Rosemary Ouseph and Richard A. Ward. 7, 2010, Nephrol Dial Transplant , Vol. 15, pp. 1927-1935.

79. Effect of increasing dialyzer mass transfer area coefficient and dialysate flow on clearance of protein-bound solutes: a pilot crossover trial. Luo FJ, Patel KP, Marquez IO, Plummer NS, Hostetter TH, Meyer TW. s.l. : 53, 2009, Am J Kidney Dis, Vol. 6, pp. 1042-1049.

80. Microchip Dialysis of Proteins Using in Situ Photopatterned Nanoporous Polymer Membranes. Simon Song, Anup K. Singh,Timothy J. Shepodd, Brian J. Kirby. 8, 2004, Analytical Chemistry, Vol. 76, pp. 2367-2373.

81. Application of internal reflux in the raffinate phase for membrane extraction in cross-flow rectangular modules. Yeh, H.M.

82. Analysis of dialysis coupled with ultrafiltration in cross-flow membrane modules. H.M. Yeh, T.W. Cheng, Y.J. Chen. 1997, Journal of Membrane Science, Vol. 134, pp. 151-162.

83. Mass transfer for dialysis through parallel-flow double-pass rectangular membrane modules. H.M. Yeh, Y.H. Chang. 2005, Journal of Membrane Science, Vol. 260, pp. 1-9.

84. Mass transfer for dialysis with ultrafiltration flux declined in cross-flow membrane modules. H.M. Yeh, T.W. Cheng, Y.J. Chen. 2000, Journal of Chemical Engineering of Japan, Vol. 33, pp. 440-448.

85. Analysis of membrane extraction through rectangular mass exchanger. H.M. Yeh, Y.S. Hsu. 1999, Chemical Engineering Science, Vol. 54, pp. 897-908.

86. Solvent extraction in multipass parallel-flow mass exchangers of microporous hollow-fiber modules. H.M. Yeh, C.M. Huang. 1995, Journal of Membrane Science, Vol. 103, pp. 135-150.

87. Solvent extraction through a double-pass membrane channel with recycle. H.M. Yeh, Y.Y. Peng, Y.K. Chen. 1999, Journal of Membrane Science, Vol. 163 , pp. 177-192.

88. Numerical Analysis of Mass Transfer in Countercurrently Paralle-flow Rectangular Dialyzer with internal recyle for improved performance. H.M.Yeh. 4, 2011, Tamkang Journal of Science and Engineering, Vol. 14, pp. 351-358.

89. Numerical Ananlysis of mass trasnfer in double –pass parallel-plate dialyzers with external recycle. H.M.Yeh. 2009, Computers and Chemical Engineering, Vol. 33, pp. 815-821.

90. Limits of mass-transfer in parallel plate dialyzers. Spas D.Kolev, Willem E. van der Linden. 1992, Analytica Chimica Acta, Vol. 2562, pp. 301-305.

91. Hemodialyzer mass transfer-area coefficients for urea increase at high dialysate flow rates. The Hemodialysis (HEMO) Study. Leypoldt JK, Cheung AK, Agodoa LY, Daugirdas JT, Greene T, Keshaviah PR. 6, 1997, Kidney International, Vol. 51, pp. 2013-2017.

92. Jakob, M. Heat Transfer. New York : John Wiley & Sons, Inc, 1957. Vol. 2.

93. Friedrich, Craig. Laser Ablation. [Online] 1998. [Cited: 20 4 2015.] http://www.me.mtu.edu/~microweb/chap4/ch4-2.htm.

94. Effective deep ultraviolet photoetching of polymethyl methacrylate by an excimer laser. Y. kawamura, K. Toyoda, S.Namba. 5, 1982, Applied Physics Letters, Vol. 40, pp. 374-375.

95. Sensing cyanide ion via fluorescent change and its application to the microfluidic system. Soo Kyung Kwon, Songzi Kou, Ha Na Kim, Xiaoqiang Chen, Hyejin Hwang, Seong-Won Nam, So Hyun Kim, K. M. K. Swamya, Sungsu Park, Juyoung Yoon. 2008, Tetrahedron Letters, Vol. 49, pp. 4102-4105.

96. Comparison of Co-Current and Counter-Current Flow Fields on Extraction Performance in Micro-Channels. Benny Malengier, Subramaniam Pushpavanam. 2012, Advances in Chemical Engineering and Science, Vol. 2, pp. 309-320.

97. Cheryan, Muni. Ultrafiltration and microfiltration handbook. s.l. : CRC Press LLC. p. 94.

98. Advanced functional polymer membranes. Ulbricht, Mathias. 2006, Polymer, Vol. 47, pp. 2217-2262.

99. Characterization of UF Membranes Membrane Characteristics and Characterization Techniques. Smolders, F. P. Cuperus and C. A. 1991, Advances in Colloid and Interface Science, Vol. 78, pp. 135-173.

100. Characterization of Ultrafiltration Polymeric Membranes. P. Abaicchio, A.Boitino, G.Camera Rodax, G.Capannell, S.Munari. s.l. : Elsevier Science Publishers, 1990, Desalination, Vol. 78, pp. 235-255.

101. Yoon, S. Principle and Application of Membrane Bioreactor Process. Online MBR Information. [Online] [Cited:] http://www.onlinembr.info/Membrane%20process/Pore%20size.html.

102. K.Scott. Industrial Membrane Separation Technology. s.l. : Springer Science & Business Media, 1996. pp. 5-7.

103. The Method To Define The Pore Diameter And Its distribution for Porous Membrane. Lu Xiaolong, Ma Shihu Chen Yi. s.l. : Tianjin Montian Company, 2005.

104. A review on membrane fabrication: Structure, properties and performance relationship. Boor Singh Lalia, Victor Kochkodan, Raed Hashaikeh, Nidal Hilal. 2013, Desalination, Vol. 326, pp. 77-95.

105. Characterization and properties of micro- and nanowires of controlled size, composition, and geometry fabricated by electrodeposition and ion-track technology. Toimil-Molares, Maria Eugenia. 2012, Beilstein J. Nanotechnol., Vol. 3, pp. 860–883.

106. Nuclear Tracks in Solids: Principles and Applications. R. Robert, Louis Fleischer, Paul Buford Price, R.M. Walker. s.l. : University of California Press, 1975.

107. Hahnemuhle. TEM – Track Etched Membranes Unique technology - Precise Features - Advanced Performance. Hahnemuhle. [Online] [Cited:20.11.2015] http://www.hahnemuehle.com/fileadmin/user_upload/bilder/filtration/pdf/FILTRATION_Flyer_6seiter_TEM_Track_Etched_Membranes_EN.pdf.

108. Surface charge density of the track-etched nanopores in polyethylene terephthalate foils. Jianming Xue, Yanbo Xie, Yu Yan, Jin Ke, and Yugang Wang. 2009, BIOMICROFLUIDICS, pp. 2240-2248.

109. Sterlitech. Sterlitech. Sterlitech Corporation. [Online] http://www.sterlitech.com/filters/membrane-disc-filters/polyester-membrane-filters/polyester-pete-membranes.html. [Cited:] http://www.sterlitech.com/filters/membrane-disc-filters/polyester-membrane-filters/polyester-pete-membranes.html.

110. Properties of Films Composed of Cellulose Nanowhiskers and a Cellulose Matrix Regenerated from Alkali/Urea Solution. Haisong Qi, Jie Cai, Lina Zhang, Shigenori Kuga. 2009, Biomacromolecules, Vol. 10, pp. 1597-1602.

111. Sterlitech. Sterlitech Coporation . [Online] [Cited:] http://www.sterlitech.com/filters/membrane-disc-filters/polyethersulfone-pes-membrane-filters.html.

112. Metal Nanoparticle Modified Polysulfone Membranes for Use in Wastewater Treatment: A Critical Review. Heidi Lynn Richards, Priscilla G. L. Baker, Emmanuel Iwuoha. 2012, ournal of Surface Engineered Materials and Advanced Technology, Vol. 2, pp. 183-193.

113. Carlos A. Costa, Joaquim S. Cabral. Chromatographic and Membrane Processes in Biotechnology. s.l. : Kluwer Academic Publishers, 1990. pp. 179-180.

114. Characterization of anisotropic UF-membranes: top layer thickness and pore structure. F.P. Cuperus, D. Bargeman and C.A. Smolders. s.l. : Elsevier Science Publishers, 1991, Journal of Membrane Science, Vol. 61, pp. 73-83.

115. An osmolyte-based micro-volume ultrafiltration technique. Ghosh, Raja. 2014, Lab Chip, Vol. 14, p. 4559.

116. A New Method to Determine the Skin Thickness of Asymmetric UF-Membranes Using Colloidal Gold Particles. F.P.Cuperus, D. Bargeman, K.Smolders. 2, 1990, Journal of Colloid and Interface Science, Vol. 135, pp. 486-495.

117. Critical points in the analysis of membrane pore structures by thermoporometry. F.P. Cuperus, D. Bargeman and C.A. Smolders. 1, 1992, Journal of Membrane Science, Vol. 66, pp. 45-53.

118. Preparation, characterization and performance of polyethersulfone ultrafiltration membranes. B.K.Chaturvedi, AK.Ghoshb, V.Ramachandhranb, M.K.Trivedi, M.S.HanTab, B.M.Misrab. 2001, Desalination, Vol. 3, p. 140.

119. Protein Diffusion in Living Skeletal Muscle Fibers: Dependence on Protein. Simon Papadopoulos, Klaus D. Jurgens, Gerolf Gros. 2000, Biophysical Journal, Vol. 79, pp. 2084-2094.

120. Modification of regenerated cellulose ultrafiltration membranes by surface-initiated atom transfer radical polymerization . Nripen Singha, Zhen Chenb, Namrata Tomera, S.Ranil Wickramasingheb, Neil Soice , Scott M. Husson. 2008, Journal of Membrane Science, Vol. 311, pp. 225-234.

121. Electrical conduction studies through microporous track etch membranes of equal pore density and porosity. Ravish Garg, Vijay Kumar, Dinesh Kumar, S.K. Chakarvarti. 2, 2014, ISST Journal of Applied Physics, Vol. 5, pp. 101-105.

122. Electrolytic transport through cylindrical etched pores in polyethylene terphthalate track etch membrane. S. Kumar, S.K. Chakarvarti. 14, 2008, Modern Physics Letters B, Vol. 22, pp. 1415-1421.

123. Measurement of average etched pore radius in ion track membranes through conductometric technique. S. Kumar, S.K. Chakarvarti. 30, 2008, Modern Physics Letters B, Vol. 22, pp. 2993-2998.

124. Characterization of regenerated cellulose membranes hydrolyzed from cellulose acetate. Yun Chen, Xiao-peng Xiong, Guang Yang, Li-na Zhang, Sen-lin Lei, Hui Liang. 4, 2002, Chinese Journal of Polymer Science, Vol. 20, pp. 369-375.

125. E.L.Cussler. Diffusion : Mass Transfer in fluid systems. 2nd. s.l. : Cambridge University Press, 1997.

126. Effect of Protein on Hemoglobin and Hematocrit Assays with a Conductivity-Based Point-of-Care Testing Device: Comparison with Optical Methods. Sidney M. Hopfer, Francesca L. Nadeau, Marilyn Sundra, Gregory S. Makowski. 1, 2004, Annals of Clinical & Laboratory Science, Vol. 34.

127. Microfabricated ultrarapid desalting device for nanoelectrospray ionization mass spectrometry. Tibavinsky IA, Kottke PA, Fedorov AG. 6, 2015, Analytical Chemistry, Vol. 87, pp. 351-356.

128. The past, present and future of cell-free protein synthesis. Katzen F, Chang G, Kudlicki W. 3, March 2005, Trends Biotechnology, Vol. 23, pp. 150-156.

129. Solution additives that desalt protein ions in native mass spectrometry. Flick TG, Cassou CA, Chang TM, Williams ER. 17, 2012, Analytical Chemistry, Vol. 84, pp. 7511-7517.

130. Qingyuan Hu, Hongwei Hou. Tobacco Smoke Exposure Biomarkers. s.l. : CRC Press, 2015. p. 20.

131. Baker, Richard W. Membrane Technology and Applications. 2. s.l. : McGraw-Hill, 2004.

Chapter 10: Appendix 1

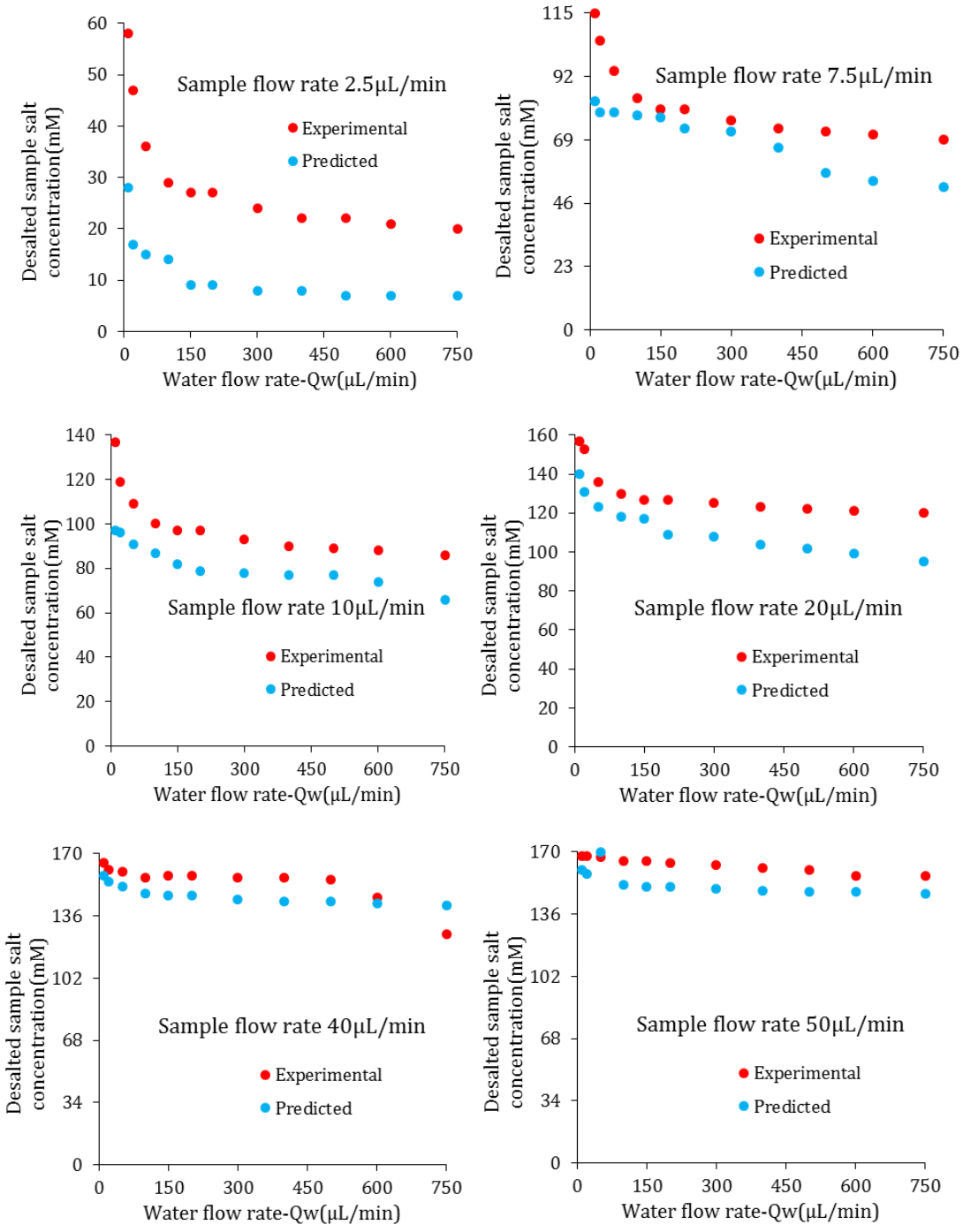

Figure 10.1: Comparison between the post-dialysis sample salt concentration as determined by conductivity measurements and the theoretical salt concentration as calculated with the mass transfer equations.